Methods for Enhancing Power Line Communication over Low Voltage Networks

Teză destinată obţinerii
titlului ştiinţific de doctor inginer
la
Universitatea Politehnica Timişoara
în domeniul
INGINERIE ELECTRONICĂ, TELECOMUNICAȚII ȘI TEHNOLOGII INFORMAȚIONALE
de către

Ing. Sebastian Avram

Preşedintele comisiei:	prof.univ.dr.ing. Dan-Florentin Lascu
Conducător ştiinţific:	prof.univ.dr.ing. Radu Adrian Vasiu
Referenţi ştiinţifici:	prof.univ.dr.ing. Corneliu Burileanu
	prof.univ.dr.ing. Dorin Petreuș
	prof.univ.dr.ing. Cătălin-Daniel Căleanu

Ziua susţinerii tezei: 03 Noiembrie 2023.

Seriile Teze de doctorat ale UPT sunt:

1. Automatică
2. Chimie
3. Energetică
4. Inginerie Chimică
5. Inginerie Civilă
6. Inginerie Electrică
7. Inginerie Electronică şi Telecomunicaţii
8. Inginerie Industrială
9. Inginerie mecanică
10. Ştiinţa Calculatoarelor
11. Ştiinţa şi Ingineria Materialelor
12. Ingineria Sistemelor
13. Inginerie Energetică
14. Calculatoare şi Tehnologia Informaţiei
15. Ingineria Materialelor
16. Inginerie şi Management
17. Arhitectură
18. Inginerie Civilă și Instalații
19. Inginerie Electronică, Telecomunicații și Tehnologii Informaționale

Universitatea Politehnica Timişoara a iniţiat seriile de mai sus în scopul diseminării expertizei, cunoştinţelor şi rezultatelor cercetărilor întreprinse în cadrul Şcolii doctorale a universităţii. Seriile conţin, potrivit H.B.Ex.S Nr. 14 / 14.07.2006, tezele de doctorat susţinute în universitate începând cu 1 octombrie 2006.

România, 300223 Timişoara, Bd. Vasile Pârvan 2B
Tel./fax 0256 404677
e-mail: editura@upt.ro

Foreword

This thesis was developed during my doctoral studies at the Department of Communications, Politehnica University Timişoara. My research is focused on improving narrow band power line communication, a cost-effective and efficient solution to enable communication over power lines. It is a subject of significant importance because as of 2020 more than 123 million smart meters use NB-PLC as communication protocol in Europe and their number is expected to increase to more than 200 million by 2024.

To achieve this goal, I thoroughly examined the existing literature and identified two main areas where improvements can be brought. In the next stage, I have prepared both theoretical and practical means of implementing the improvements, ultimately validating them in laboratory conditions.

Primarily, I express my heartfelt appreciation to my esteemed thesis advisor and mentor, Professor Radu Vasiu, whose expertise, encouragement, and continuous monitoring have been indispensable. His commitment to fostering intellectual curiosity and scholarly excellence has been an inspiration, and I am deeply grateful for the trust he placed in my abilities.

To my colleagues and fellow researchers, thank you for engaging in stimulating discussions, sharing your knowledge, and fostering a collaborative academic environment that has nurtured my growth as a scholar.

As I present this thesis, I carry in my heart the memory of my father, whose belief in my academic journey was a driving force. This work is dedicated to his memory and the unwavering love and support he bestowed upon me.

Finally, I express profound gratitude to my family and friends for continuously inspiring and providing unwavering support throughout this entire journey. Their comprehension of my responsibilities and patience with the demands of my PhD studies proved invaluable in assisting me in surmounting various challenges along the way.

Timişoara, August 2023 Sebastian Avram

For my familiy

Avram, Sebastian

Methods for Enhancing Power Line Communication over Low Voltage Networks Teze de doctorat ale UPT, Seria X, Nr. YY, Editura Politehnica, 2023, xx pagini, yy figuri, zz tabele.

ISSN:
ISBN:

Cuvinte cheie
Power Line Communication, Smart metering, Smart Grid, Power Line Carrier

Rezumat: Temele abordate în această teză au ca scop să aducă îmbunătățiri comunicației de date de bandă îngustă de frecvență prin liniile de joasă tensiune (Narrow Band Power Line Communication NB-PLC).

Numărul mare de dispozitive (peste 123 milioane doar în Europa) care folosesc NB-PLC ca să comunice în rețeaua inteligentă de distribuție a energiei electrice (smart grid) cât și directivele europene (2019/944, 2009/73/EC și 2012/27/EU) care cer un grad ridicat de implementare al smart grid justifică nevoia de a identifica, valida si implementa metode de îmbunatățire a NB-PLC.

Autorul propune teoretic, implementează practic și validează în condiții de laborator două technici de îmbunătățire a NB-PLC cu aplicabilitate directă în smart grid.

Contents

LIST OF FIGURES

LIST OF TABLES

LIST OF ABBREVIATIONS

AC	alternating current
ADC	analog to digital converter
AFE	analog front end
AMI	advanced metering infrastructure
AMR	automatic meter reading
ARIB	association of radio industries and businesses
ATX	advanced technology extended
AWGN	additive white Gaussian noise
BB	broadband
CCFL	cold cathode fluorescent lamp
CE	Conducted emissions
CISPR	Comité International Spécial des Perturbations Radioélectriques
COSEM	companion specification for energy metering
CSMA	carrier sense multiple access
CT	current transformer
D8PSK	differential eight phase shift keying
DA	distribution automation
DAB	digital audio broadcasting
DBPSK	differential binary phase shift keying
DC	data concentrator
DLMS	device language message specification
DQPSK	differential quaternary phase shift keying
DSP	digital signal processor
DVB-H	digital video broadcasting - handheld
DVB-T	digital video broadcasting – terrestrial
EDGE	enhanced data rates for GSM evolution
EMC	electromagnetic compatibility
EMI	electromagnetic interference
FCC	federal communications commission
FFT	Fast Fourier Transform
FRA	frequency response analyser
GPRS	general packet radio service
GSM	global system for mobile communications
HDLC	High-level Data Link Control
HPLC	high speed power line communication
IDE	integrated development environment
IEC	International Electrotechnical Commission
IFFT	inverse fast Fourier transform
MAC	media access control
MB	medium band
MoCA	multimedia over coax alliance
MOV	metal oxide varistor
MV	medium voltage
NB	narrow band
OBIS	object identification system
OFDM	orthogonal frequency division multiplexing
PAPR	peak to average power ratio

PC	personal computer
PER	packet error rate
PHY	physical
Pk_{Max}	peak detector
PLC	power line communication
PLF	power line filter
PRIME	power line intelligent metering evolution
PSD	power spectral density
PSTN	public switched telephone network
QAM	quadrature amplitude modulation)
RBW	resolution bandwidth
RCD	residual current protective device
RCS	ripple control system
RSSI	received signal strength indicator
RTC	real time clock
SG	smart grid
SM	smart meter
SNR	signal to noise ratio
SPI	serial peripheral interface
SPICE	simulation program with integrated circuit emphasis
SWT	sweep time
TCP/ IP	High-level Data Link Control
TMOV	thermally protected metal oxide varistor
UART	universal asynchronous receiver/ transmitter
UMTS	enhanced data rates for GSM evolution
U-NB	ultra narrow band
UWB	ultra-wideband
VBW	video bandwidth
VNA	vector network analyser
WiMAX	worldwide interoperability for microwave access,
Z_{in}	input impedance
Z_L	load impedance
Z_S	source impedance

1 Introduction and Motivation

This chapter outlines the rationale behind selecting enhancement techniques for NB-PLC as the focal point of the thesis. It also offers a compilation of articles in which I have been the first author, all closely aligned with the subject of my doctoral research and created during that timeframe. Within this chapter, the thesis's scope, objectives, assumptions, and constraints are all expounded upon.

1.1 Background and Overview

The primary focus of this thesis is centered around enhancing NB-PLC through low voltage lines with the wider scope of improving SGs with PLC.

With over 123 million devices exclusively in Europe [1] utilizing NB-PLC for SG communication and supported by European directives (2019/944, 2009/73/EC, and 2012/27/EU) stressing enhanced SG integration, the necessity to identify, validate, and apply strategies to enhance NB-PLC is well-founded.

In the thesis I will presents two distinct PLC enhancement methodologies researched by me during the doctoral studies, both theoretically and practically, which are subsequently validated within controlled laboratory settings. These techniques hold immediate relevance for enhancing NB-PLC within the context of the SG.

1.2 Published articles

During my research on this subject, I had the opportunity to present my work through several papers at international conferences as well as to publish an article in an academic journal. These endeavors were instrumental in confirming the validity of my work. To demonstrate the relevance of the research areas explored in my thesis, I am pleased to provide a comprehensive list of the articles I have authored or co-authored, all of which were produced in conjunction with and during the progress of my thesis:

1. Sebastian Avram, Radu Vasiu. 2023. "Passive Power Line Communication Filter Design and Benchmarking Using Scattering Parameters" Applied Sciences 13, no. 11: 6821. (Q2 journal), DOI: 10.3390/app13116821, WOS: 001006564200001.

2. Sebastian Avram, Radu Vasiu, Loredana Nicoleta Paven, Maria Lucia Crauciuc, Dan Chiciudean, "Hardware and Software Implementation of a Self-Calibrating Smart Meter with Tamper Detection," 2021 10th International Conference on ENERGY and ENVIRONMENT (CIEM), Bucharest, Romania, 2021, pp. 1-5, DOI: 10.1109/CIEM52821.2021.9614900.

3. Sebastian Avram, Cătălin Daniel Căleanu, Radu Vasiu, Andreea-Mirela Safta, Horatiu George Belei, "Hardware and Software Integration of an Electrophoretic display on a smart meter," ITM Web Conf. 29 03003 (2019), DOI:10.1051/itmconf/20192903003.

4. Sebastian Avram, Andreea -Mirela Safta, Cătălin Daniel Căleanu, Radu Vasiu, "Hardware and software implementation of an embedded metering webserver," 2017 40th International Conference on Telecommunications and

Signal Processing (TSP), Barcelona, Spain, 2017, pp. 43-46, DOI: 10.1109/TSP.2017.8075933, WOS: 000425229000009.

5. Sebastian Avram, Vladislav Plotenco, Lorendana Nicoleta Paven, "Design and development of an electricity Meter Test Equipment," 2017 International Conference on Optimization of Electrical and Electronic Equipment (OPTIM) & 2017 Intl Aegean Conference on Electrical Machines and Power Electronics (ACEMP), Brasov, Romania, 2017, pp. 96-101, DOI: 10.1109/OPTIM.2017.7974954. WOS: 000426909600014.

6. Sebastian Avram, "Power line communication channel noise source detection using smart meters," 2016 12th IEEE International Symposium on Electronics and Telecommunications (ISETC), Timisoara, Romania, 2016, pp. 103-106, DOI: 10.1109/ISETC.2016.7781067, WOS: 000390717800024.

1.3 Motivation for choosing PLC

This part seeks to give a thorough knowledge of the reasons for the selection of PLC as the study's subject. It will examine the high (and rising) pace of adoption, the specific advantages of PLC, and the difficulties in implementing the SG with NB-PLC.

The primary advantage of NB-PLC is that it makes use of the current electrical grid infrastructure and makes it possible to include SMs into the SG.

In the European Union (EU-28), there will be around 123 million SMs installed by the year 2020, or nearly 43% of all power consumers [1]. By 2024, it is anticipated that there will be 223 million installed SMs, and by 2026, there will be 266 million. 16 of the EU's 28 member states have chosen to use NB-PLC as their preferred means of communication between SMs and DCs [2] .

In comparison to the results of [1], a research by the Joint Research Centre [2] shows greater rollout rates. But according to a market analysis done by the end of 2020, 130 million SMs had been installed in Europe, with 72% of them using PLC [3].

The CENELEC A, B, C, and D bands (3 kHz to 148.5 kHz) [4] are used by NB-PLC in Europe for communication, which is impacted by gaps as well as more permissive limits for EMC and EMI CE. CISPR and IEC organizations have both drawn attention to these two areas of concern, which have been thoroughly covered in scholarly publications [5]–[16]. Currently, actions are being done to address these gaps, such as suggested changes to standards like CISPR 16-1-2, CISPR 32 and corresponding IEC standards.

The use of NB-PLC in SG applications is significant (and growing), and given the gaps in standardization and the existence of grid-connected devices that operate at frequencies lower than 150 kHz, there is a need for the mitigation of these issues in order to maintain and enhance the communication between SG devices.

1.4 Scope and Objectives

In this section I will outline the scope and objectives of the thesis by defining the specific aspects of PLC that will be addressed. Additionally, the intended outcomes and goals of the research will be stated.

This thesis provides extensive answers for these questions:

1. How and why is PLC integrated into the electricity grid, and what are its primary objectives and benefits?
2. What specific challenges does NB-PLC encounter within the power distribution grid, and how do these challenges impact its performance and reliability?
3. What could be non-invasive techniques or solutions available to address the challenges faced by PLC within the SG without the need for grid modifications? If so, what are these techniques, and how can they be effectively implemented?
4. In order to enhance PLC performance, what potential modifications or improvements might be required in the power grid infrastructure, and what strategies can be employed to successfully implement these modifications?

For developing this thesis I have focused on three primary research areas: the identification, avoidance, and filtering of CE within the electricity grid, specifically in the NB-PLC frequency band. These techniques have the scope to enhance the reliability, decrease the error rate, decrease latency, and increase data rate.

1.5 Assumptions and Limitations

Acknowledging the assumptions made within the thesis is essential to maintain transparency and establish the boundaries of the research. This section will discuss the limitations of the research, such as specific environments or scenarios that are not considered.

The concepts researched by me and presented in this thesis have been developed for CENELEC A, B, C, and D bands and validated in laboratory environment using measurement setups that are derived or identical to international standards, which are suitable for AC European power grid. Extension of the usage towards FCC (9-490kHZ) [17] and ARIB (10-450kHZ) [18] PLC bands as well as different power grid standards (i.e. North American electricity grid) is possible but it will require redesign due to different topologies, frequency bands and standards.

1.6 Thesis structure

The thesis is structured in the following manner:

Chapter 1 presents the motivation for choosing enhancement methods of NB-PLC as subject of the thesis together with the list of articles, in which I served either as the main author, all pertaining to the topic of my doctoral research and produced during that period. The scope and objectives together with the assumptions and limitations of the thesis are presented in this chapter.

Chapter 2 provides an introduction into PLC thus covering the following aspects: PLC working principle, communication channel characteristics, PLC applications in the power distribution grid, standardization together with standardization gaps, PLC protocols and frequency spectrum allocation, PLC signal coupling techniques, as well as an overview of the two most used PLC standards for smart metering (PLC-G3 and PRIME).

Portions of this introduction have previously served as the start point for my scientific articles [19]–[24]. To compose this introduction, I conducted an extensive literature review, referencing over 110 bibliographical sources.

Chapter 3 presents an innovative method for detecting devices connected to the power line that generate CE in the frequency band of PLC. The approach involves utilizing SM to establish a link between energy measurements of the load and the communication quality reports obtained from the PLC-G3 modem. By observing practical results, a clear relationship between energy measurements and the noise generated by specific loads becomes evident thus allowing the creation of a transmission schedule for PLC.

The theoretical principles and experimental results presented in this chapter constitute a part of my research activities, and they have been published in scientific publications as referenced in [19], [21], [22], [24], [25].

Chapter 4 discusses my research study that introduces a novel approach for designing and simulating PLFs using S-parameters. Although S-parameters have been applied in other high frequency designs in the past, this work is the first to employ this particular strategy for designing PLFs for filtering applications in NB-PLC frequency band. A 13^{th} order passive PLF was created to show the viability of the proposed design framework. Based on the outcomes, it is possible to develop PLFs that perform better compared to the ones available on the market, in terms of NB-PLC frequency band insertion loss, quiescent power, and input/ output impedance.

The theoretical principles and experimental outcome presented in this chapter originate from my prior scientific publications as referenced in [20], [21].

Chapter 5 marks the concluding segment of my thesis. It commences with overarching conclusions drawn from the research conducted over the past years. The theoretical contributions that this thesis makes to the field of PLC research are then presented, together with the newly developed practical contributions. I finish by providing prospective future routes in this particular field of study that would be interesting for myself or for other experts.

2 Introduction into PLC

The chapter starts with an in-depth examination of the working principles of PLC, where the working principle of how this technology utilizes power lines as physical medium for data transmission is delved into. Within this context, I have also presented in a structured manner the challenges that PLC faces in electricity grid: CE in the power line, standardization gaps, attenuation, and low access impedance.

To appreciate the significance and trajectory of PLC, a step back in time will be taken to trace its historical evolution. My intention is to show the evolution of PLC, from its inception as first-generation systems to the third-generation technologies that define its landscape today. These aspects will not only emphasize the significant progress in PLC but also underscore its increasing importance in contemporary power grid applications.

PLC is used in both AC and DC power systems. This thesis focuses on PLC in AC systems however; it is worth to note that PLC uses the same principles in both AC and DC power systems.

Furthermore, I will delve into the subjects of PLC protocols and frequency spectrum allocation. The intricacy of these topics highlights the wide range of standards and regulations that govern PLC. These aspects are presented to provide a comprehensive understanding of the communication standards in this field.

Signal coupling methods are a key component of PLC technology, and these methods, including antenna coupling, capacitive coupling, inductive coupling, and resistive coupling, will be explored. Each of these coupling techniques has its own applications and unique characteristics, which are detailed and explained.

In the sections that follow, the technical aspects of PLC protocols and transceivers will be delved into, using the foundational knowledge laid out here as basis for the chapters that will follow.

Portions of this introduction have previously served as the foundation for my scientific articles [19]–[21], [25], [24], [22]. To compose this introduction, I conducted an extensive literature review, referencing over 110 bibliographical sources.

2.1 PLC working principle

PLC is using the existing power lines as transmission medium on which a relatively high frequency signal of low amplitude is superimposed on the low frequency high amplitude mains voltage [26].

The fundamental components and operational principles of PLCs are graphically represented in Figure 2.1 and Figure 2.2, and their explanations are provided below:

- Signal Modulation: Data is first modulated onto a carrier signal. The data is typically represented by variations in voltage or current at specific frequencies as well as digital frames.
- Signal Coupling: The modulated signal is coupled to the power line at a substation or directly at the point of use. This can be achieved using various coupling methods, the most common one are using transformers or capacitors.
- Signal Propagation: The modulated signal travels along the power lines, reaching its destination, which can be another substation, a SM, or any other PLC-equipped device.

- Signal Demodulation: At the receiving end, the signal is demodulated to extract the original data.

Figure 2.1 illustrates the fundamental coupling principle of PLC signals in AC power systems, where a relatively high-frequency signal is superimposed or coupled onto the relatively low frequency high amplitude mains voltage waveform. In Figure 2.2, two PLC devices are depicted communicating with each other, with a particular focus on the types of signals associated with their respective locations.

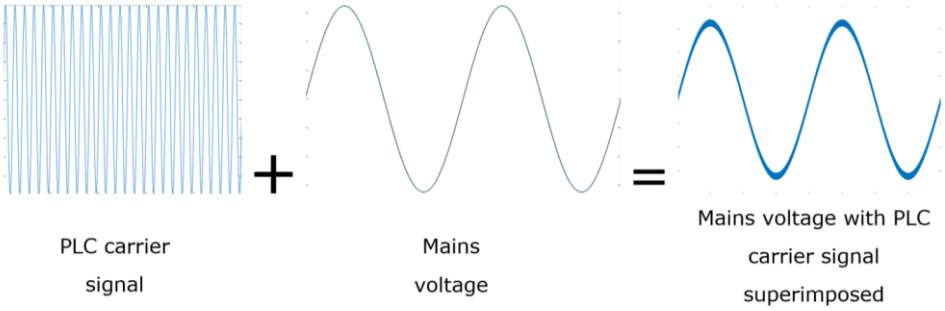

Figure 2.1 PLC signal basic principle

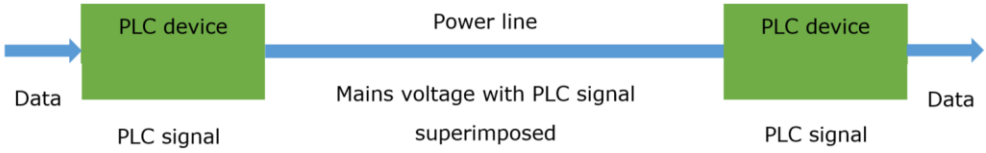

Figure 2.2 Two PLC devices communicating

The below figures provide a detailed overview of a typical PLC signal coupled on the mains power line in SM application of European grid. It is worth to note that PLC is being used in a variety of AC and DC power systems and this is just an example of waveform on which the PLC signal can couple:

- Figure 2.3 depicts a standard 230V_{RMS} 50Hz mains voltage waveform, which I have selected as an example because the upcoming chapters in this thesis will delve into both the theoretical and practical aspects associated with this specific mains standard.
- Figure 2.4 illustrates a PLC carrier signal with a frequency of 40kHz and an amplitude of 1VPP. This carrier signal example aligns with the established standards for PLC in electricity utilities, meeting both amplitude and frequency specifications [27]. I have opted for this specific example because the subsequent chapters in this thesis will utilize PLC signals that follow the same standard.
- Figure 2.5 shows the composition between mains voltage VRMS =230V, f=50Hz waveform and PLC signal waveform having a carrier frequency of fc=40kHz. The depicted waveform is a FSK type of communication. The introduction of the PLC signal into the mains is typically achieved through coupling, commonly capacitive or inductive coupling, which will be extensively discussed in section 2.6.
- Figure 2.6 provides an in-depth perspective of Figure 2.5, with a particular focus on highlighting the disparities in frequency and amplitude between the mains voltage waveform and the PLC carrier. The PLC signal, characterized

by its high frequency at 40kHz and a smaller amplitude can be observed on the 230V, 50Hz mains voltage waveform.

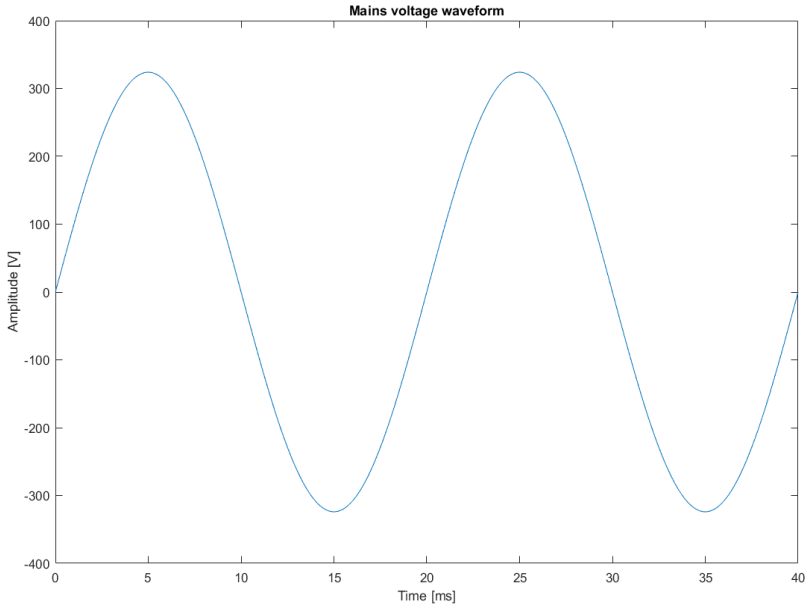

Figure 2.3 Mains voltage waveform

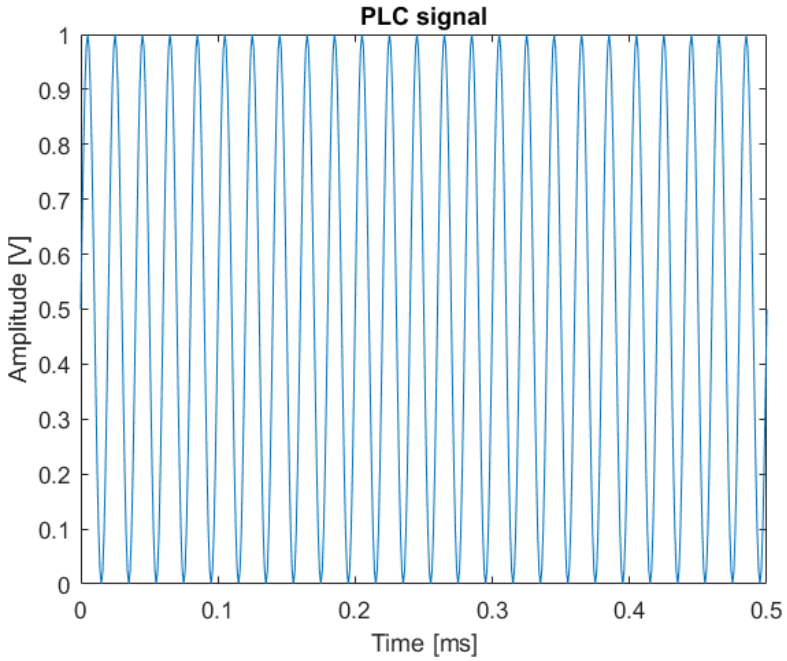

Figure 2.4 PLC signal waveform

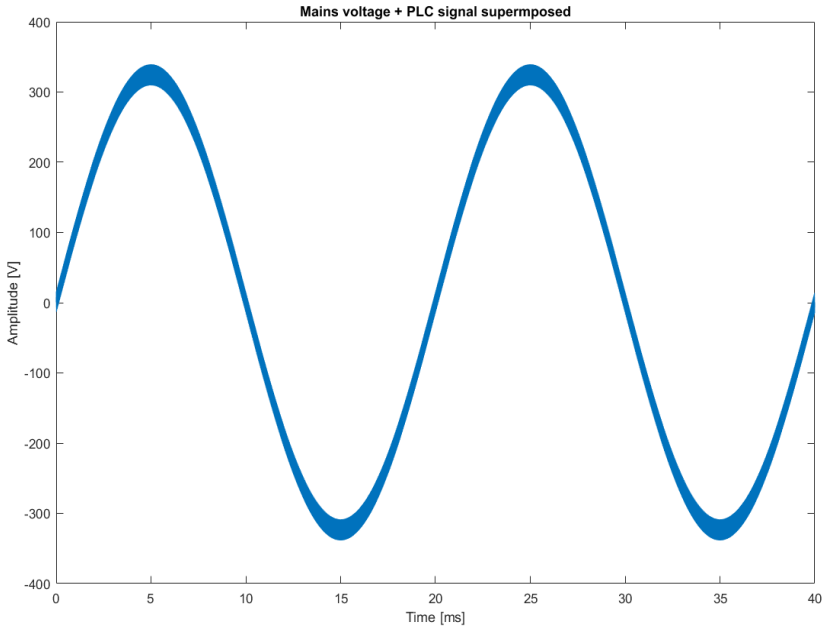

Figure 2.5 Mains voltage waveform with PLC signal waveform superimposed

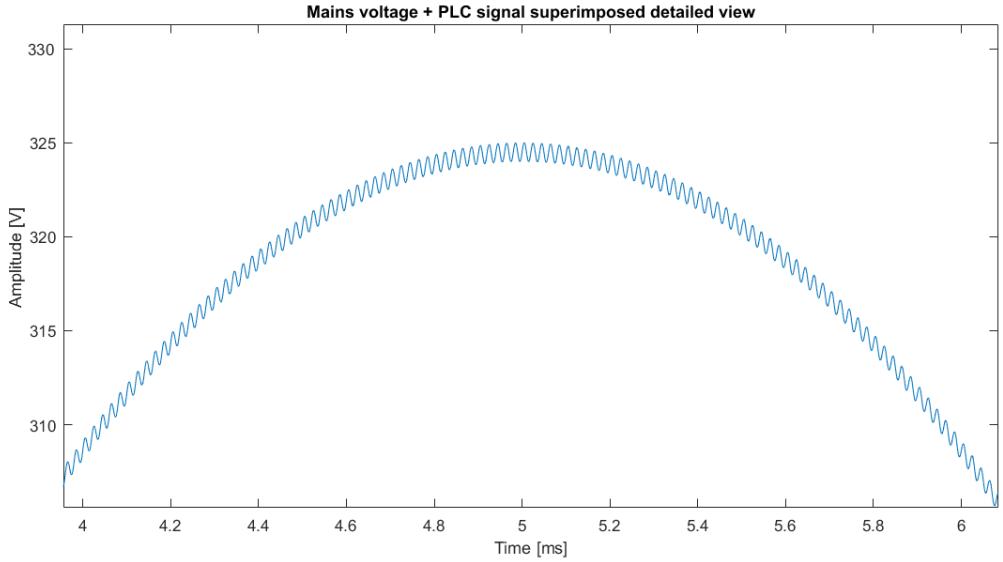

Figure 2.6 Mains voltage waveform with PLC signal waveform superimposed detailed view

2.2 PLC Channel

PLC makes use of already-existing power lines as a communication channel that offers a wide range of advantages thanks to the efficient use of this extensive infrastructure. These benefits include broad coverage, reduced deployment costs, independence from other communication infrastructures developed for other purposes (such as mobile data communication) as well as less environmental impact.

However using the existing electrical grid poses numerous challenges such as uncontrollable network topology, noise, attenuation and low impedances.

Figure 2.7 illustrates the simplified PLC channel model, which represents the behaviour of data transmission over electrical power lines. This model typically encompasses essential elements that describe the characteristics and components involved in PLC communication:

- Channel Response: This describes how the PLC signals propagate through the power lines. The channel response accounts for the attenuation, distortion, and delays introduced by the power lines. It characterizes how the signal strength and phase change with frequency and distance. In simple models, this may be represented as a frequency-dependent transfer function.
- Noise: Noise in the PLC channel is typically due to various electrical interferences and can degrade the quality of the transmitted signal. This noise can be thermal (thermal noise), impulsive (caused by electrical devices turning on/off), or due to external electromagnetic interference. The noise is usually represented as an additive component that affects the received signal.
- TX End: This part of the model represents the signal source, modulation techniques, and encoding methods used to transmit data over the power line. The TX end shapes the data signal before it is injected into the power line.
- RX End: The RX end represents the receiver equipment. It includes components for signal detection, demodulation, decoding, and error correction. The receiver's job is to extract the transmitted data from the received signal, accounting for noise and channel distortion.

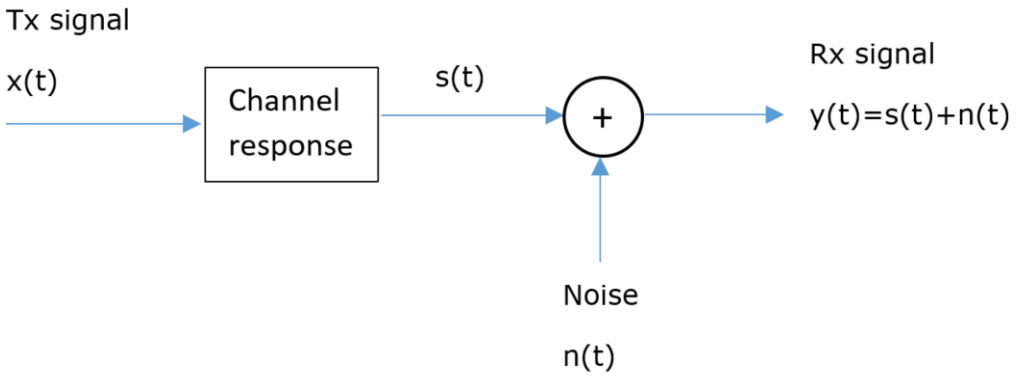

Figure 2.7 PLC channel simplified model

This section summarizes PLC channel characteristic with emphasis on CE present in the electrical grid, CE standardization gaps, signal attenuation and access impedance.

2.2.1 Power line noise

Noise in PLC systems refers to unwanted or undesirable signals that disrupt or interfere with the communication between PLC transceivers. These noise signals can originate from various sources and manifest as electrical disturbances or interference in the power lines or communication medium.

The presence of noise can degrade the quality of the transmitted signals, leading to errors or loss of data integrity. This is a common challenge in PLC systems, and addressing and mitigating noise is a crucial aspect of ensuring reliable and efficient communication between PLC devices. Techniques like signal filtering, error correction, and adaptive modulation are often employed to combat the effects of noise and maintain the integrity of the communication.

This noise arises from spurious CE emitted by electrical appliances (loads), which are directly connected to the electrical power system such as: SMPS, phase fired controllers, motor driven appliances, high frequency electronic equipment and inverters [28], [29]. The constant on and off switching of the electrical loads leads to varying noise levels over time. The total noise at a specific electrical connection results from the combination of unwanted emissions propagated by various noise sources connected to electrical grid [29], [30].

Power-line noise can be classified into five different types all of which are listed below and detailed throughout this section:

- Coloured background noise.
- Narrowband noise.
- Periodic impulsive noise synchronous to mains frequency.
- Periodic impulsive noise asynchronous to mains frequency. asynchronous impulsive noise [19], [31].

Coloured background noise: This type of noise cannot be accurately modelled as additive AWGN throughout the entire NB-PLC frequency band. It is better described as coloured noise with a decreasing power spectral density. The lowest frequency bands of the NB-PLC spectrum experience the most interference from this background noise [31].

Figure 2.8 shows a normalized signal, which appears as a waveform or data transmission, with the presence of both AWGN and colored noise. When generating in Matlab the figure depicting this type of noise in Figure 2.8, I considered the following factors:

- AWGN noise is characterized by its statistical properties. It is "additive" because it is added to the original signal, "white" because it has a constant PSD across all frequencies, and "Gaussian" because its amplitude follows a Gaussian distribution. This noise introduces randomness and interference into the signal, which can affect its RSSI and SNR.
- Additionally, there is "colored noise" superimposed on the signal. Colored noise is different from white noise in that its power spectral density varies with frequency, meaning it has more power at some frequencies than others. This noise can be generated in various ways and can introduce specific frequency-dependent distortions or artifacts to the signal.
- Normalizing all the values in this context likely means that the amplitudes of the signal and the noise have been adjusted to a common reference level, making it easier to analyze and compare their impact on the signal. The normalization helps ensure that the signal and noise can be appropriately balanced and evaluated.

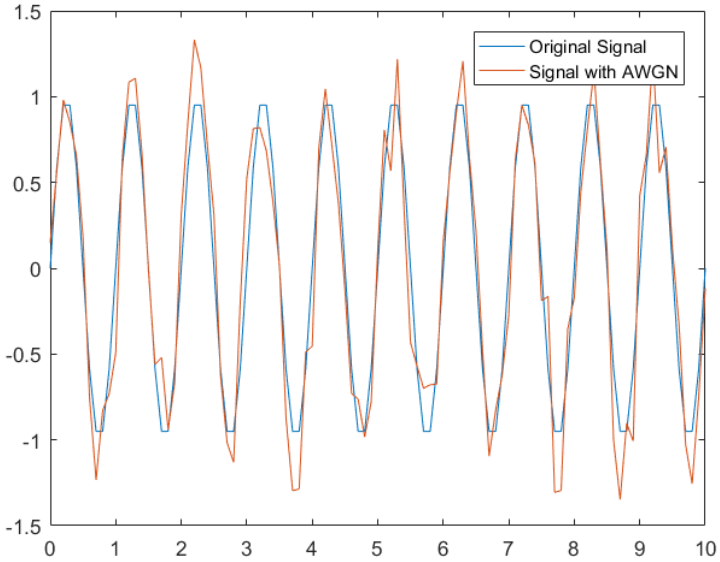

Figure 2.8 AWGN colored noise superimposed on signal

Narrowband noise: This type of noise in PLC systems include continuous-tone jammers and amateur radio devices emitting spurious signals that occupy an extremely narrow part of the PLC spectrum. PLC systems employing single-frequency carriers for data modulation can be particularly affected by the significant noise power at these spectral locations [31].

The illustration in Figure 2.9 helps visualize the challenge posed by narrowband noise in PLC systems. It highlights how spurious signals at specific frequencies can potentially disrupt communication in PLC systems, particularly those using single-frequency carriers. The SFDR value serves as a quantitative measure of the system's ability to handle these spurious emissions while maintaining a strong and reliable carrier signal. Figure 2.9 represents the PLC spectrum with a carrier f_c=9.8 kHz and spurious emissions at f=14.7 kHz, the spurious free dynamic range is SFDR=80.13 dB. Below I provide a comprehensive breakdown of the components depicted in Figure 2.9:

- Carrier Frequency (fc=9.8 kHz): The central element of the spectrum is the carrier signal with a frequency of 9.8 kHz. This carrier is where the primary data transmission occurs in the PLC system.
- Spurious Emissions at f=14.7 kHz: Surrounding the carrier signal, one can observe additional signals or noise at a frequency of 14.7 kHz. These signals represent spurious emissions. Spurious emissions are unwanted or unintended signals that are emitted at frequencies other than the primary carrier frequency. In this case, they occupy a narrow part of the PLC spectrum. These spurious signals can be caused by various sources, including continuous-tone jammers and amateur radio devices. These emissions are particularly problematic for PLC systems employing single-frequency carriers for data modulation.
- Spurious Free Dynamic Range (SFDR=80.13 dB): This figure also provides a key metric to assess the system's performance in the presence of narrowband noise. The Spurious Free Dynamic Range (SFDR) is a measure of how much

stronger the desired signal (the carrier) is compared to the unwanted spurious signals. In this case, the SFDR is specified as 80.13 dB, indicating a substantial dynamic range for the carrier signal compared to the spurious emissions.

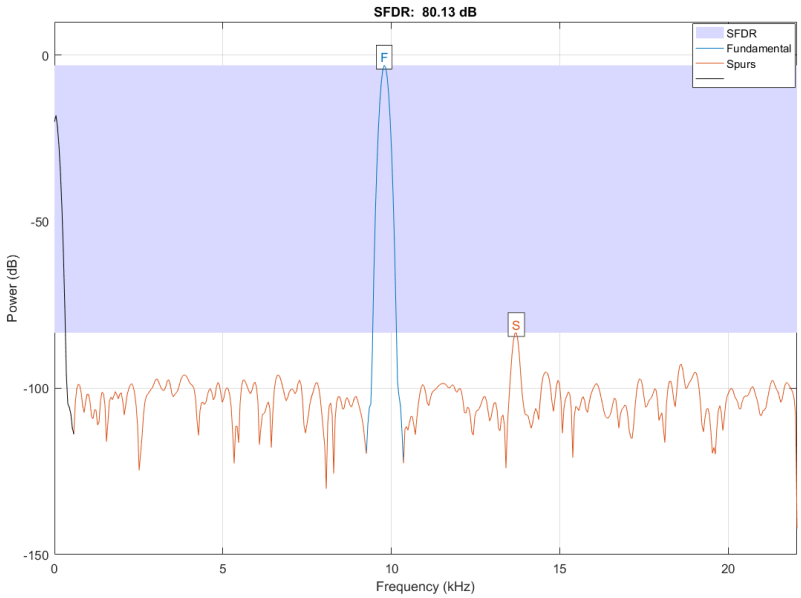

Figure 2.9 PLC spectrum with spurious emissions

Periodic impulsive noise synchronous to mains frequency: This noise is caused by the switching actions of silicon-controlled rectifiers and AC to DC rectifier circuits found in many electrical appliances. It occurs at the mains frequency or its integer multiples and is synchronous with the variations of the AC mains voltage.

Figure 2.10 serves as an example to visually represent this periodic impulsive noise that is synchronized with the mains sinusoidal waveform [31]. It helps in understanding the challenges and potential interference that can arise in PLC systems due to this type of noise, especially when it coincides with the timing of the mains voltage variations. Characteristics of the Signal depicted in Figure 2.10 are presented below:

- Periodic Nature: The noise follows a recurring pattern or cycle, and it synchronizes with the mains frequency. In other words, it occurs at the same frequency as the AC mains supply, which is typically 50Hz or 60Hz depending on the region. Furthermore, it can also manifest at integer multiples of the mains frequency.
- Origin: The primary source of this noise is the operation of electrical appliances containing silicon-controlled rectifiers and AC to DC rectifier circuits. These components are essential in converting AC to DC in many devices. Their switching actions create disturbances in the electrical signal, leading to the appearance of this impulsive noise.
- Synchronization: One main aspect of this noise is its synchronization with the variations of the AC mains voltage. As the AC voltage goes through its sinusoidal waveform, the noise occurs at specific points in the waveform, often associated with the switching actions of the rectifiers. This

synchronization can introduce regular impulses in the mains signal, potentially affecting the quality of PLC.

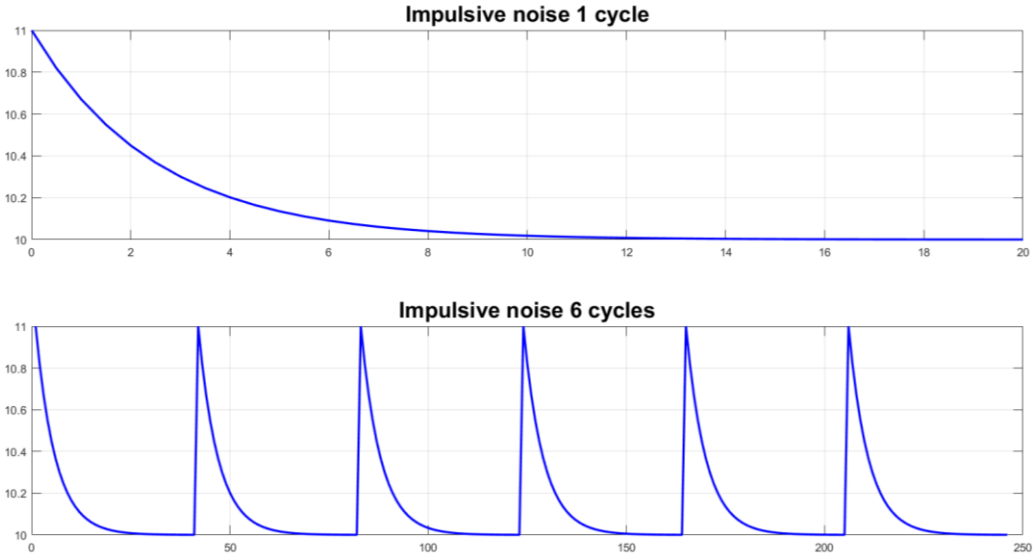

Figure 2.10 Periodic impulsive noise

Periodic impulsive noise asynchronous to mains frequency: The majority of electronic devices in use today, including those equipped with SMPSs, can inadvertently generate a specific type of noise referred to as "asynchronous periodic impulsive noise". Unlike its synchronous counterpart, this type of noise does not synchronize to the mains frequency cycle but occurs at times related to switching cycle.

Asynchronous periodic impulsive noise shares the same impulsive shape as a single period of the synchronous periodic impulsive noise. This impulsive shape results from the high-frequency switching actions inherent to SMPSs and other electronic components. These high-frequency periodic switching events, characteristic of SMPSs, introduce disturbances in the mains, leading to the formation of impulsive noise patterns [31].

The impact of asynchronous periodic impulsive noise on PLC systems should not be underestimated. These disturbances can disrupt PLC communication, introducing irregular interference into the power line. Consequently, data integrity and communication reliability may be compromised. Addressing and mitigating this type of noise are necessary to ensure the dependable operation of PLC-based communication systems amid the presence of various electronic devices.

Asynchronous impulsive noise: This noise results from the sudden connection and disconnection of electrical loads on the power line. This type of switching events generate intermittent CE, leading to PLC error bursts. Inductive devices and universal motors commonly found in household appliances are primary sources of aperiodic impulsive noise. When these devices are turned on or off, they generate electromagnetic interference that affects PLC. Examples include refrigerators, washing machines, and vacuum cleaners. The inductive nature of these devices, such as the coils in electric motors, creates sudden changes in current and voltage when they are switched [31].

Figure 2.11 is a graphical representation of asynchronous impulsive noise that has the following key properties:

- Aperiodic characteristic: Aperiodic impulsive noise does not follow a regular or periodic pattern. It is unpredictable in its occurrence, happening as electrical loads are activated or deactivated. This irregularity can make it challenging to anticipate and mitigate.
- Intermittent Noise Effects: Aperiodic impulsive noise introduces intermittent disturbances into the power line. These disturbances can lead to bursts of errors or data corruption in PLC systems. The irregularity of these noise bursts can be particularly problematic for reliable data transmission.

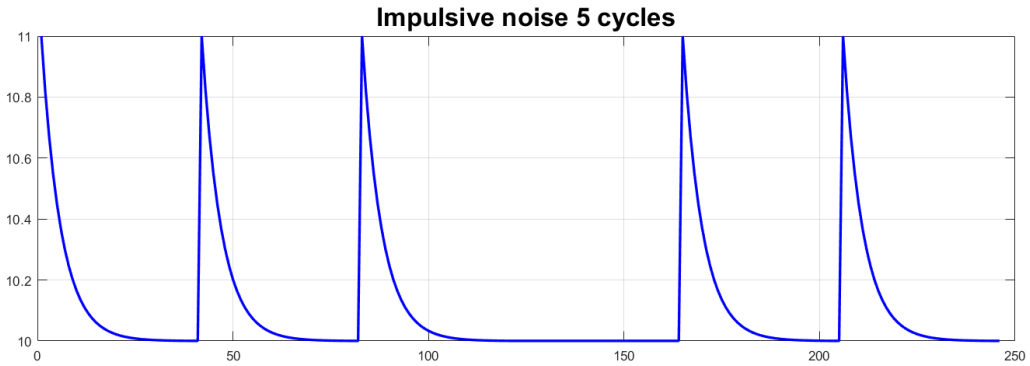

Figure 2.11 Aperiodic impulsive noise

Figure 2.12 presents the time domain representation of a sinusoidal signal in its original form, along with the same sinusoidal signal superimposed with asynchronous impulsive noise. All values in this figure have been normalized thus are dimensionless.

- Original Sinus Signal: This represents a clean and continuous sinusoidal waveform. In many cases, such a waveform is used as the carrier signal for data transmission in PLC systems. The sinusoidal waveform is characterized by its regular and predictable oscillations, making it suitable for data encoding.
- Superimposed Asynchronous Impulsive Noise: This portion of the figure depicts how aperiodic impulsive noise, which occurs due to the connection and disconnection of electrical loads, affects the original sinus signal. The superimposed noise introduces irregular disturbances, resulting in deviations from the clean sinusoidal waveform. These deviations represent the impact of asynchronous impulsive noise on PLC communication.
- The normalized values in Figure 2.12 allow for a clear visual representation of how asynchronous impulsive noise can disrupt a sinusoidal signal commonly used in PLC systems.

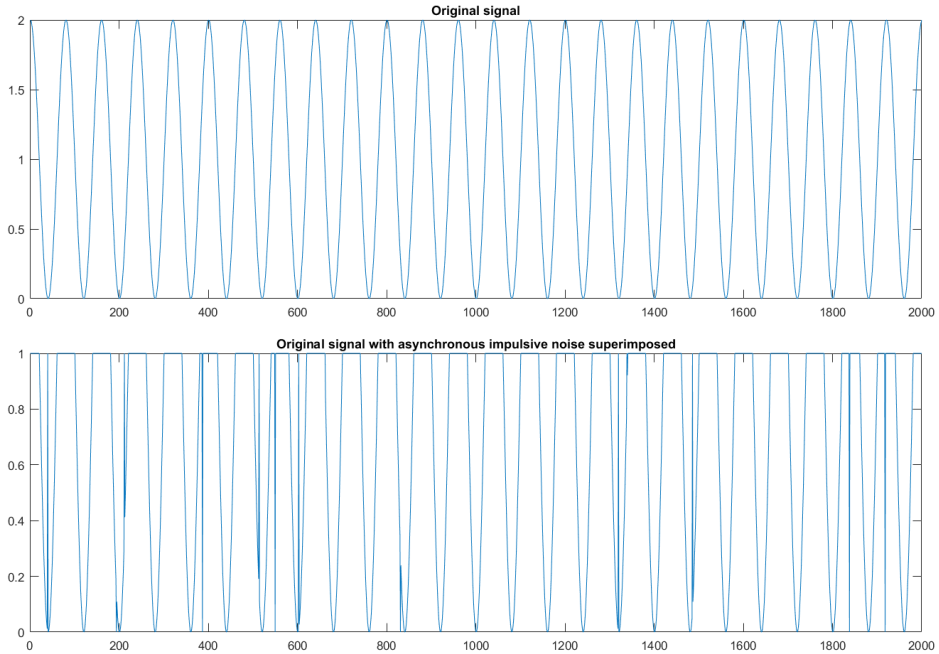

Figure 2.12 Asynchronous impulsive noise in PLC spectrum

The presence of noise, particularly continuous background noise, continuous narrowband noise, and synchronous periodic impulsive noise, can negatively affect NB-PLC communication performance. Additionally, EMC standardization flaws allow for interference between NB-PLC and multiple devices.

In Table 2.1 I have provided the summarized properties and sources of noise types in a side-by-side comparison, allowing for an easy comparison between noise types and the acquisition of a comprehensive understanding of their properties and sources in a structured and organized manner. Usually in the power line all types of noise are present and have a cumulative effect upon PLC.

Table 2.1 Power line noise types and key characteristic [19], [31]

Noise name	Properties	Source
Colored background noise	Low PSD, varying with frequency	Addition of various low power noise sources
Narrow-band noise	Sinusoidal waveform shape Amplitude modulated Time variable	Radio Broadcast
Periodic impulsive noise asynchronous to the mains frequency	Frequency spectrum is spatially shaped according to the impulse repetition rate ranging from 5 µs to 20 µs	SMPSs

Periodic impulsive noise synchronous to the mains frequency	PSD decreasing with frequency Impulse shape with kHz range occurrence rate	Synchronous rectifiers and phase fired controllers
Asynchronous impulsive noise	High PSD which can reach 50dB Shaped as impulses with a repetition rate in the range of kHz to MHz Occurring randomly	Transients in the power line generated by switching

2.2.2 Standardization gaps and SMPS CE

The CENELEC A, B, C, and D bands (with a frequency band of 3 kHz-148.5 kHz) are used by NB-PLC throughout Europe. However, this utilization is affected by gaps in the standardization of EMC CE and EMI from devices. These aspects have become the focal point of research articles [5]–[11], [13]–[16], [32] and have garnered the attention of both CISPR and IEC. To address these shortcomings, efforts are now being made, including modifications to standards like CISPR 16-1-2, CISPR 32, and a selection of IEC standards.

It has been observed that CE limits within the 3–148.5 kHz frequency band are explicitly specified in only a few instances: the NB-PLC specific standard [27], lighting equipment [33], and a single domestic appliance category (inductive ovens) covered by the EMC standard [34]. Figure 2.13 shows the IEC EMC standards that apply to the majority of mains-powered equipment in Europe as well as the frequency bands they cover. The majority of these standards establish emission limits above 150 kHz.

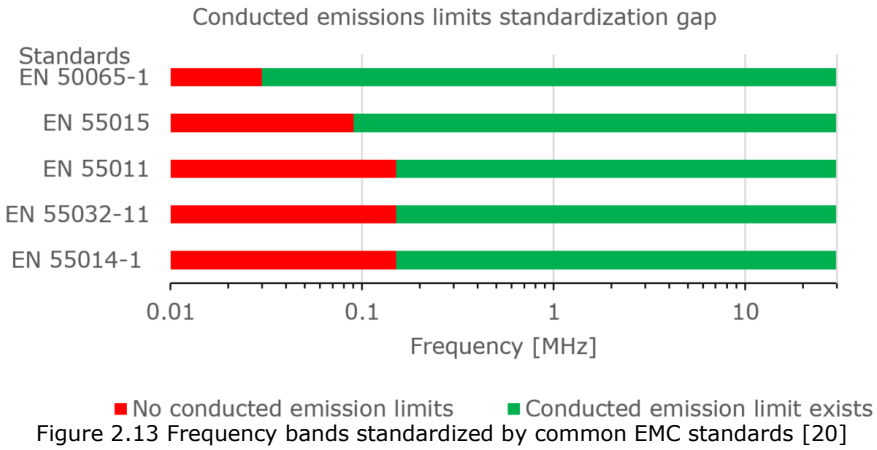

Figure 2.13 Frequency bands standardized by common EMC standards [20]

SMPSs and inverters that are connected to the electricity grid frequently use switching frequencies up to 150 kHz. These devices thus generate CE that affect NB-PLC [32], [35]. A number of important aspects justify the usage of SMPS switching frequencies below 150 kHz [36]:

- Efficiency: The total efficiency of the SMPS increases when switching frequencies are reduced. Lower operating frequencies increase conversion

efficiency and decrease power dissipation in power semiconductors like transistors and diodes by reducing switching losses.

- EMC: Emissions increase due to higher switching frequencies with lower rise and fall times generating harmonics. The lack of or more relaxed emission limits below 150 kHz also contributes to the preference for lower frequencies.
- Thermal considerations: With a lower switching frequency, the components have more time between switching cycles to dissipate the heat produced by the switching components in SMPS.
- Component choice: The losses and dimensions of passive components employed in SMPS tend to rise as the frequency increases. Therefore, utilizing lower frequencies can help mitigate these limitations.

2.2.3 Power line attenuation

The attenuation of PLC signal due to power cables varies significantly with cable type, length, and signal frequency. This characteristic is primarily influenced by dielectric losses in the cable insulation and has a significant impact on signal propagation within power line networks. Additionally, the various cable types in existing installations and devices connected lead to multiple reflections in the PLC signal propagation path, caused by changes in network access impedance. Experimental results have proven that it is possible to achieve with NB-PLC protocols point to point distances of up to 1.5km in a 3-wire LV power line network [37]. The characteristics of power cables in relation to PLC signal propagation within power line networks is described as follows:

Low-Pass Characteristic of Power Cables: The low-pass characteristic of power cables varies significantly depending on factors such as cable type, length, and signal frequency. This characteristic is primarily influenced by dielectric losses in the cable insulation, and as a result, it significantly impacts signal propagation in power line networks [38].

Impact of Cable Types and Connected Loads: Moreover, the diversity of cable models in the electrical grid and variations in loads lead to multiple reflections in the PLC signal propagation path. These reflections occur due to changes in network access impedance, consequently affecting overall signal quality and performance.

Signal Attenuation and Electrical Phases: In addition, the attenuation of signals in PLC can vary based on whether transceivers are connected to the same electrical phase or different phases [39]. Even when connected to the same phase, PLC links might experience unequal attenuation levels due to varying circuit loading between nodes on that phase [40].

Narrowband Frequency-Selective Fading: PLC signals are susceptible to narrowband frequency-selective fading, resulting in notches in the PLC channel response at specific frequencies. These notches can be caused by factors such as reactive loading, multipath propagation, or standing waves on the power line. Additionally, excessive fading at the carrier frequency in single-carrier PLC systems can significantly degrade system performance.

Time Domain Effects: In the time domain, it has been reported that signals experience periodic fading attributed to loads such as DC supplies without transformers [40]. For instance, residential buildings typically experience lower attenuation compared to high-rise buildings. This difference is likely due to longer signal distances and increased circuit loading in high-rise buildings.

Variability in PLC Signal Attenuation: Consequently, the attenuation of PLC signals can vary significantly across different buildings due to differences in circuit

loading and electrical system characteristics [40]. As a result, deploying robust PLC signalling, error-correction, and access-control schemes becomes essential for maintaining reliable communication.

Careful consideration of trade-offs between noise and attenuation levels is necessary when selecting PLC carrier frequencies. It is important to note that noise levels typically decrease with increasing frequency, while attenuation tends to increase.

2.2.4 PLC access impedance

The RSSI is reduced by impedance mismatch in the electrical grid, which is brought on by the existence of diverse cable kinds and lengths and varied types of switched-on and switched-off loads in both residential and industrial settings. In turn, this causes the transmission range to be reduced [41], the data rate to noticeably drop, and, in the worst situation, connection between devices to be lost. If impedance fluctuates within the PLC transmission channel's frequency range in addition to the consequences already discussed, the effect of impedance may be considerably more significant.

Figure 2.14 serves as a visual representation of the impact of power line impedance on PLC signal quality. The changes in grid impedance inside the PLC transmission channel cause considerable fluctuations in the received by the receiver. As a result, under such circumstances, communication quality may noticeably deteriorate. Predicting the effects of this kind of deterioration is difficult since the impact is made worse by the time-varying nature of the grid impedance [42], [43]. The plots from Figure 2.14 are represented on the same axis for a better view of the impact of power line impedance upon PLC signal and are described as follows:

- PLC TX (Unaffected) and PLC RX (Affected by Line Impedance two frequency spectrums are depicted on the same axis. The first spectrum represents the transmitted PLC signal (TX) before it is affected by the power line's impedance, as measured at the transmitter end. This spectrum is labeled as "PLC TX (Unaffected)". The second spectrum represents the RX PLC signal after it has been influenced by the power line's impedance, as measured at the receiving end. This spectrum is labeled as "PLC RX (Affected by Line Impedance).
- Alongside the two frequency spectrums, an impedance measurement of the power line is also presented. This measurement indicates the electrical impedance characteristics of the power line within the PLC transmission channel. It helps visualize how the impedance values vary with respect to different frequencies within the PLC signal's frequency range together with the impact on the RX signal level.

The PLC access impedance topic is continued in section 3.2.1 as part of broader discussion regarding measurement setups for PLC signals in a controlled environment emulating the real power line.

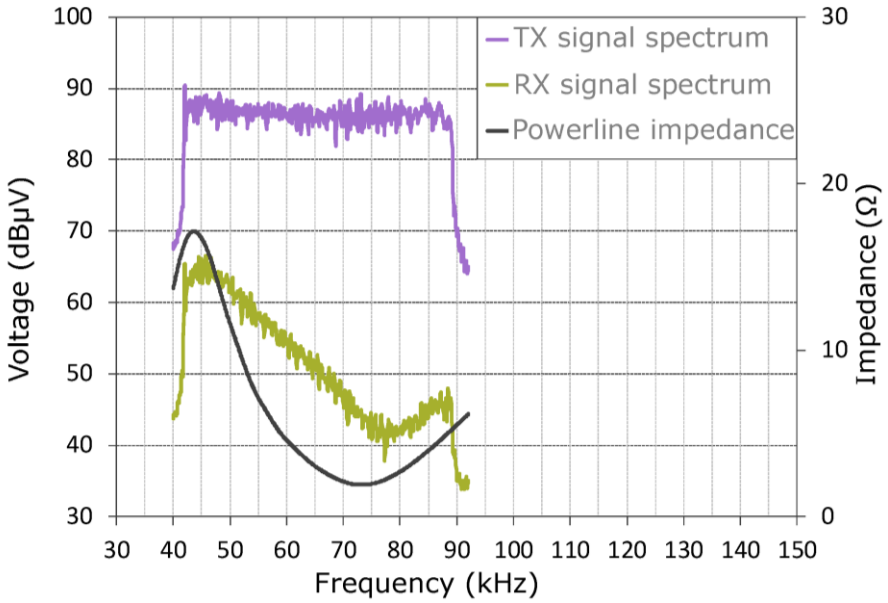

Figure 2.14 Power line impedance influence on PLC signal frequency spectrum [44]

2.3 The history of PLC

The concept of using the power lines as communications medium occurred to multiple persons in various locations around the globe at the beginning of the 20th century. It seems that from technical point of view the concept of transmitting multiple voice messages over a singular telephony circuit utilizing multiple carrier frequencies has been the trigger of using the power line for transmitting voice messages [45]. The below notable events, sorted in chronological event have been identified to be a part of the genesis of PLC:

- In 1910-1911, Major George Squier of the US Army Signal Corps showed the use of a carrier-frequency technology to transmit several telephone channels over a single telephone circuit [46].
- The Imperial Japanese Electro-Technical Laboratory carried first commercial usage of telephony over power lines in 1918 in Japan on a 144km long power line owned by Kinogawa Hydro-Electric Co. in Tokyo. Subsequently, commercial operation commenced in December 1918, utilizing the Fuji Hydro-Electric Co.'s 22kV power line [47].
- By the late 1920s, telephony over power lines had become extensively adopted across Europe and the United States. According to a 1929 estimate mentioned in an Austrian journal, approximately 1000 systems had been installed in Europe and the United States by that time, with a majority of the European installations concentrated in Germany [48].

With the help of Brown's article [49] I have extracted a list of notable events that served as basis for the usage of PLC in metering applications:

- As far back as 1838, Edward Davy introduced the concept of remote electricity supply metering. His proposal aimed to monitor the voltage levels of batteries at unmanned locations along the London - Liverpool telegraph system.

- Joseph Routin and C.E.L. Brown, hailing from Zurich, Switzerland, obtained British Patent No. 24833 for their powerline signalling electricity meter in the year 1897.
- The power line signalling electricity meter was followed by Chester Thoradson's patent in 1905. Developed in 1902, this remote reading system for electricity meters employs an additional signaling wire. However, despite its potential, the scheme did not gain commercial traction due to inadequate cost benefits, leading to its discontinuation.
- In 1913, the production of automatic electromechanical meter repeaters began, and in 1927, the patent for using vacuum tubes in metering was granted. In 1936, the indirectly heated vacuum tubes eliminated the need for batteries , while in 1947, the miniature vacuum tubes, and later in 1960, the transistor, significantly reduced the meter's size [50].
- By 1967, integrated circuits became prevalent, and by 1980, microprocessors started appearing worldwide in various applications. Towards the late 1980s and early 1990s, there were proposals for relatively advanced error control coding, along with their implementation on wide scale and relatively accessible microcontrollers within the hardware of a PLC modem.

2.4 PLC for electric power grid applications

The commercial usage of PLC in the electric power grid can be split into three generations [51]:

- First Generation are represented by RCSs which provide unidirectional communication for centralized load management and peak consumption curve flattening in power distribution grids.
- Second Generation are composed out of low data rate PLC systems which were proposed in the 1990s, AMR systems were deployed based on this technology.
- Third Generation PLC devices used for electric power grid applications are OFDM-based systems with significantly higher data rates with applications in SGs, DA, and AMI.

2.4.1 First generation PLC systems

In the 1950s, companies like Landis & Gyr [51] and Brown Boveri & Cie [50], [52] developed RCSs for load management in electrical grids, specifically to mitigate load peaks. These systems have have seen extensive deployment and continue to be used in various European countries [53], [54] as well as in other countries around the globe [55] for load control and operational purposes, even when other telecontrol links are unavailable.

Ripple control operates by injecting low frequency signals (audio frequency range) in the MV grid. Frequencies are carefully chosen to avoid harmonics of the mains frequency, typically ranging from 0.15 kHz to 1.35 kHz. Lower frequencies below 0.25 kHz are favoured for longer distances being lesser impacted by attenuation [56]. Different distribution grid operators utilize distinct frequencies to prevent interference. Depending on the mains voltage level at the signal coupling point, the injected signal can have a strength of up to 5% of the mains voltage level, which corresponds to transmission power of up to 150 kVA.

For a better and pragmatic overview, I have listed the key characteristics regarding RCSs:

- Signal coupled in the MV lines can easily pass via MV/ LV transformers, allowing them to reach all RCS receiving apparatus linked to the LV grid over great distances because of the ripple control signal's low frequency and high power.
- The distribution grid operator is the only source of transmission. However, supervisory receivers monitor the setup and communicate with the transmitter via other communication channels (such copper cables) to deliver acknowledgement signals.
- The system's telegrams are made up of a series of carrier pulses. Data is sent at a rate of around 10 b/s because bits are encoded as on off keying pulses lasting several hundred milliseconds.
- Telegrams, which last several seconds to minutes, convey messages with a size of about 50 bits. Receivers decipher the communicated sequence and turn on or off their electric relays in accordance, managing appliances like hot water boilers and electric heaters.
- More recent systems include advanced features including remote receiver timer programming, error checking, and message fragmentation. Although the ripple control theory is widely used, system providers own the individual designs.

RCSs are commonly employed by distribution utilities for load peak limitation. When the total power consumption approaches a preconfigured limit, specific loads (e.g., HVAC, water boilers, heat storage tanks) are switched off following a pre-programmed priority list for a configurable maximum duration.

Additionally, ripple control is used to transmit orders for time-based tariff switching to the meters. The typical RCS deployed in the power grid is represented in Figure 2.15 and consists out of the following elements [57]:

- The core of the RCS system is the Broadcast Center connected to the HV grid, serving as the central control hub. It comprised out of the Control Unit and a central modem. The Control Unit is responsible for generating control signals, while the central modem facilitates communication with other components in the system.
- At the MV grid level, there are two critical components: The first one is the local Modem, which acts as an intermediary for data communication, ensuring connectivity between the Broadcast Centre and local devices. The second is the Local Control Unit, which receives and interprets control signals from the Broadcast Centre and can relay these signals to the devices on the MV and LV grid. Third component is the Line Coupler, which is designed to efficiently transmit control signals generated by the Control Unit from the Broadcast Centre to the MV grid.
- In the LV Grid, the primary role of Ripple Control Receivers is to govern an array of load control devices by executing received commands, typically involving the activation or deactivation of devices like heaters, boilers, and lighting. This capability allows for remote and automated load management within the LV grid, leading to optimized power distribution and a responsive approach to shifting power demands.

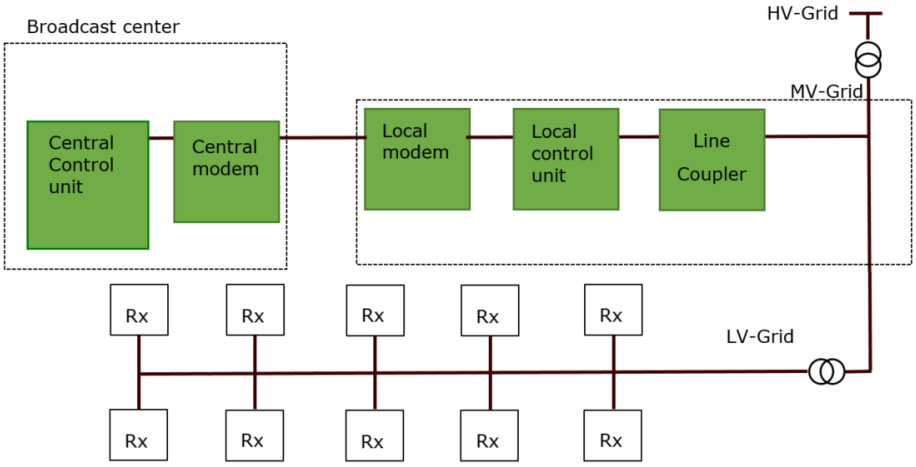

Figure 2.15 RCS installation in the power grid

2.4.2 Second generation PLC systems

RCSs are unable to offer the two-way communication that DA applications, AMR, and AMI demand. There is a need for more increased bandwidth thus higher carrier frequencies are used, at the expense of decreased communication range.

However, challenges arise due to the utilization of higher signal frequencies and the limited transmit signal levels from consumer end devices in the LV grid. These factors make it difficult for signals to pass through MV/ LV transformers. Consequently, a network architecture is proposed, consisting of a backbone network, possibly utilizing MV-PLC, to DC situated at the MV/ LV substations. These DCs then enable LV-PLC communication to the SMs or devices attached to the specific LV grid branch. At the beginning of the 2000s, the DCs started using mobile data or Ethernet connection to communicate with the backbone.

CENELEC issued the European Norm EN 50065-1 [27] in 1991, which restricts the maximum PLC output level in the range 120 dBµV $\leq V_{PLC} \leq$ 134 dBµV as well as the frequency bands for MV/ LV PLC.

Figure 2.16 offers a comprehensive and visually accessible reference of the frequency spectrum allocation in Europe for NB-PLC by providing the following information: frequency bands, regulatory information, and designated usage [17], [20].

Frequency	3 kHz	95 kHz	125 kHz	140 kHz	148.5 kHz
Frequency band	CENELEC-A	CENELEC-B	CENELEC-C	CENELEC-D	
Brief description of the allocated frequency spectrum	Electricity distribution companies and their licensees.	Consumer use without access protocol.	Consumer use, with EN 50065-1 compliant CSMA access	Consumer use without access protocol.	

Figure 2.16 NB-PLC Frequency Spectrum allocation in Europe

The CENELEC A-band is specifically allocated for communications of electricity distribution companies for DA, AMR and AMI, while the other bands are intended for

consumer-site applications, for example, for household devices. The standards define output power requirements of either 1 W or 5 W and define spectral masks for these PLC devices communicating beyond 17.5 kHz.

Since the 1980s, several bidirectional MV/ LV PLC technologies operating at frequencies up to 150 kHz have been developed and implemented [58], [59]. Some of these solutions remained proprietary [60], [61], while others are IEC compliant. The modulation used by the second generation systems is SFSK and FSK which are standardized by IEC 61334-5-1 [62] and IEC 61334-5-2 [63].

One of the most widespread 2nd generation, PLC systems utilize two carriers at 63.3 kHz and 74.5 kHz, which are FSK-modulated with a data rate of up to 1.2 Kb/s. The wide separation of the carrier frequencies allows diversity reception, improving performance in AMR, especially in Italy, France and Sweden, where a large-scale implementation was performed [64], [65].

The standardization process turned IEC 61334-5-1 [62] into an International Standard, IEC 61334-5-2 [63] and IEC 61334-5-5 [66] have remained Technical Specifications. The FSK system by ENEL of Italy is included in IEC 61334-5-2 [63], using a carrier at f=82 kHz for LV and f=72 kHz for LV, FSK-modulated achieving a 600 bps on LV, and 1200 bps on MV [67]. ENEL has made significant strides in expanding its infrastructure for remotely managing meters, with substantial expansion efforts beginning in the early 1990s and reaching completion by the early 2000s [67]–[69].

Two PHY layer profiles with different modulations have been proposed (not deployed in mass-rollouts) by ABB and have been included in the below technical specifications [70]:

- IEC TS 61334-5-4:2001 describes Multiple-carrier Modulation with DPSK for PLC on MV [71].
- IEC TS 61334-5-5:2001 describes Spread Spectrum Fast Frequency Hopping with applications for PLC on LV [66].

The expansion of SGs necessitates greater access to energy consumption data from users for effectively managing the grid. In this regard, DLMS/COSEM serves as a robust protocol that standardizes communication between SMs and utility backbone servers [72]. It achieves this by seamlessly integrating device models from various makers. The DLMS/ COSEM smart metering protocol is versatile and not limited to electricity metering; it extends its applicability to utilities such as gas, water, and heat.

This comprehensive set of standards is developed and maintained by the DLMS User Association and has received adoption by the International IEC as part of the IEC 62056 series of standards.

While OBIS is in charge of naming and recognizing objects within the system, COSEM acts as the universal object model applicable to a variety of applications. The application layer protocol known as DLMS facilitates the conversion of data into messages.

Figure 2.17 offers a comprehensive representation of the DLMS/ COSEM communication model and its various communication options and corresponding PHY technologies. It visually demonstrates how data is structured, how communication protocols are applied, and how information flows through different layers of the model. Newer communication protocols are available but I have focused on the ones that were used in parallel with second generation PLC systems [69], [73]. The key components and layers of the DLMS/ COSEM communication model diagram shown in Figure 2.17 are:

- The data model is the top layer of the diagram representing the DLMS/ COSEM data model, which includes interface classes and object models. This layer defines how data is organized and structured for communication.
- The Application layer handles the interpretation of data and the execution of various DLMS/ COSEM services.
- The data link layer, represented beneath the application layer, includes the use of HDLC as the communication protocol. It manages data framing and error detection.

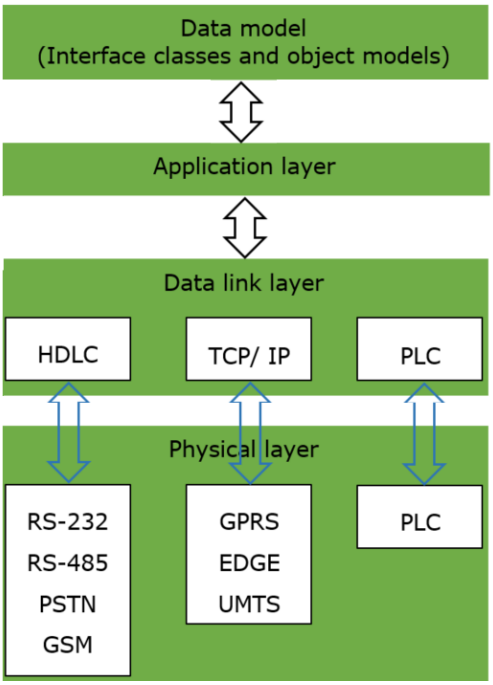

Figure 2.17 DLMS/ COSEM communication model

Figure 2.18 presents the architecture of a SG using NB-PLC as last mile communication protocol between LV-Grid connected SMs and DC as well as internet or MV-PLC for the connection between DCs and central system. Internet connectivity is the preferred option for connecting DCs with PLC and central system. This preference arises from several factors such as high number of SM using PLC (meaning that it might be a bottleneck), low data rate of MV-PLC and expensive PLC coupling implementation. As basis for creating Figure 2.18 the following references have been used [74]–[77]. The SG architecture presented in Figure 2.18 includes the following key elements:

- At the bottom of the figure, there are LV grid-connected SMs represented as individual devices. These meters are deployed at the customer premises and are equipped with NB-PLC communication capabilities.
- Positioned centrally within the figure is the DC, which acts as an intermediary between LV grid-connected SMs and the higher-level communication networks. The DC is equipped to communicate with SMs using NB-PLC.

- Above the LV grid-connected components, there are two communication pathway variants between DC and backbone: MV-PLC and internet.

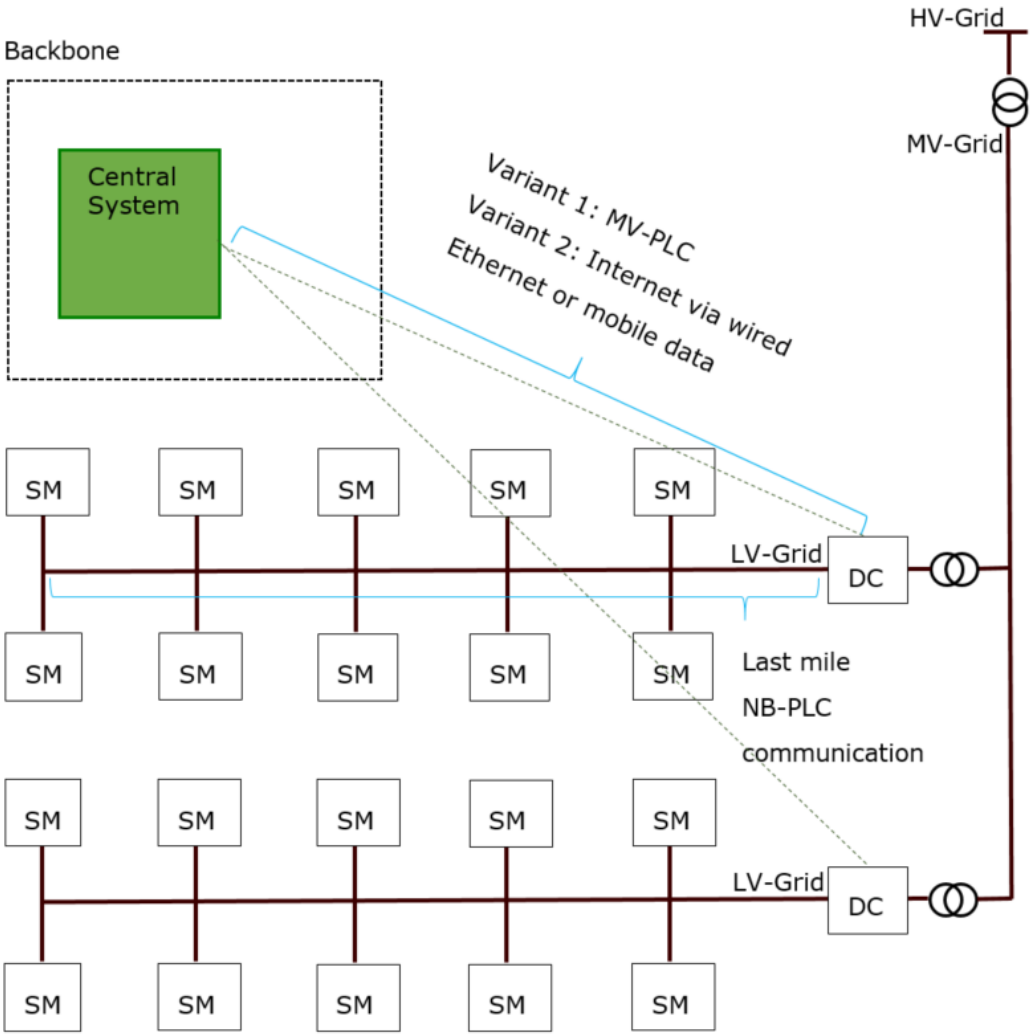

Figure 2.18 PLC installation in the SG

2.4.3 Third generation PLC systems

Real-time DA applications and AMI require increased transfer rates compared to the ones offered by 2nd generation PLC systems [74]. To achieve these higher data rates, larger bandwidths are needed, and the CENELEC A-band, with a bandwidth 35 kHz to 91 kHz using multiple carrier frequencies, provides a suitable solution. However, at such wide frequency bandwidths, the frequency-selectivity of the channel transfer functions of LV and MV electrical lines is quite high requiring the usage of

OFDM [78]. iAd© pioneered the use of OFDM for PLC, which became the basis for the REMPLI system, capable of speeds up to 60 kb/s in the CENELEC bands [12].

Closely spaced orthogonal carriers are used in the digital multi-carrier modulation technique known as OFDM to convey data. To produce a lengthy OFDM time domain signal, these subcarriers are PSK- or QAM-modulated and merged using IFFT. In order to prevent inter-symbol interference in the time domain and guarantee orthogonal subcarriers at the receiver despite signal distortion, a brief guard interval (cyclic prefix) is added between the symbols. Due to this characteristic, OFDM is robust to challenging channel circumstances, such as frequency-selective distortion brought on by signal reflections in the electrical grid and attenuation of high frequencies in long electrical lines.

OFDM has gained popularity in modern communication systems, being used in various technologies such as xDSL, terrestrial wireless distribution of television signals (DVB-T, DVB-H), and IEEE's high-rate wireless LAN standards (802.11a and 802.11g). It has been adopted in many communications standards, including WiMAX, DAB, 3 cellular telephony, IEEE 802.16, IEEE P1901, among others [79], [80].

In the context of PLC, various efforts have been made to set a global standard up to 150 kHz for the PHY and MAC layers. One such initiative is PRIME, which suggests the application of OFDM to the CENELEC A-band. PRIME Alliance, with 27 key industry members, focuses on defining standard PHY and MAC layers for a license-free PLC-based SG communication technology [81].

PLC-G3 addresses the CENELEC A-band with a variant for the US FCC-allocated PLC bands. It utilizes PHY layer parameters similar to those of PRIME, while its MAC layer is based on the wireless IEEE 802.15.4 standard [65].

IEEE P1901.2 working group was initiated to develop a standard for low frequency (up to 500 kHz) NB-PLC for SG Applications on LV and MV grids. This standard is based on OFDM, drawing inspiration from PRIME and PLC G3.

ITU-T G.hnem, focuses on defining a NB-PLC standard for energy management applications that can coexist with the BB-PLC ITU-T G.hn system [82]. This effort aims to harmonize with IEEE P1901.2.

These initiatives reflect the ongoing efforts to develop standardized and efficient PLC systems for various applications in the energy and communication sectors.

2.5 Overview of PLC protocols and frequency spectrum allocation

The wide range of applications for PLC has resulted in the need to adhere to numerous specifications while developing standards. Regulatory efforts focus on ensuring the coexistence of PLC systems with other devices sharing the medium and/ or frequency band.

PLC protocol can be classified based on the frequency bands it uses. This classification distinguishes between:

- U-NB, 125-3000 Hz
- NB, 3-500 kHz
- MB, 0.7-1.8 MHz
- BB, 1.8-250 MHz

U-NB PLC operates at very low data rates, going up to 100bps, but it has the advantage of communicating over long distances 150 km or more. Early deployments of PLC involved UNB-PLC technologies like the RCSs [83], Turtle System [84] and TWACS [61]. Despite the low data rate per link, these systems use effective

addressing techniques that facilitate scalability. Although UNB-PLC solutions have been used for decades since the deployment of protocols using NB-PLC their usage has decreased.

NB-PLC protocols are quite used in the SG, because they provide the optimum compromise between range and data rate. Besides smart metering these protocols are used in home and industrial automation. The most used standards in this frequency band are PRIME and PLC-G3.

MB-PLC protocols are intended for SMs and IEEE 1901.1 is the applicable standard. One of the PLC protocols using this frequency band is HPLC [85].

BB-PLC protocols support high transmission speeds, reaching hundreds of Mbps. They are used for mostly for home applications but it can be extended to smart metering and building applications [86]–[89].

Figure 2.19 illustrates the spectrum allocation for PLC across different areas, including ARIB, FCC, and CENELEC, categorizing it into U-NB, NB, MB, and BB segments, highlighting the regulatory distribution of PLC frequencies.

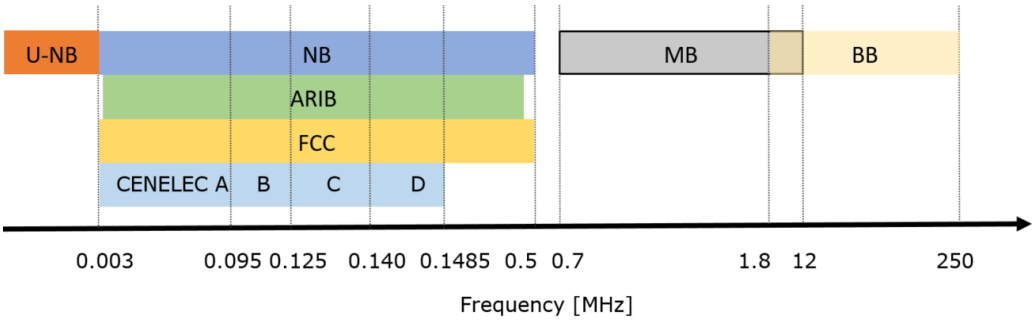

Figure 2.19 Spectrum allocation of PLC

Table 2.2 provides a comprehensive categorization of PLC protocols by linking them to their main characteristics, including frequency band, protocol, maximum data rate, transmission range, and corresponding standards.

Table 2.2 Overview of international PLC related standards, protocols and frequency bands

Frequency band	Protocol	Maximum data rate	Transmission range	Standard
U-NB	Turtle	up to 100bps	Ultra long range	IEC 14908-3 IEC 61334-5-2
	TWACS			IEC 14908-3 IEC 61334-5-2
	Ripple control			IEC 62054-11
NB	Prime	up to 1Mbps	Long range	ITU-T G.9901 ITU-T G.9904 IEEE 1901.2
	G3-PLC	up to 280kbps		ITU-T G.9901 ITU-T G.9903 IEEE 1901.2
	LonWorks™	up to 1.25Mbps		IEC 14908-4 IEC 14908-3

				IEC 14908-2 LONMARK Interoperability Guidelines
MB	HPLC	150kbps-10Mbps	Medium range	IEEE 1901.1
BB	HD-PLC	62.5Mbps-1.0Gbps	Short range	IEEE 1901 ITU-T G.9905
	HomePlug™	0.2Gbps-1.3Gbps		IEEE 1901
	G.Hn	0.3Gbps-2.0Gbps		ITU-T G.9960 G.9961 G.9962 G.9963 G.9964

BB-PLC and MB-PLC maximize data rate but trade-off communication range while U-NB has extremely low data rates. For utility applications, extensive coverage has greater importance than data rate, making NB PLC a preferable choice. NB-PLC has the potential to reach challenging locations, making it more suitable for utility applications. Consequently, I will not delve further into U-NB, MB and BB PLC, thus focusing in devices using NB-PLC communicating in the frequency bands below 150 kHz.

2.6 PLC signal coupling methods

The coupling between the PLC amplifier and the power line is a complex topic due to the characteristics of electric power grids, various installation types, broad range of protocol and diverse regulatory constraints.

PLC couplers are devices, which inject or receive PLC signal into electric power cables. In this context of PLC, power cables can carry either AC or DC, and the PLC transceivers' signals are coupled to them using a coupling circuit. For AC power lines, the coupling circuit must also filter out the AC mains signal, while for DC electric power grids, the coupling circuit solely blocks the DC mains voltage.

This section focuses on the physical connection aspect, which primarily involves injecting and extracting PLC signals into and from the power line. Four coupling methods have been identified based on their physical configuration for connecting to the power line, namely: antenna coupling, capacitive coupling, inductive coupling and resistive coupling.

Coupling PLC transceivers with the communication medium presents significant challenges, mainly due to the variability of access impedance, which changes over time and with frequency due to dynamic loads connected to the grid. Additionally, the low impedance of electricity distribution network to which reduces technical losses in energy delivery poses a problem because typical coupling devices are designed with access impedances much higher compared to the ones present in the communication medium.

Figure 2.20 illustrates the six main characteristics of PLC couplers obtained by summarising the following references [90]–[94]. These attributes collectively

define the functionality and compatibility of PLC couplers in various applications and settings.

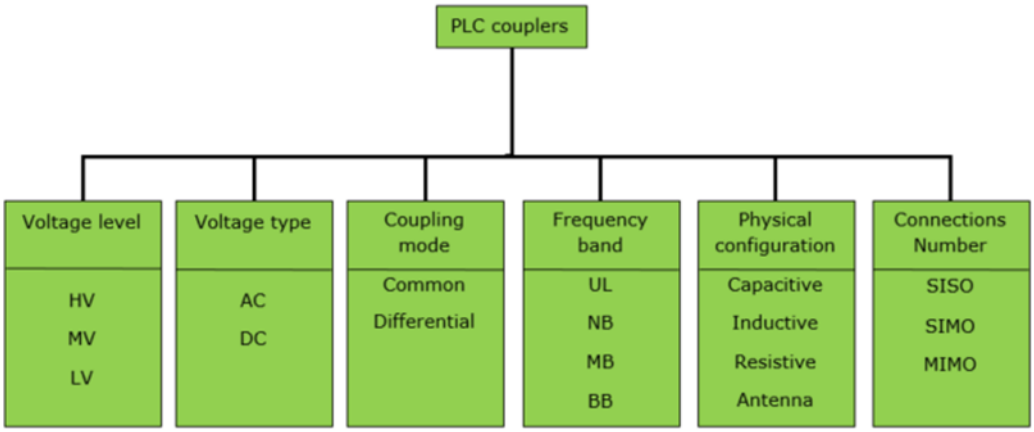

Figure 2.20 PLC couplers classification

In recent years, designing a PLC coupler that addresses impedance matching, maintains a flat frequency response to minimize distortions, provides efficient immunity against transients, and remains economical has been a major focus [95], [96]. Accomplishing such a design requires addressing several issues to create a practical PLC coupler suitable for the target application.

2.6.1 Antenna coupling

PLC first utilized the antenna coupling method for telephony over power lines, which involved running a parallel wire or antenna alongside the conductor carrying mains voltage to induce or extract communication signals in the line [45]–[48]. This approach was particularly favored for high voltage transmission lines due to its safety, as it did not require direct contact with the electrical power line. Instead, it used air as a dielectric insulation, minimizing the risk of progressive deterioration, which could occur with air dielectric-based capacitors. The antenna connection method also had the benefit of having exposed cables that were simple to examine and maintain.

However, one drawback of the antenna coupling system was the need for additional wires to be strung at the substation, potentially necessitating reinforcement of supporting structures or towers [90]. Although the efficiency of the telephony system over power lines was considered to be sufficient [97] the complexity of the coupling system most likely led to the replacement of the antenna coupling method by the capacitor coupling method.

Researchers have renewed their interest in the antenna coupling method, especially in the context of enhancing wireless systems coverage using PLC [98]–[100]. Straight power line antenna model is presented in [101] by the means of an analytical and numerical approach to solve the Pocklington integro-differential equation that depicts the distribution of induced current caused by an antenna positioned over a limited conducting ground in an overhead wire. Proposes a hybrid between RF and PLC technologies in buildings with multiple floors by exploring the use of the building wiring system as an antenna [100].

Another notable development is the work presented in [99], where researchers introduced a contactless PLC system. The cable acts as an antenna for

coupling with the power line enabling the propagation and radiation of 2.45 GHz Wi-Fi signals up to 40 m. A resonant quarter wave antenna is formed by exposing the coaxial cable thus radiating the maximum power onto the power line. The length of the antenna from Figure 2.22 can be calculated as follows:

$$\lambda = \frac{v_{coax}\left[\frac{m}{s}\right]}{f\left[\frac{1}{s}\right]} = \frac{0.65 * 3 * 10^8}{2.45 * 10^9} \approx 8\ cm \tag{2.1}$$

$$L = \frac{\lambda}{4} = 2cm \tag{2.2}$$

Figure 2.21 provides a visual representation of how RF signals can be transmitted via traveling waves along power lines. It illustrates the key components involved in this communication method and how it can be integrated into the existing power grid infrastructure, offering a means of data exchange and communication.

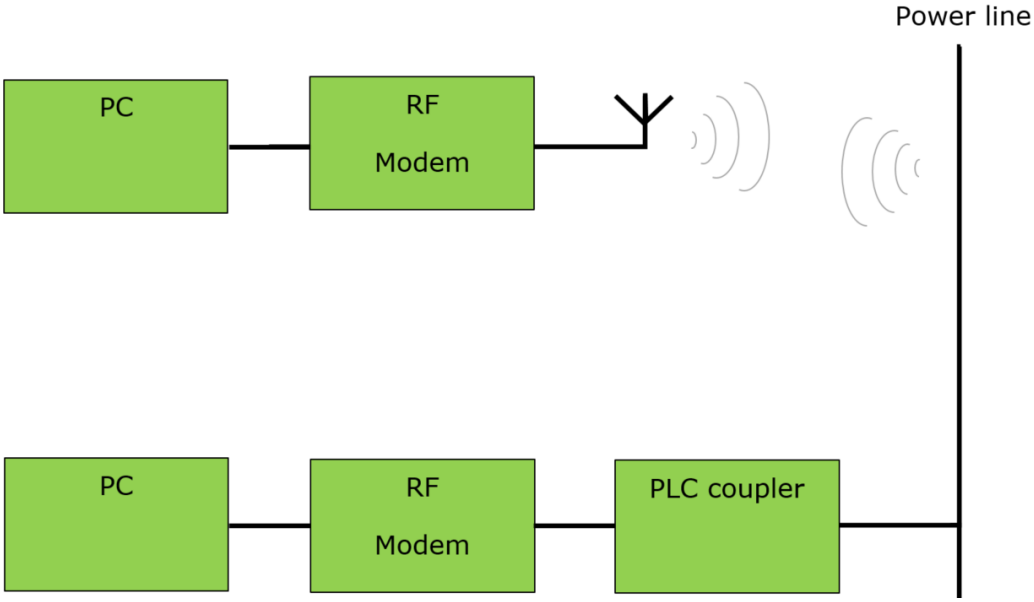

Figure 2.21 RF communication via contactless PLC [99]

Figure 2.22 presents the antenna coupling circuit for PLC which uses as coupler a quarter-wavelength antenna along the power line. The coupler is interfaced with the antenna port, facilitating a reliable coupling between the RF modem and the external antenna, thus optimizing signal transmission and reception, enabling effective data communication over power lines. Depending on the transmission power and frequency, antenna coupling may not be required at both ends; there might be the case that RF signals will couple sufficient signal level to communicate.

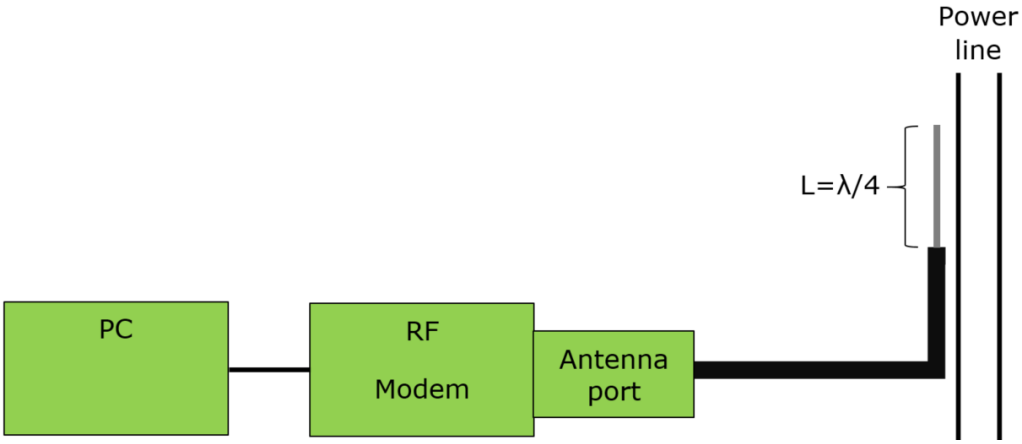

Figure 2.22 Antenna coupling circuit [99]

2.6.2 Capacitive coupling

Capacitive coupling is one of the most used types of PLC coupling methods because it is reliable and can be tuned for any kind of frequency band. The basic functionality of the coupling filter is that it acts as a high pass or band pass filter so that it couples and decouples PLC signal from the power line. Subsequently the PLC coupler has two different impedances one at frequencies closer to mains frequency and the other at higher frequencies closer to PLC frequencies.

Figure 2.23 presents the behaviour of mains frequency and PLC signal frequency impedance of a capacitor and inductor having common values for NB PLC coupling [103], by looking from the mains side the coupler actually forms a high pass filter. By choosing the right components, capacitive coupling is suitable for all types of voltages, frequencies and PLC protocols.

Figure 2.24 is the S11 measurement using VNA of a real 470nF film capacitor suitable for operating in mains conditions [102], from the smith chart it can be seen that the impedance of the capacitor between 9kHz and 1MHz is quite low thus making it suitable for coupling PLC signal.

Figure 2.25 is the S11 measurement using VNA of a real 22μH inductor suitable for operating in mains conditions, from the smith chart it can be seen that the impedance of the inductor between 9 kHz and 1 MHz makes it suitable for it to be part of the PLC coupler.

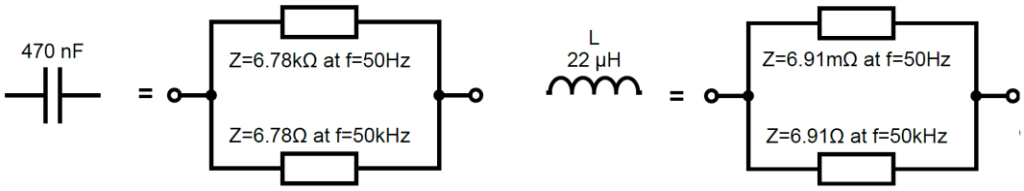

Figure 2.23 Mains frequency and PLC signal frequency impedance of capacitor and inductor

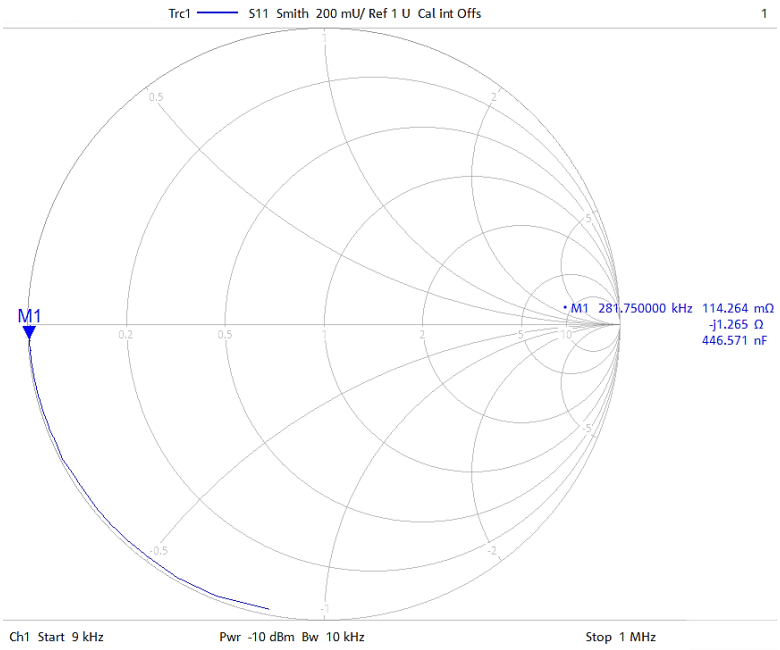

Figure 2.24 S11 measurements of a 470nF capacitor

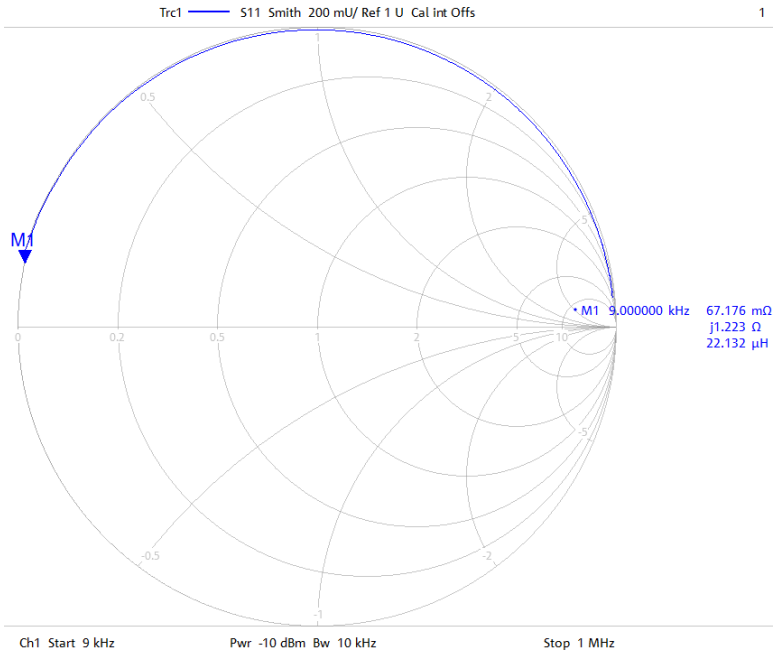

Figure 2.25 S11 measurements of a 22μH inductor

There are two types of PLC capacitive coupling methods:

The non-isolated capacitive coupling method involves the use of a combination of components, specifically a capacitor and an inductor, to establish a PLC signal connection with the electrical grid [21]. The described configuration permits the exchange of PLC signals while retaining a non-isolated connection to the grid. This setup can be an effective coupling method for single phase SMs that utilize a shunt to measure the current flow. In such cases, it is important for the internal ground of the SM to be at the same electrical potential as the phase. Figure 2.26 visually represents this type of coupler, illustrating the main components and their connection to the grid outlining its mains frequency and PLC frequency behavior. The capacitor facilitates signal transfer, while the inductor helps manage impedance and prevent unwanted interference. This method is suitable for applications where isolation from the electrical grid is not required.

The isolated capacitive coupling method employs a more complex configuration that includes a capacitor, an inductor, and a transformer to establish PLC signal connection with the electrical grid. This type of coupler, is depicted in Figure 2.27. The transformer serves as an isolation barrier, ensuring that PLC signals can be transmitted without galvanic connection to mains potential. This method is particularly used in three phase meters and other PLC equipment. The combination of components allows for efficient signal transmission while maintaining galvanic isolation.

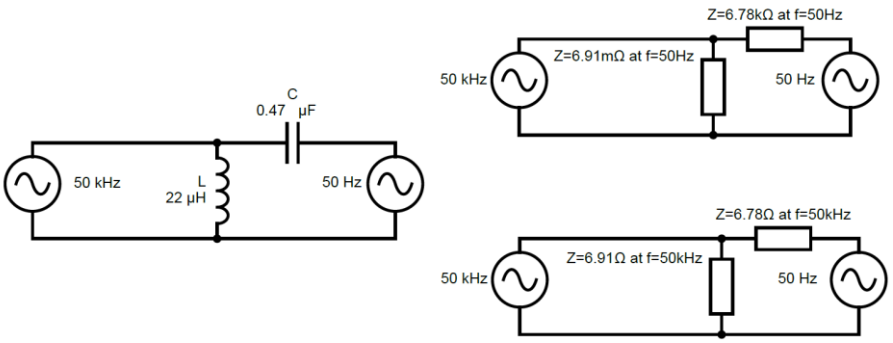

Figure 2.26 Mains frequency and PLC signal frequency impedance of non-isolated capacitive coupler

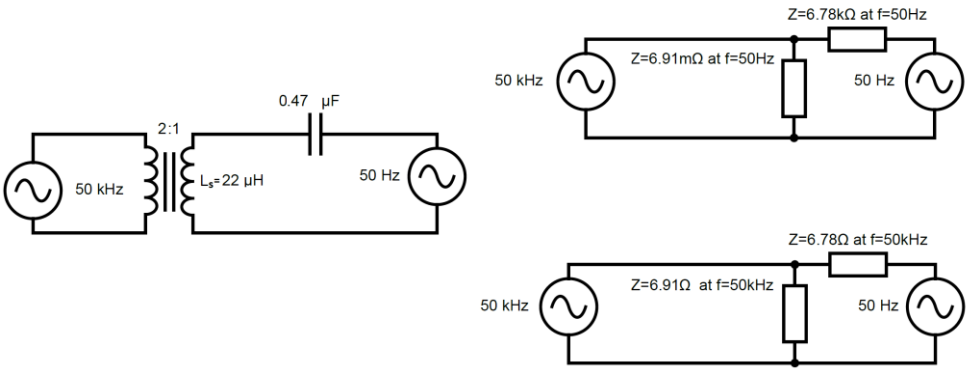

Figure 2.27 Mains frequency and PLC signal frequency impedance of isolated capacitive coupler

2.6.3 Resistive coupling

This type of coupling method is still in early experimental stages and can be considered only for PLC receiver applications because the output of the transmission power amplifier has to be decoupled from the mains voltage and frequency in order to function properly. Comparing the resistive coupling method with the capacitive coupling method one can see that the PLC signal level is reduced significantly more compared to the PLC coupler proposed in [108] while the mains voltage is 45% higher in the case of the resistive coupler. Below equations present a comparison between the voltage division ration of the resistive PLC coupler proposed in [108] and the capacitive coupler presented in section 2.6.2.

$$V_{out} = \frac{Z_2}{Z_1 + Z_2} * Vin \tag{2.3}$$

$$V_{out_{resisitive\ at\ 50Hz}} = V_{out_{resisitive\ at\ 50kHz}} = \frac{4.7k\Omega}{100k\Omega + 4.7k\Omega} * Vin \tag{2.4}$$

$$V_{out_{resisitive\ at\ 50Hz}} = V_{out_{resisitive\ at\ 50kHz}} = 4.5\% * Vin \tag{2.5}$$

$$V_{out_{capacitive\ at\ 50Hz}} = \frac{6.91m\Omega}{6.91m\Omega + 6.78\Omega} * Vin = 1‰ * Vin \tag{2.6}$$

$$V_{out_{capacitive\ at\ 50kHz}} = \frac{6.91\Omega}{6.91\Omega + 6.78\Omega} * Vin = 50\% * Vin \tag{2.7}$$

2.6.4 Inductive coupling

There are two methods of coupling the PLC signal onto the power line using transformers: series inductive coupling and shunt inductive coupling. Both methods seem to be best suited for PLC communication in shielded underground MV power lines. For writing this section I have used the following references [90], [91], [104]–[107].

Series inductive coupling is connected in series with the power cables shield. To do this, one end of the device should be connected to the shield of the power cable, while the other end should be grounded. This series connection ensures a reduced insertion loss of about 1dBm±0.5 when compared to non-inductive coupling. Additionally, this type of inductive coupler enables signal transmission over distances exceeding 5 km [104]. The installation of the series connected inductive coupling is more complex compared to the shunt inductive coupling method because it requires direct contact between the coupler transformer and conductor. Figure 2.28 provides the overview of the integration of series connected inductive couplers in an underground MV shielded cable installation. This type of coupling method transmits between the shield of the underground cable and ground.

Shunt inductive coupling is based on the principle of electromagnetic induction, which is similar to what CTs are doing in the power distribution grid but in this case instead of measuring the induced voltage proportional to the current passing through the conductor the transformers is used for injecting signal. Using this method signal attenuation levels are ranging from -20dB to -35dB. Nevertheless, this method exhibits larger coupling attenuation compared to the intrusive inductive coupling method, consequently limiting the maximum data transmission distance to approximately 5 km [104]. The main benefit of this coupling method is that it does not require direct contact to the conductor thus installation is much simpler compared to the series inductive coupling. Premo manufactures inductive couplers which operate at NB-PLC frequencies which do not require direct contact to the conductor thus are easy to install [105]. Figure 2.29 illustrates the inclusion of shunt inductive-

coupled PLC modems within an underground MV shielded cable installation. These type of coupler is using as transmission medium all lines passing through it.

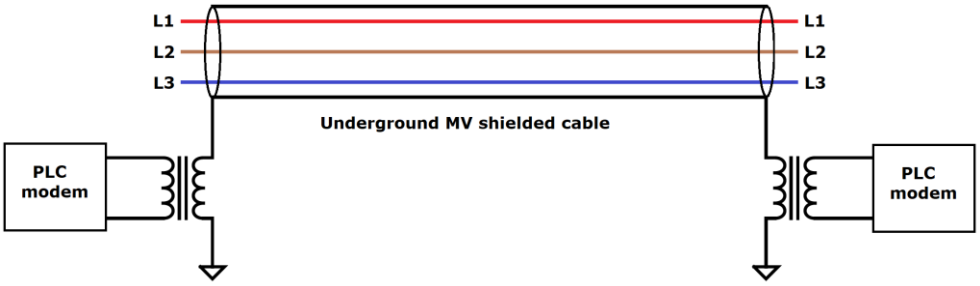

Figure 2.28 Series connected inductive coupling

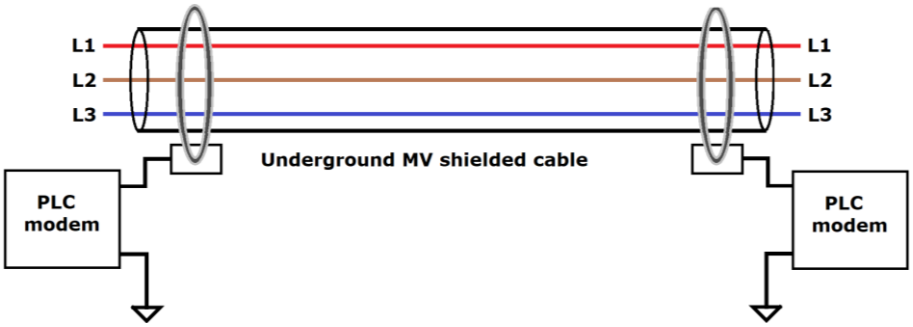

Figure 2.29 Shunt inductive coupling

2.7 PLC transceiver overview

In this section I present a generic PLC transceiver thus creating the necessary overview for the next sections. For developing this section I have performed a thorough bibliographical research using multiple references [103], [109]–[113].

PLC transceivers utilize modulation techniques to imprint data onto the power line signal. The transmitter modulates the data onto the carrier signal, and the receiver demodulates the received signal to recover the transmitted data. Common modulation schemes include BPSK, QPSK, OFDM, and more.

As presented in section 2.5 PLC systems can operate in different frequency bands. The choice of frequency band depends on factors like transmission distance, available bandwidth, and regulatory constraints. The PLC coupling interface needs to be adapted.

The main characteristic and features of a PLC transceiver are presented below.

Noise and Interference Handling: Power lines are susceptible to various types of noise and interference, including impulsive noise, white noise, and radio frequency interference. PLC transceivers incorporate techniques like error correction coding, interleaving, and adaptive modulation to mitigate the effects of noise and interference.

Channel Estimation: Due to the changing nature of the power line channel, PLC transceivers often employ channel estimation techniques. These techniques help

the receiver adapt its demodulation parameters to account for channel variations, enhancing the reliability of communication.

Protocol Implementation: PLC transceivers adhere to specific communication protocols, such as PRIME, G3-PLC, HomePlug, and IEEE 1901. These protocols define how data is structured, transmitted, and received over the power line network.

Security: PLC transceivers implement security measures to protect the transmitted data from unauthorized access or tampering. Encryption, authentication, and access control mechanisms are commonly used to ensure data privacy and integrity.

Adaptive Power Control: PLC transceivers often incorporate adaptive power control mechanisms to adjust transmission power based on the channel conditions. This helps optimize the communication link and reduce interference to other devices on the power line.

Mains zero crossing detection: is performed by the PLC transceiver and it has the following purposes, based on the PLC protocol used: synchronization, data demodulation, reduce inter-symbol interference, power control.

Figure 2.30 presents a generic PLC transceiver diagram in which TX and RX signal paths are highlighted with red and green.

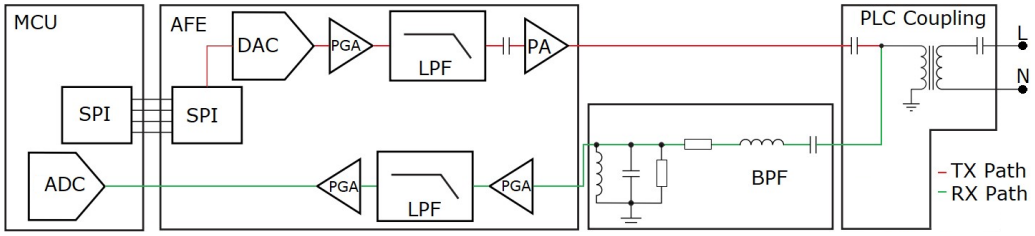

Figure 2.30 PLC transceiver diagram

2.8 Overview of PLC-PRIME and PLC-G3 protocols

PRIME and PLC-G3 stand out as two highly recognized and used protocols in the latest generation of NB-PLC protocols. Both of these protocols emerged as open standards, initially pioneered by a compact consortium of telecommunications and electricity distribution companies. However, these initiatives have since evolved into expansive alliances with a growing roster of participants. Despite their shared aim of serving various applications within SGs, these protocols exhibit significant distinctions as well as similarities, which will be explored in this section. The information presented in this section have the purpose of creating the theoretical background for the PLC enhancement techniques described in Section 3 and Section 4. Due to the similarities between PLC-Prime and PLC-G3 semiconductor manufacturers offer PLC modems that allow the implementation of both using the same HW components, just the software and configuration for the modem differs [110], [111], [114].

Table 2.3 is a side-by-side overview of PLC-G3 and PLC-PRIME protocols. In order to create this overview I have used multiple references [109], [112], [113], [115]–[117]. The table provides a comparative analysis of these two protocols across various parameters, as follows:

Table 2.3 Overview of PLC-G3 and PLC-PRIME

Parameter	PLC-G3	PLC-PRIME
Bandwidth in CENELEC A	35 kHz to 91 kHz	42 kHz to 89 kHz
Number of carriers	36	84 header 96 payload
Carrier frequency spacing	1.56 kHz	488.28 Hz
Pilot subcarriers	Not used	13 header 1 payload
Cyclic prefix	75 μs	192 μs
OFDM symbol timing	715 μs	2240 μs
Preamble timing	6080 μs	2048 μs PRIME 1.3.6 8192 μs PRIME 1.4
FFT interval	640 μs	2048 μs
Interleaving	Each data packet	Each OFDM symbol,
Windowing	Available	Not available
Forward error correction	Convolutional code Reed-Solomon Repetition code	Convolutional code Repetition code
Max data rate	33.4 kbps	128.6 kbps
Modulation Differential encoding	DBPSK, DQPSK, ROBO In time	DBPSK, DQPSK, D8PSK In frequency

PLC-G3 PHY layer uses differential and coherent modulation types, ranging from DBPSK/ BSPK (1 bit per symbol) to D8PSK/8PSK (3 bits per symbol). Another modulation, known as ROBO, employs DBPSK/BPSK with a 4-fold repetition to enhance its capabilities in severe power line conditions.

PLC-PRIME PHY layer does not have ROBO modulation type, but it uses D8PSK which allows PLC-PRIME to have almost 4 times more data rate compared to PLC-G3, but it needs higher SNR.

A major contrast between G3-PLC and PRIME lies in their frame structures. In PRIME, a linear chirp signal spans the entire OFDM spectrum, whereas G3-PLC adopts a repetition of the OFDM symbol approximately 9.5 times. Both protocols incorporate a preamble for synchronization purposes. In the case of G3, this preamble serves the dual purpose of estimating the channel transfer function. Furthermore, in G3, the final symbol within the preamble also acts as a reference point for measuring the phases of the subcarriers in the header [116].

Figure 2.31 presents the PLC-PRIME frequency spectrum as it is measured on a standard LISN and Figure 2.32 presents the PLC-G3 spectrum in the same conditions. In Figure 2.32 the 36 carriers can be observed due to the high PAPR which is explained in detail in section 3.2.

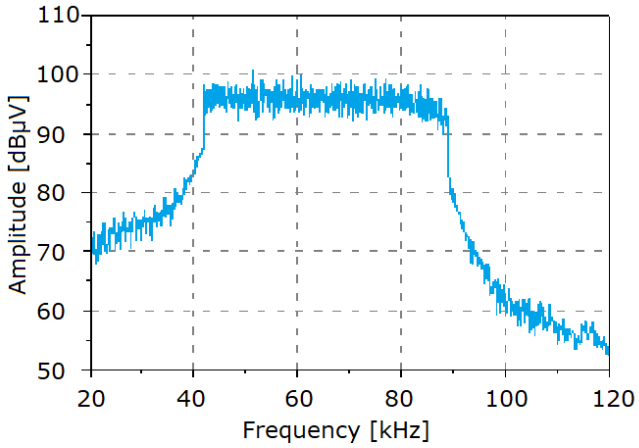

Figure 2.31 PLC-PRIME frequency spectrum in TX mode

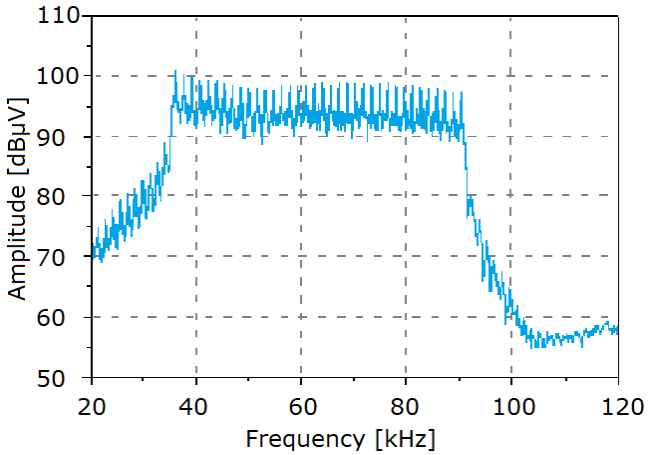

Figure 2.32 PLC-G3 frequency spectrum in TX mode

2.8.1 Modulation types used

Data bits undergo mapping for differential modulation techniques such as DBPSK, DQPSK, and D8PSK. In place of employing the phase reference vector φ, each phase vector utilizes the preceding symbol on the same subcarrier as its phase reference. In this way of calculating the phase uncertainty if the constellation is rotated due to communications channel through which the signal passes is mitigated.

Coherent and non-coherent modulation schemes are two different approaches to modulating a carrier signal with information. They differ primarily in how they handle the carrier phase information during modulation and demodulation [118].

In coherent modulation, both the transmitter and the receiver have synchronized carrier oscillators, which means they know the exact phase of the carrier signal. This synchronization allows the receiver to extract the phase and amplitude information from the received signal. Coherent modulation is typically more sensitive to carrier phase changes and provides higher data rates and better performance in terms of error rates.

Non-coherent or differential modulation, on the other hand, does not require carrier phase synchronization between the transmitter and the receiver. The receiver does not attempt to recover the carrier phase; instead, it focuses on extracting the amplitude and phase changes that are caused by the modulated signal. Non-coherent modulation is less sensitive to carrier phase variations and is often used in scenarios where carrier phase information cannot be reliably transmitted, such as in frequency-selective fading channels or when using low-cost equipment.

In summary, the key difference between coherent and non-coherent modulation schemes lies in how they handle carrier phase information. Coherent modulation requires synchronized carrier oscillators and can achieve higher data rates but is more sensitive to phase variations. Non-coherent modulation does not rely on carrier phase synchronization and is more robust in situations where carrier phase information is difficult to maintain.

Table 2.4 provides a comprehensive overview of the modulation types available for PLC-G3 in the CENELEC A frequency band, with a distinctive focus on the distinction between non-coherent and coherent modulation methods. This table highlights the modulation options in PLC-G3, distinguishing between non-coherent, suitable for challenging environments, and coherent modulation methods, offering different data rates and performance characteristics.

Table 2.4 PLC-G3 modulation types available in CENELEC A frequency band

Non-coherent (differential modulation)	**Coherent modulation**
Robust mode	Robust mode
DBPSK modulation	BPSK modulation
DQPSK modulation	QPSK modulation
D8PSK modulation	8PSK modulation

Figure 2.33 constellation diagram of DBPSK, DQPSK, and D8PSK graphically explain digital modulation schemes which employ a finite set of symbols for conveying information. These symbols are assigned specific magnitude and phase values on the I/Q plane, forming what is known as constellation points. Modulation schemes with a higher number of constellation points have the capacity to transmit more information per symbol. In simpler terms, the greater the number of symbols in a modulation scheme, the more bits a single symbol can represent [119] . For instance, in BPSK, each symbol can convey only a binary choice of 0 or 1, owing to its two constellation points, thereby transmitting one bit per symbol. In the case of QPSK, which features four constellation points transmit 2 bits/ symbol. As a general rule the number of constellation points is $2^{n\ (\text{bits/ symbol})}$.

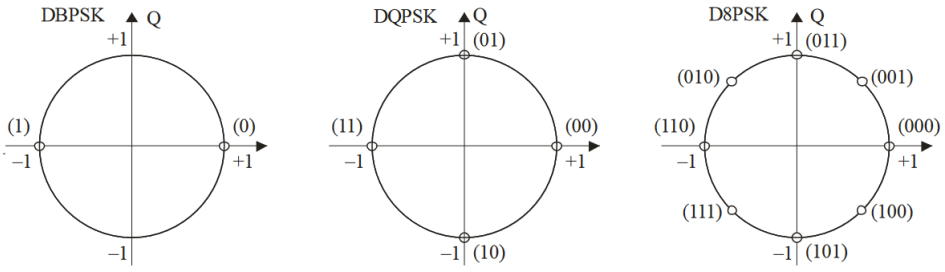

Figure 2.33 Constellation diagram [113]

Although it is tempting to use high data rate PSK modulations the power line is a communication channel with a lot of interferences thus communication robustness against noise is more important than increased data rate. Figure 2.34 presents the theoretical BER vs. SNR of the signal processing methods associated to each type of modulation used in PLC-G3 and PLC-PRIME under the influence of white noise [120].

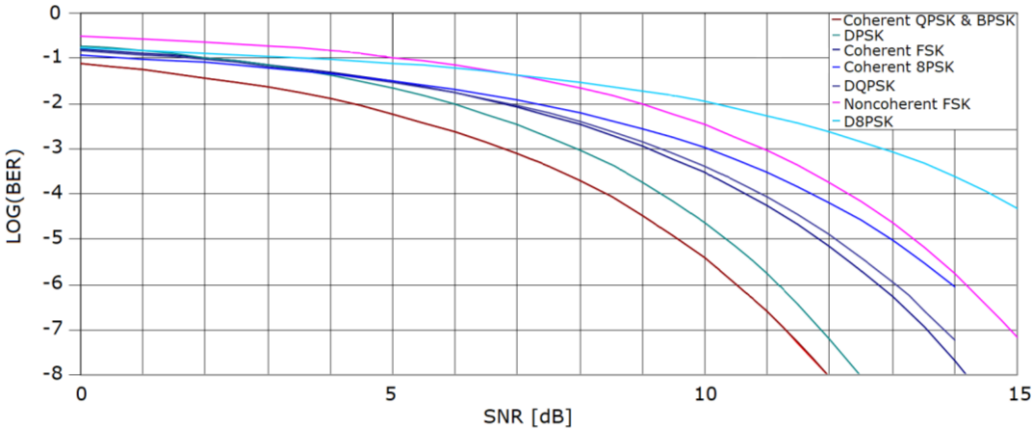

Figure 2.34 BER vs. SNR of modulations used in PLC-G3 and PLC-Prime

2.8.2 OFDM transceiver implementation in PLC

Both PLC-G3 and PLC-PRIME are using OFDM because it is as an efficient means of maximizing the use of constrained bandwidth channels, enabling the incorporation of advanced channel coding methods.

The available bandwidth is partitioned into numerous sub-channels, akin to independent subcarriers modulated with PSK and operating at distinct non-interfering (orthogonal) frequencies. Redundancy bits are introduced through Convolutional and Reed-Solomon coding, allowing the receiver to recover lost bits caused by both constant background noise and abrupt impulsive noise disruptions. Employing a time-frequency interleaving scheme serves to minimize the correlation of received noise at the decoder's input, thereby introducing diversity.

The generation of the OFDM signal is achieved through the application of an IFFT on the complex-valued signal points, which are a product of differentially encoded phase modulation and are assigned to individual subcarriers. An OFDM symbol takes shape as a cyclic prefix is appended to the outset of each block yielded by the IFFT process. The length of this cyclic prefix is carefully chosen to ensure that the channel's group delay does not incite undue interference between successive OFDM symbols. Furthermore, windowing curtails the out-of-band leakage from the transmitted signals.

For adapting to varying link conditions, channel estimation comes into play. Depending on the received signal's quality, the receiver may, upon request from the transmitter, furnish suggestions regarding the optimal modulation scheme to be employed in forthcoming packets destined for the same receiver. Additionally, the system discerns subcarriers with suboptimal SNR and abstains from transmitting data on those channels.

Figure 2.35 offers a visual representation of the OFDM transmitter's complex structure, displaying the above described techniques and strategies employed to ensure reliable and efficient data transmission.

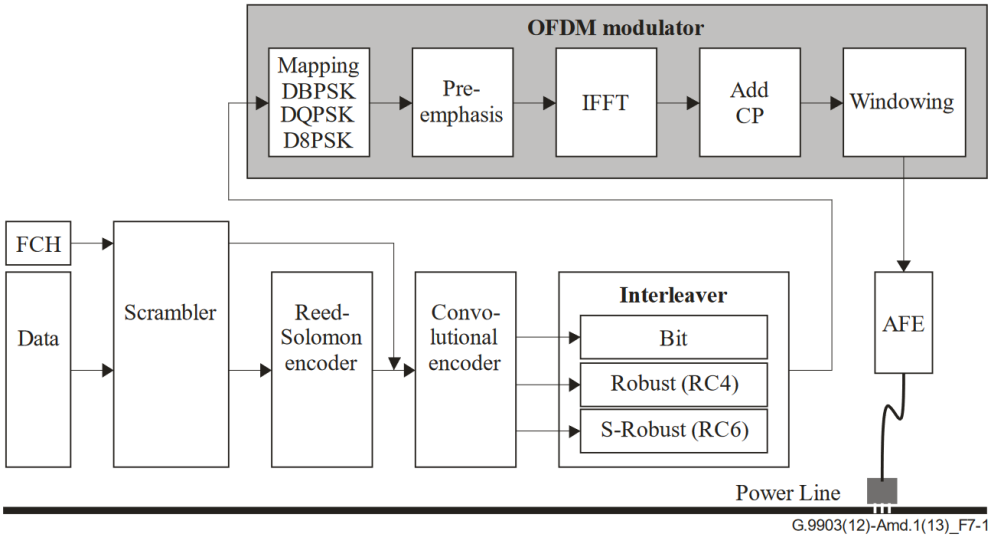

Figure 2.35 OFDM transceiver block diagram [121]

2.9 Chapter summary

In conclusion, this introductory chapter has established the foundation for understanding PLC in the context of modern power grid applications. The chapter initiated with an in-depth examination of PLC's fundamental working principles, revealing the utilization of power lines as a physical medium for data transmission. Within this context, a structured presentation of the challenges faced by PLC within the electricity grid, including power line CE, standardization gaps, signal attenuation, and low access impedance, was provided.

The historical context of PLC was examined, tracing its development from first-generation systems to the cutting-edge third-generation technologies. This historical perspective highlights the remarkable advancements that have taken place in the field of PLC, underscoring its growing relevance in contemporary power grid applications.

Furthermore, the exploration delved into the intricate domains of PLC protocols and frequency spectrum allocation, revealing the multitude of standards and regulations governing this technology. This exploration was performed with the purpose to enhance my understanding of communication standards within the PLC field.

Additionally, signal coupling methods, a important component of PLC technology, were explored, encompassing various techniques such as antenna coupling, capacitive coupling, inductive coupling, and resistive coupling, each with its own applications and characteristics.

The subjects presented in this chapter serve as a basis for the subsequent chapters, where a deeper dive into the technical intricacies of PLC protocols and transceivers will be undertaken.

Portions of this introduction have previously served as the basis for my scientific articles [19]–[21], [25], [24], [22], and this chapter was developed through an extensive literature review referencing over 110 bibliographical sources.

I have made theoretical contributions in the field of PLC across several primary topics using extensive literature review as research method:

Integration of PLC in the Electricity Grid: In sections 2.4, 2.5 and 2.6 of my research, I have delved into the "how" and "why" of PLC's utilization as a communication protocol using power lines as physical transmission medium. My work emphasizes the significance of using the existing extensive network of power lines within the electricity grid for communication purposes, obviating the need for laying additional dedicated communication cables or deploying costly wireless systems. Notably, PLC serves as a last-mile communication protocol, facilitating communication between SMs and DCs.

Challenges Faced by PLC in Power Distribution Grids in the Context of SGs: My research has identified and discussed the multitude of challenges that PLC must overcome to ensure effective communication within the electricity grid. These challenges include CE arising from standardization gaps, signal attenuation due to line losses and low power line impedances.

A major theoretical contribution of my research is the in-depth analysis of the challenges posed by CE in the grid on NB-PLC. I have categorized these emissions, identified their sources, and emphasized their impact on communication. Additionally, I have outlined the need for enhancing NB-PLC by developing methods for detecting, avoiding, and filtering out CE within the NB-PLC communication frequency band.

I have detailed how these challenges affect PLC's signal quality and communication reliability. The types of CE present in the electricity distribution grid, signal attenuation, and power line impedance are thoroughly explored in sections 2.2.1, 2.2.2, 2.2.3.and 2.2.4 of the thesis and are also discussed in my scientific articles [19], [20].

3 Conducted noise source detection and avoidance technique

In this chapter, I put forth a novel approach to identify loads that generate noise within the frequency band of PLC. The method involves leveraging SMs to establish a correlation between energy measurements of the load and the quality reports obtained from the PLC-G3 modem channel. By examining practical results, clear connection between energy measurements and the noise originating from specific loads can be observed. To further validate the need of such an enhancement method, spectrum measurements using PLC-G3 on power lines with both low and high impedance were conducted, allowing for a comprehensive comparison with the noise spectrum. The correlation allows the creation of a transmission schedule based on when the loads generating noise are operated.

An alternative effective method for reducing noise is the utilization of a PLF positioned between the electricity meter and the consumer. This filter serves the purpose of eliminating noise within the PLC band, but it comes it introduces losses at mains frequency and additional deployments costs. This option of improving PLC is presented in chapter 4.

To prevent noise altogether, there is the option to choose PLC frequency bands that operate above 150 kHz, which are covered by standardized CE regulations. The available PLC frequency bands include FCC and ARIB, although in Europe, only the CENELEC-A band is allocated specifically to PLC communication for utilities. The spectrum allocation together with the PLC protocols is presented in section 2.5.

The theoretical concepts and experimental results presented in this chapter are built upon my published scientific articles [19], [21], [22], [24], [25].

3.1 SM Concept

The concept developed by me implies harnessing the capabilities of SMs so that the loads that introduce CE in the PLC frequency band on the consumer side can be effectively identified. This is achieved by utilizing channel quality reports obtained from the PLC modem and energy measurements acquired from the metrology ADC. Figure 3.1 is the block diagram of a SM with PLC [19], [22], [24], [25], [122], [123] that is capable of creating a correlation between load power consumption and the noise generated by the load. Table 3.1 explains the components and sub-blocks used in Figure 3.1. SMs have precise RTCs, used for multi tariff implementation, which can be further used in order to develop the optimum PLC transmission schedule. The concept was designed to utilize standard market-available components, making it feasible to integrate it to some extent into existing deployed SMs.

The proposed architecture represents from functional point of view a single phase shunt based SM utilizing a capacitive, non-isolated type of PLC coupling, thus the ground of the SM electronic components will be at phase potential. In this case the most cost efficient and energy efficient power supply topology is to use a non-isolated flyback converter with 15V output for the PLC AFE and a buck converter from 15V to 3.3V for supplying the digital part. The concept can be implemented towards all types of electricity meters: poly-phase, indirect connected, semi-direct, semi-indirect. I have chosen the to detail upon the single phase architecture because it is the most common used type of meter and it is easy to up-scale towards other types of meters.

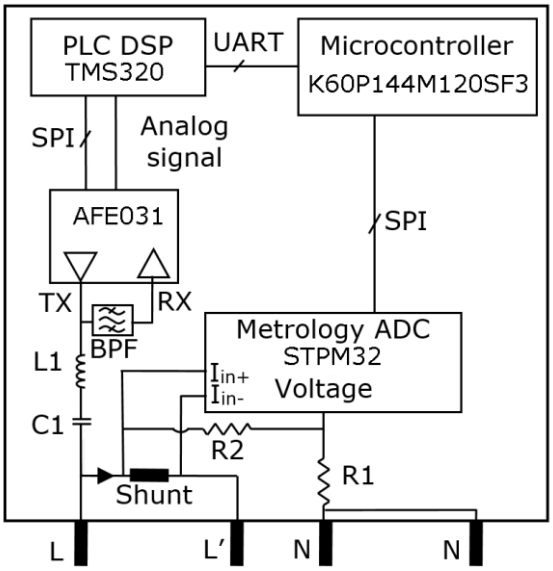

Figure 3.1 Architecture of a single-phase SM with PLC

The SM comprises several essential components carefully selected for optimal performance and compliance.

The PLC solution is provided by Texas Instruments™, featuring the TMS320F28069 microcontroller and the AFE031 PLC AFE.The analog Band-Pass Filter for the RX path is constructed using passive components. While the PLC mains coupling in the CENELEC-A frequency band, uses a capacitive non-isolated solution with polypropylene capacitor C1=0.47μF and a ferrite core semi-shielded inductor L1= 470μH.

To ensure accurate measurement, an STPM32 metrology ADC from STMicroelectronics™ is integrated, using a Copper-manganin shunt of 1mΩ resistance, ensuring precision within a <0.1% error margin across the 24mA to 120A range, meeting the accuracy standards set by EC Directive 2014/32/EU.

Managing the SM's core functions is the NXP™ K60P144M120SF3 microcontroller, built on the ARM Cortex M4 architecture. To facilitate mains connections, a DIN-type terminal block is employed, recognized as the standard variant in Europe. These thoughtfully chosen components collectively allow the SM to deliver accurate and reliable performance while pre-complying with European regulatory directives.

Table 3.1 summarizes the role of each major component in the SM architecture.

Table 3.1 Single-phase SM with PLC block diagram explanations

Components	Explanation
PLC DSP	PLC digital signal processor, which is used to modulate and demodulate the PLC signal. Channel quality reports are also computed inside the DSP.
AFE	The PLC AFE is responsible of the PHY layer implementation of the PLC modem.

BPF	Analog band pass filter is required on the Rx path before the signal is amplified by the AFE.
L1, C1	PLC signal coupling elements, at mains frequency they behave almost as an open circuit Z while at PLC signal frequencies the impedance is low facilitating signal coupling.
Shunt	Used as current measuring element. The voltage drop is measured using the differential inputs of the metrology ADC I_{in+} and I_{in-}.
R1, R2	Voltage divider that is used in the mains voltage measurement chain. An array of series connected resistors is recommended for increasing voltage withstand.
Metrology ADC	Provides instrumentation and energy readings such as: load current, voltage, phase shift and power measurements.
Microcontroller	The correlation between load power consumption and its conducted noise can be done inside the microcontroller.
L, L', N	L is the mains connection from the power grid while L' is the connection towards the load. N is the mains neutral connection.

3.2 CE source detection and avoidance technique evaluation setups

In this section, I expound upon the procedures undertaken to establish a laboratory test configuration that closely approximates the characteristics of the power grid. To achieve this objective, an exhaustive analysis of scholarly literature and adherence to international standards were conducted.

3.2.1 Power line impedance simulation circuit

The loads connected to the power line determine the access impedance of a NB-PLC modem [124]. This section provides an extensive examination of the literature pertaining to power line impedances and offers a pragmatic approach of its integration into the test setup through the utilization of an impedance adaptation circuit in conjunction with a standard LISN [125].

PLC access impedance at frequencies below 500 kHz is in focus among researchers for quite some time. In 1976, Malack and Engstrom conducted a comprehensive study, publishing the largest collection of power line impedance measurements to date [126]. This study involved measuring the impedance of 86 AC power distribution systems within the frequency range of 20 kHz to 20 MHz. Subsequent research has confirmed the ongoing relevance and accuracy of their findings. To demonstrate this, Figure 3.2 presents a graphical representation of impedance measurement results obtained from [43], [126]–[129] and impedance value proposed in the EMC standard which characterizes the standard LISN [125] , focusing on the frequency range of 20 kHz to 150 kHz.

The purposes of Figure 3.2 are to:

1. Establish that the impedance results obtained by Malack and Engstrom [126] remain valid.
2. Emphasize that the noise and PLC level measurements presented in the following section are based on real-world impedance encountered in practical scenarios.

3. Show the discrepancy of the LISN impedance proposed in international standard EN55016-1-2 [125] compared to the real power line impedance.

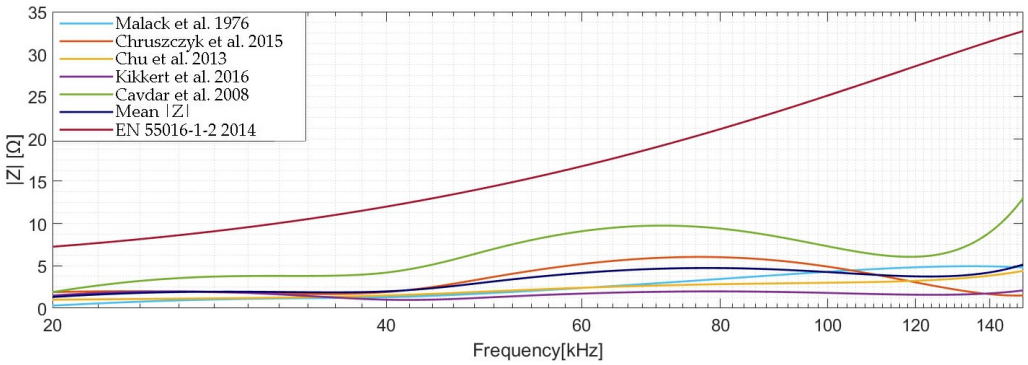

Figure 3.2 Power line impedance and LISN impedance [43], [125]–[129]

In order to achieve a power line impedance closer to values encountered in field conditions impedance circuit from Figure 3.3 is used as part of the LISN. L' is the live terminal of the LISN while N' is the neutral and PE protective earth. I have implemented this type of adaptive circuit using a thick film high power resistor (20W), polypropylene capacitor and power inductor.

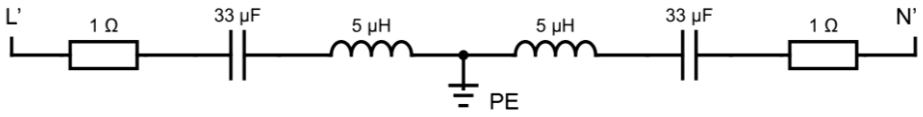

Figure 3.3 Adaptive impedance circuit

Figure 3.4 presents the impedance and phase of the circuit simulating electrical grid impedance from Figure 3.3. Impedance values obtained with the adaptive impedance circuit are very close to the mean impedance of the power line.

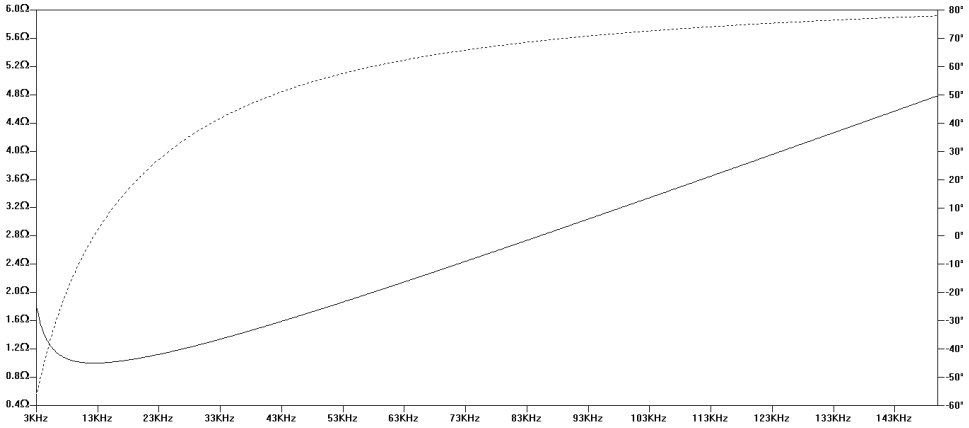

Figure 3.4 Impedance and phase plot for half of the adaptive impedance circuit

The power consumption of the low impedance simulation circuit depicted in Figure 3.3 is approximately P ≈ 1 kW at the mains frequency f = 50 Hz. This power consumption is significantly lower in comparison to using a purely resistive 2Ω load, where the power consumption would be P ≈ 26.5 kW. The calculations for quiescent power drain are elaborated in Equations (3.1) - (3.11).

$$Z = \sqrt{R^2+(X_L - X_C)^2} \tag{3.1}$$

$$R = 1\ \Omega \tag{3.2}$$

$$X_L = 2\,\pi\, fL = 1.5\ m\Omega \tag{3.3}$$

$$X_C = \frac{1}{2\,\pi\, fC} = 95.5\ \Omega \tag{3.4}$$

$$Z = 95.5\ \Omega \tag{3.5}$$

$$\varphi = tan^{-1}(\frac{X_L - X_C}{R}) = -25.5^{\circ} \tag{3.6}$$

$$cos\,\varphi = 0.9 \tag{3.7}$$

$$I_{RMS}/_2 = \frac{V_{RMS}/_2}{Z} = \frac{115}{95.5} = 1.2\ A \tag{3.8}$$

$$P_{1/2\ adaptive\ circuit} = U_{RMS} I_{RMS}\, cos\,\varphi = 230 \times 2.4 \times 0.9 = 496.8\ W \tag{3.9}$$

$$P_{adaptive\ circuit} = 2 * P_{1/2\ adaptive\ circuit} = 992\ W \tag{3.10}$$

$$P_{2\Omega\ Load} = \frac{U_{RMS}^2}{R} = \frac{52900}{2} = 26.45\ kW \tag{3.11}$$

3.2.2 PLC signal level and CE measurement setup

The LISN depicted in Figure 3.5 represents a customized version of the CISPR16 LISN, characterized by a symmetrical configuration relative to ground [123], and it exhibits the impedance profile depicted in Figure 3.4. This particular LISN serves the purpose of facilitating measurements of conducted noise levels and PLC frequency spectrum on an impedance characteristic more closely aligned with that encountered in actual power line scenarios.

There are three main types of LISNs each of them with having specific usage: V-LISN, M-LISN inserted between the power cord and DUT, T-ISN used for telecommunication lines [130]. The LISN depicted in Figure 3.5 is a V-LISN, below is it's description:

V-LISNs are primarily used to measure the unsymmetric disturbance voltage between one of the mains lines (L or N) and ground. There are two main types of V-LISNs with different inductance values: 5 µH and 50 µH. V-LISNs with 5 µH inductance are typically employed for testing equipment designed for vehicles, boats, and aircraft that are connected to on-board power systems with DC or 400 Hz frequencies. On the other hand, V-LISNs with 50 µH inductance, according to international standards [131], are intended for testing equipment that operates at mains frequencies of 50 Hz or 60 Hz.

To conduct measurements on a higher impedance, such as the one presented in the EN55016-1-2:2014 standard trace depicted in Figure 3.4, specific modifications to the LISN illustrated in Figure 3.5 [125] are necessary:

- C5=C6=3,3μF
- L5=L6=0Ω
- R5=R6=1kΩ

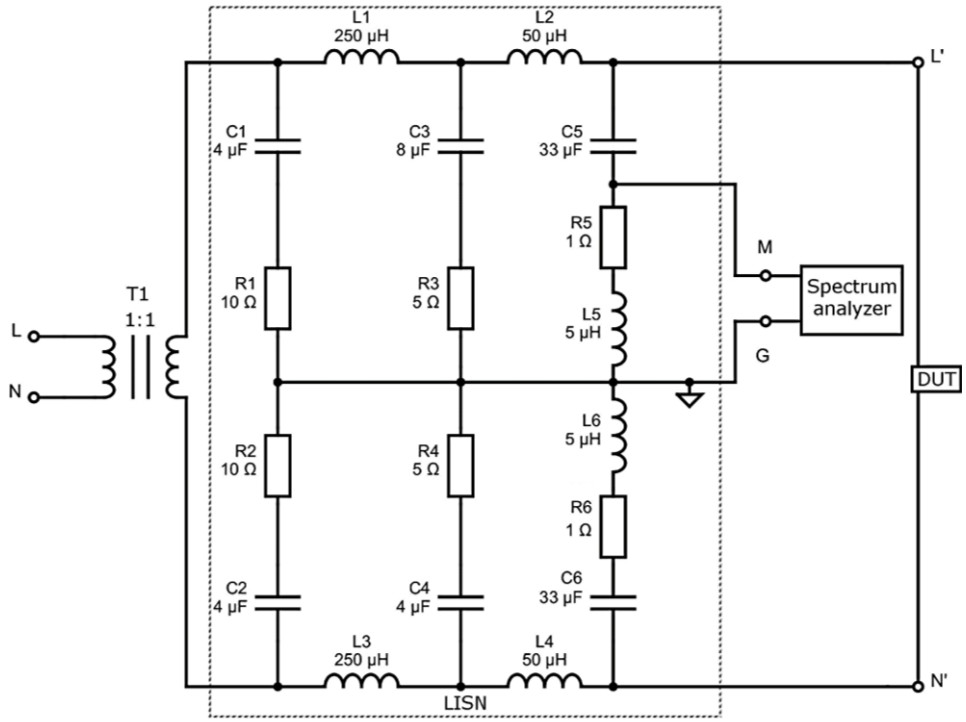

Figure 3.5 PLC signal level and CE measurement setup

Table 3.2 provides explanations regarding the components used in the measurement setup from Figure 3.5.

Table 3.2 Noise level measurements and PLC signal measurement setup explanations

Components	**Explanation**
T1	For safety reasons an isolation transformer is used.
L1 to L4, R1 to R4 and C1 to C4	These components are employed to achieve a noiseless AC power supply characterized by a predetermined impedance profile. This involves the utilization of L-C filters, featuring air-core inductors and film capacitors.
C5, R5, L5, L6, C6 and R6	The components are part of the low impedance simulation circuit depicted from Figure 3.3 .
Spectrum analyser	A spectrum analyser is connected through a BNC cable to the measuring port of the LISN. The conducted noise is not always symmetric so the measurements should be performed on both L' (between R5 and ground) and N' (between R5 and GND). For these measurements I have used R&S® FSL3 spectrum analyser [132].

3.2.3 PLC SNR, RSSI and power measurement setup

The purpose of this section is to provide an overview about the setup used of for PLC SNR, RSSI and power measurements.

Figure 3.6 illustrates the measurement setup featuring two LISNs, each powered from isolated mains voltage and equipped with filtering to maintain a noise-free and well-controlled impedance environment. The sole pathway through which the PLC signal can couple is via the 50Ω measurement ports, allowing for the introduction of attenuation to simulate the effects of a power line segment. Each LISN is paired with a modem, with one operating in TX (transmit) mode and the other in RX (receive) mode. On the RX side, a metrology ADC continuously monitors the power consumption of the load. For a detailed list of the components and devices utilized in the setup, please refer to Table 3.3.

The test configuration has been developed in accordance with both international standards for PLC [27], [133] and industry-specific standards for PLC technology [82], [112], [121]. Furthermore, to enhance its functionality, I have integrated advanced power measurement using a metrology ADC. The power measurement feature is used to establish correlations between PLC channel quality metrics and power measurements of the load allowing the identification of loads generating noise in the PLC frequency band.

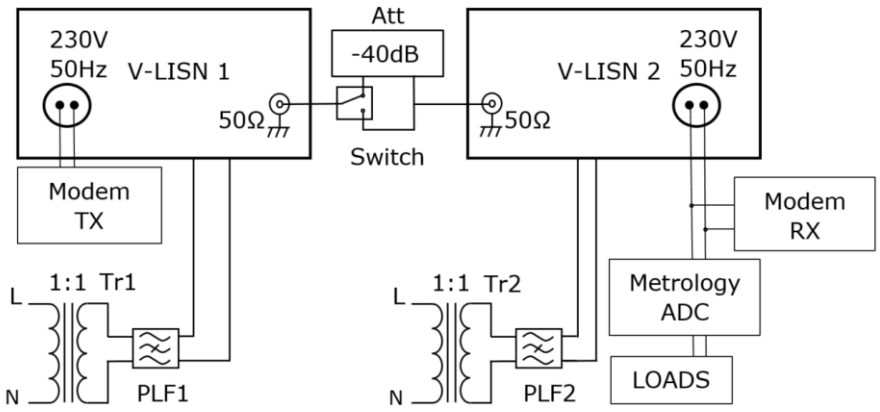

Figure 3.6 PLC SNR and RSSI measurement setup

Table 3.3 PLC SNR and RSSI measurement setup components

Components	Explanation
Tr1 and Tr2	Isolation transformer with 1:1 ratio are used for safety purposes and, dampen transients in the AC supply network and avoid ground loops [134].
PLF1 and PLF2	PLFs are used to supplement the filtering from the LISN so that it achieves the best noise floor, limited by the spectrum analyser capabilities [125].
V-LISN1 and V-LISN2	The V-LISN is utilized to quantify the unsymmetrical disturbance voltage between either line L' or N' and the ground [135]. For these measurements I have used R&S®HM6050-2 V-LISN [136].

Att	A passive attenuator serves the purpose of emulating the attenuation experienced on a power line segment connecting two modems.
Switch	The switch allows to have 2 cases, with and without -40dB attenuation.
Modem TX, Modem RX	In order to measure the SNR and RSSI one modem is configured in transmit mode –denoted TX while the other is configured in RX mode –denoted RX. In this test setup PLC-G3 modems from Texas Instruments® were used [114].
Metrology ADC	A metering AFE, called STPM32® from STMicroelectronics™ was used for metrological measurements of the loads. It's error is below 0.1% over a dynamic range of 5000:1, allowing currents in the range of 24mA to 120A to be measured with 0.1% maximum error [137].

3.3 Measurement results and analysis

This section presents the following practical results: noise level measurements, spectrum of the signal at the output of the PLC modem, PLC channel quality statistics with and without noise influence and load power measurements. The scope of this section is to provide practical validation of the concept presented in section 3.1.

3.3.1 Conducted noise and PLC signal spectrum measurement results

Noise level measurement of six common SMPS and spectrum of the PLC signal have been performed using the measurement setup described in Section 3.2.2. I have utilized a LISN HM6050-2 and an FSL 3 Spectrum Analyzer, both from R&S™. The settings of the spectrum analyzer are: RBW= 200Hz, VBW= 300Hz, SWT=60s, Detector type PkMax, Frequency sweep start=9kHz, Frequency sweep stop=150kHz.

In order to generate all the PLC-G3 carriers for spectrum measurement a PLC-G3 modem from Texas Instruments® was used [114], with the following settings: OFDM-D8PSK modulation, maximum output level, continuous transmission mode.

Figure 3.7 illustrates the spectrum analyzer measurements of CE generated by six common devices utilizing SMPS on a low-impedance setting. The most substantial noise levels are attributed to the 500W ATX PC PSU, phone charger, and CCFL light bulbs.

The PLC signal level measured at the modem output should be between 120 dBµV and 134 dBµV [27] thus the CE generated by the loads in Figure 3.7 might affect PLC communication.

Figure 3.8 and Figure 3.9 present the PLC-signal frequency spectrum at the output of a PLC-G3 modem while transmitting on low power line impedance respectively high power line impedance. These measurements serve as a practical illustration of how impedance affects PLC carriers and the frequency selectivity characteristics of the power line concerning the PLC signal.

Output level measurements were performed using channel power measurement IBW method, which uses integration in the specified bandwidth to measure the modem output level. The results of the output level measurements on simulated low electrical grid impedance respectively high electrical grid impedance

are shown in Figure 3.10 and Figure 3.11. When transmitting over a high power line impedance, the PLC signal exhibits a 6 dBµV higher power compared to transmission on a low power line impedance. The test setups for simulating both low and high power line impedance are detailed in sections 3.2.1 and 3.2.2 by explaining how the standard LISN was modified and adapted to simulate both low and high impedance conditions.

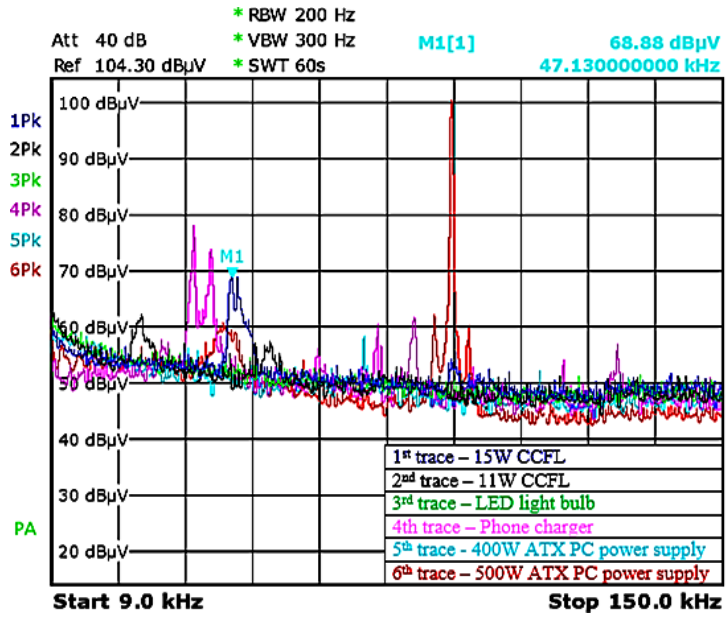

Figure 3.7 CE measurements in NB-PLC frequency band [19]

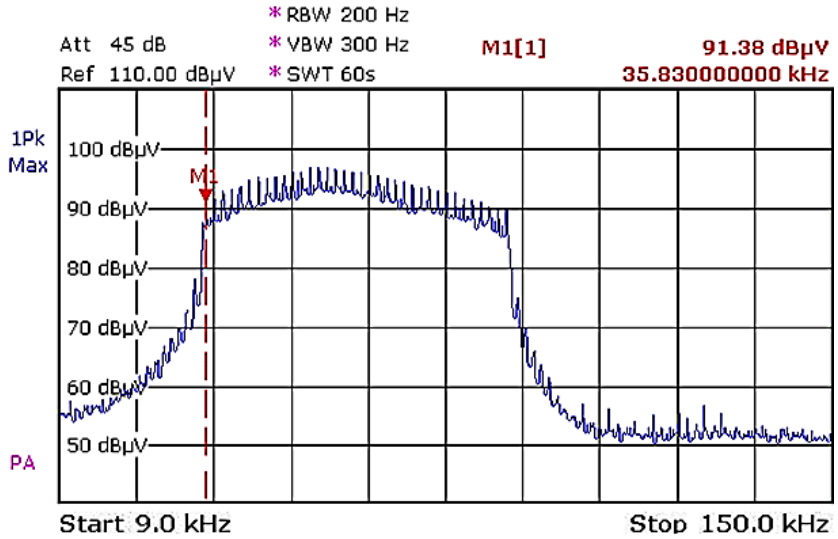

Figure 3.8 PLC-G3 signal's frequency spectrum at the modem's output on low LISN impedance [19]

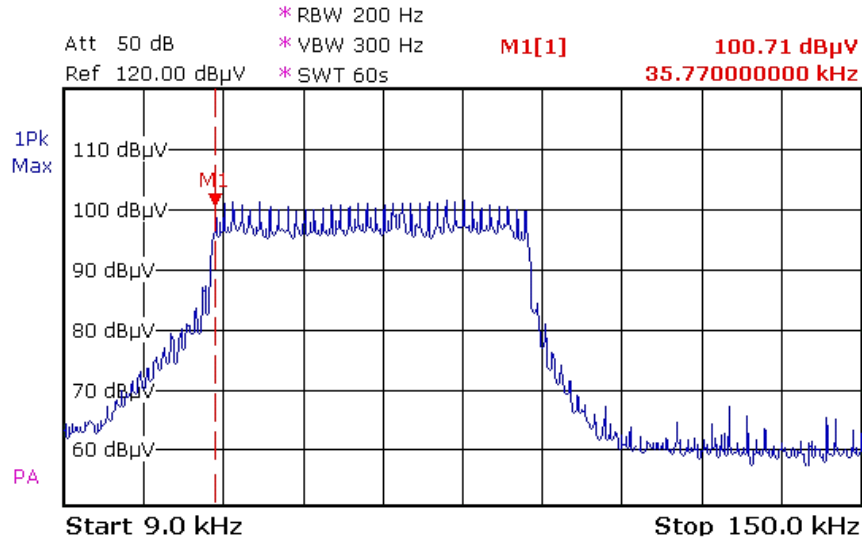

Figure 3.9 PLC-G3 signal's frequency spectrum at the modem's output on high LISN impedance [19]

Comparing Figure 3.7 against Figure 3.8 and Figure 3.9 it can be seen that 500W ATX PC supply, phone charger and 15 W CCFL generate noise that can impact the PLC-G3 communication.

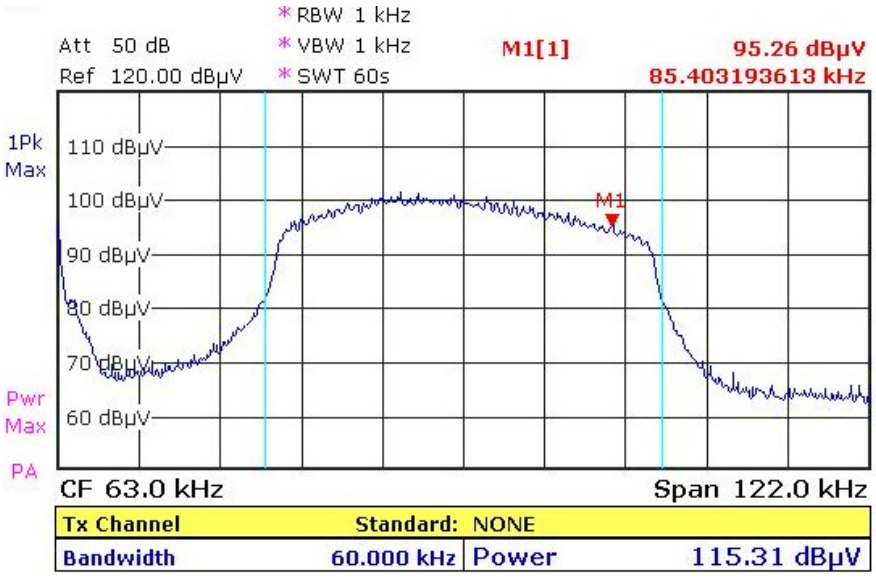

Figure 3.10 PLC-G3 signal's channel power and PSD at the modem's output on low LISN impedance [19]

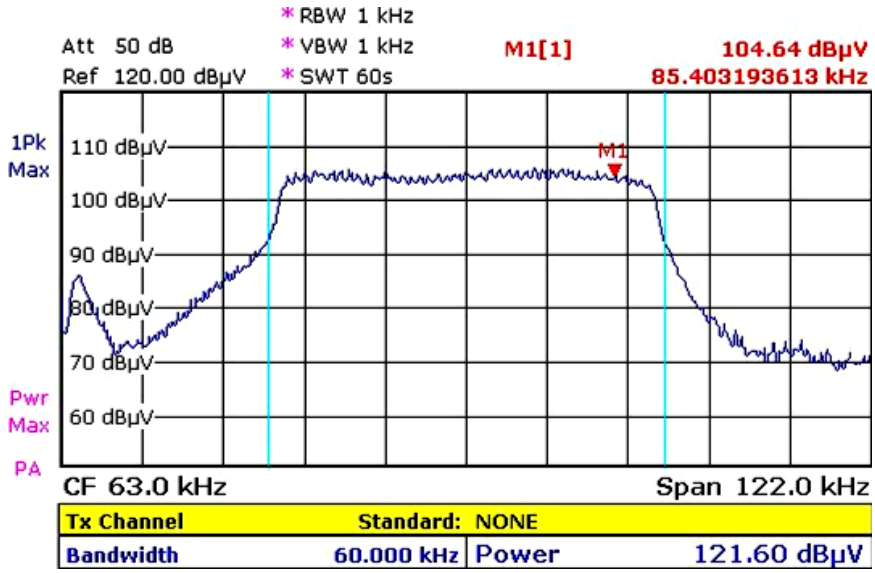

Figure 3.11 PLC-G3 signal's channel power and PSD at the modem's output on high LISN impedance [19]

PLC-G3's PAPR is rather high and equals the crest factor when expressed in decibels. PLC-G3's PAPR≈18.6 dB because it has n=36 carriers [121]. The high PAPR makes the 36 carriers visible during frequency spectrum measurements at the output of the PLC-G3 modem. Equations (3.12)-(3.15) provide a detailed calculation of PLC-G3's PAPR.

$$PAPR = \frac{|x|^2_{peak}}{x^2_{rms}} \tag{3.12}$$

$$PAPR_{dB} = 10\,log_{10}\,\frac{|x|^2_{peak}}{x^2_{rms}} \tag{3.13}$$

$$PAPR_{dB} = 10\,log_{10}\,n + 3.01dB \;\big|_{n=36} \tag{3.14}$$

$$PAPR_{dB} = 18{,}57\;dB \tag{3.15}$$

Typical values for PLC-G3 Rx sensitivity of 20 μV_{RMS} or 26 dBuV are achievable with ROBO modulation in coherent mode and a PER> 5 % [103], [111].

As practical example if one assumes a 40 dB attenuation on the power line between two modems and there is a device generating 60 dBµV noise in the PLC frequency band, the RSSI deteriorates to a point where reliable communication is no longer feasible, equations (3.16) and (3.17) describe this example:

$$RSSI_{dB} = A_{signal,dB} - A_{noise,dB} - A_{powerline,dB} = 20\;dB\mu V \tag{3.16}$$

$$20\;dB\mu V = 10\;\mu V_p \tag{3.17}$$

3.3.2 Load influence on channel quality

SNR, RSSI and power measurements have been performed using the measurement setup and test methods presented in section 3.2.3 . Figure 3.12 together with Figure 3.13 presents PLC-G3 channel quality measurements; one

modem is in TX mode and the other in RX mode. I have taken measured SNR and RSSI under the influence of the six typical loads evaluated in section 3.3.1. These measurements were conducted both with and without the presence of -40dB attenuation introduced between the two modems. This attenuation serves the purpose of emulating the characteristics of a power line segment, allowing the simulation with test conditions closer to the real-world.

The negative SNR reported by the PLC modem in Figure 3.13 when exposed to CE from the 500W ATX PSU, and in the presence of 40dB attenuation between the modems, serves as a compelling illustration of PLC-G3's OFDM technology capacity to sustain communication even when the noise level exceeds that of the PLC signal [138].

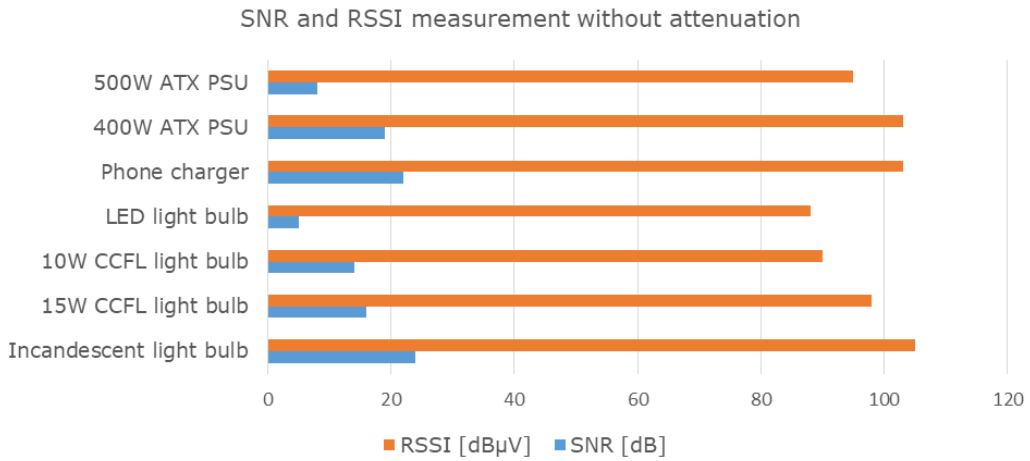

Figure 3.12 PLC-G3 SNR and RSSI measurements without channel attenuation

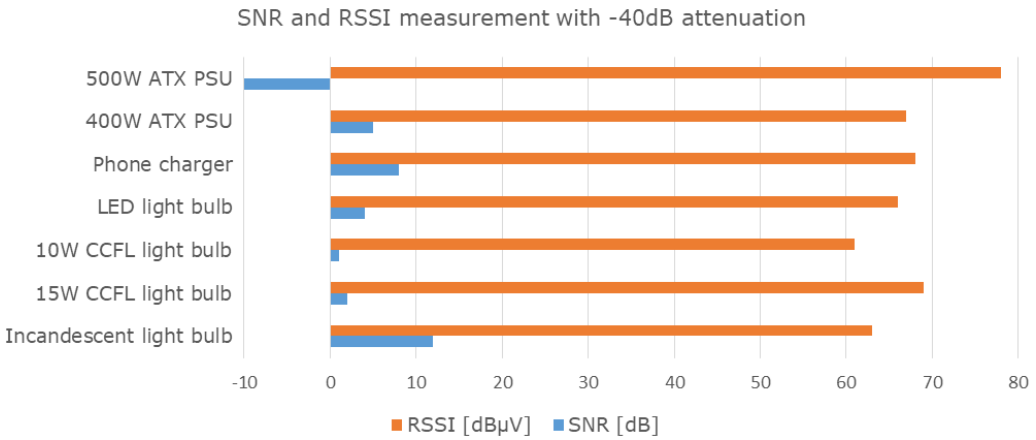

Figure 3.13 PLC-G3 SNR and RSSI measurements with -40 dB channel attenuation

Figure 3.14 presents the power measurements of the loads for which their influence in channel quality was assessed and is presented in Figure 3.12 and Figure 3.13. A reference meter having the error e<0.05% [139] was used to validate that the measurements reported by the metering ADC are accurate. The metering ADC measures current and voltage as well as the phase shift between

them and computes P, Q, S and PF. The total power consumption of the loads was found to be P= 246 W, Q= 134 VAR, S= 280 VA while PF= 0.88.

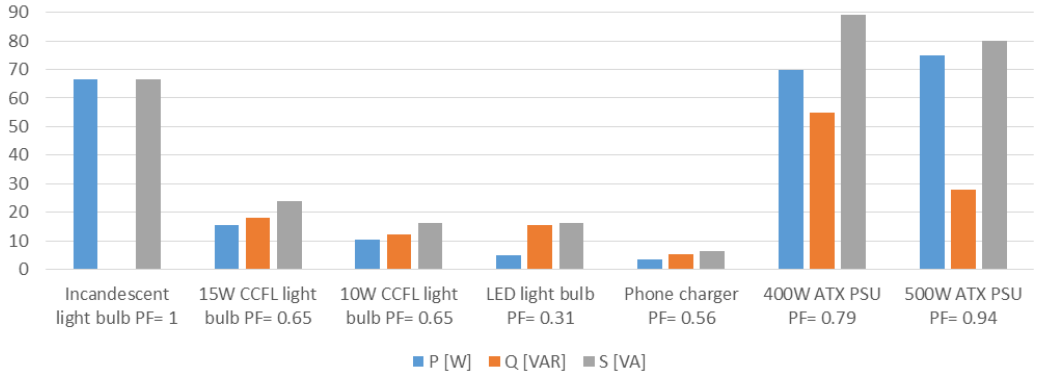

Figure 3.14 Power measurements of the six common loads

3.4 Enhanced SM concept

Beyond the SM concept discussed in section 3.1, I have designed a metering system that utilizes the same PLC-G3 modems from Texas Instruments™ [114]. However, this system incorporates a cutting-edge metrology AFE from Analog Devices™ capable of self-calibrating together with sensor supervision [140], [141] and features a power supply design comprising a non-isolated flyback converter followed by a buck converter.

The primary motivation behind the development of the new SM concept was to investigate the potential interference between the mSure™ technology utilized in the metering AFE and PLC. This is due to the fact that mSure™ superimposes a proprietary AC signal onto the mains AC waveform which passes through the metrology shunt for the purpose of self-calibration and sensor supervision [142]. Wi-Fi connectivity has been introduced to serve as a backup option for connectivity, particularly in situations where PLC communication may be unreliable. Additionally, Wi-Fi offers a reliable connection when accessible. Furthermore, Wi-Fi is incorporated to provide straightforward and easily accessible connectivity to the SM.

3.4.1 Architecture of the enhanced SM with PLC and Wi-Fi

In this section, I will introduce the key components of the enhanced SM architecture and explain its practical application as an operational SM. While the architecture is not yet fully functional as a comprehensive SM—lacking components such as metrological output (LED), buttons, and display—I have concentrated solely on the newly introduced components, particularly those that might potentially influence each other. The enhanced SM architecture proposed by me is presented in Figure 3.15. The architecture combines power supply units, microcontroller, communication modules, and metrology AFE to provide accurate energy monitoring and communication capabilities for effective SG applications. Below is a brief description of the main features:

- Compatibility with the CE detection and avoidance methodologies that were presented in section 3.2.

- High efficiency SMPS PSU comprised out of a flyback converter supplying the PLC AFE and a buck converter that further steps down the voltage to 3.3V for the digital part of the SM. The flyback converter is non-isolated so that the metering AFE can use shunt based measuring system in together with the CT used for metrology checks. The PSU implementation details are presented thoroughly in section 3.4.2.
- ESP8266 microcontroller with Wi-Fi connectivity, facilitating data communication and remote monitoring capabilities [143]. Wi-Fi is incorporated for backup connectivity in case PLC is unreliable. It also offers user-friendly access to the SM. ESP8266 is compatible with a range of development platforms for programming.
- ADE9153B is an energy metering AFE with sensor supervision and auto-calibration capabilities. Sensor supervision ensures measurement accuracy by monitoring both current and voltage channels, while auto-calibration automatically calibrates these channels over time [140], [142]. This feature is particularly valuable in maintaining accuracy as SM age. The metrology implemented in the enhanced SM is presented in section 3.4.3.
- The PLC solution utilizes the Texas Instruments™ TMS320F28PLC84 processor along with the AFE031 AFE, optimized for AMI networks in SGs, NB-PLC within the CENELEC frequency band, and complete PLC protocol stack execution [103]. PLC coupling is achieved through capacitive coupling, which is feasible from a galvanic perspective because the ground reference of the electronic components within the SM is referenced to the phase.

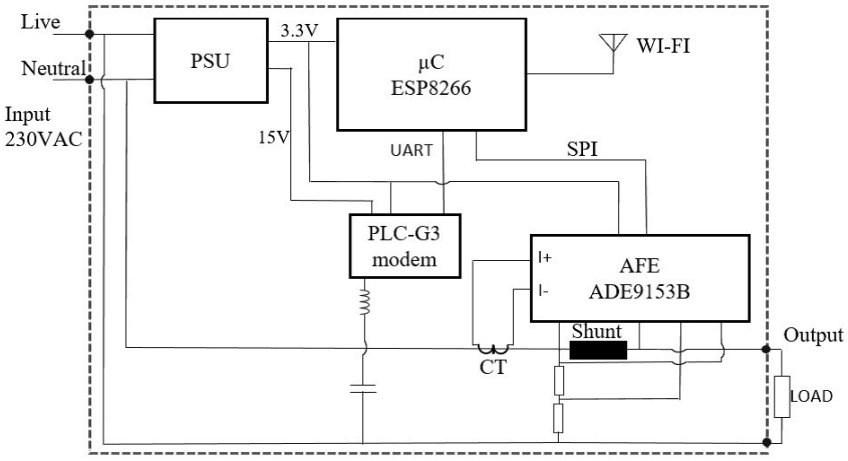

Figure 3.15 Block diagram of the enhanced SM with PLC and Wi-Fi [21]

3.4.2 Power supply implemented in the SM

The enhanced SM PSU uses a non-isolated flyback converter for stepping down to 15V the mains rectified and filtered voltage and then the voltage is further stepped down to 3.3V using a buck converter. The PLC AFE uses 15V, but the rest of the components use 3.3V. The SM PSU structure is presented in Figure 3.16 while the flyback converter and buck converter implementation is presented in Figure 3.17 and Figure 3.18 with electronic component explanations in Table 3.4.

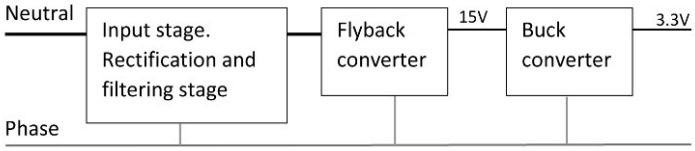

Figure 3.16 Block diagram of the SM PSU [21]

The flyback converter SM PSU composed out of the flyback converter from Figure 3.17 and buck converter from Figure 3.18 adheres to the following design criteria that is specific to electricity SM's requirements:

- It must withstand a 440VAC earth fault for 4 hours. Although this is a requirement specific for 3-phase meters this fault can occur also in single phase installations [144].
- It is optimized to achieve an efficiency of 70% under full load conditions (1.3A) with a nominal input voltage of 230VAC. Enough conversion efficiency must be achieved in order to meet the 2W power consumption when the SM is just recording energy [145].
- The design should operate effectively within an extended input voltage range of 172VAC to 265VAC and a temperature range -40°C to +85 °C [144].
- The design should also be pre-compliant with relevant EMC standards and electrical tests for SM's featuring PLC [27]. This requirement is applicable for the entire SM, but the flyback converter is the primary contributor to emissions in this case.

In this application, I have opted for Zener diode snubber over resistor-capacitor snubber for the primary side of the flyback converter. This choice is made to reduce losses and enhance efficiency, as Zener diodes conduct for a shorter duration within the primary switching pulse, and they also provide better protection for the flyback controller transistor, in this case integrated in the IC. However, for the purpose of enhancing EMC emissions, the use of a resistor-capacitor snubber will be necessary due to lower dv/dt and di/dt slopes.

The components of the SMPS described in Table 3.4 have been selected forgiven for optimum performance in terms of efficiency, output voltage stability and reliability. To achieve a robust and efficient SMPS design, during component selection, various stress factors were considered, including voltage and current ratings, switching frequency, and temperature.

Table 3.4 SM PSU component description [21]

Reference	Description
NTC1	Thermistor used for inrush current limiting
VDR1	Voltage dependent resistor for surge protection
L1,C1	LPF for suppressing CE
D1, D2	Diodes used for half-wave rectification of mains
C2,C3	Rectifier filtering capacitors
R1, R2, R3, R4	DC balancing resistors
D3, DZ1	Primary side snubber with Zener diode
T1	Transformer used by the flyback converter
D4	Flyback secondary side diode
C4, C5	Flyback secondary side filtering capacitors

R5, R6	Voltage divider for providing the feedback signal, scaled from 15V to 3.3V
D5	Prevents reverse current flow during converter start-up
R7	Limits the current flowing into internal shunt regulator of IC1
C6	decoupling capacitor, which also stores the energy necessary for IC1 during start-up phase
R8	Adjusts the amount of current flowing in the drain of IC1
C7, C8, R9	Voltage feedback loop compensation network
IC1	STMicroelectronics™ Viper26K SMPS controller IC [146]
C9, C10	Buck converter input decoupling capacitors
IC2	TPS62177DQCR buck converter controller IC from Texas Instruments™ [147]
L2	Buck converter switching inductor
R10	Power good pull-up resistor
C11, C12	Buck converter output capacitor, used for filtering

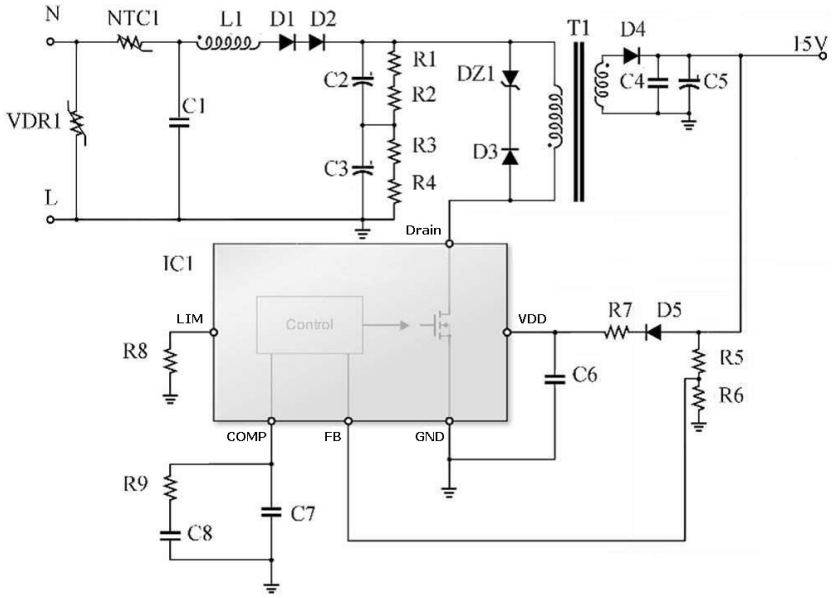

Figure 3.17 Flyback converter part of the SM PSU [21]

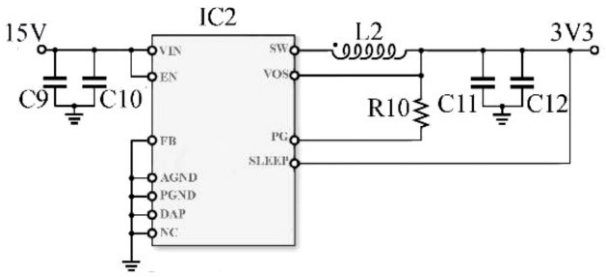

Figure 3.18 Buck converter part of the SM PSU [21]

3.4.3 Metering AFE implemented in the SM

The ADE9153B is an energy metering AFE with sensor supervision and auto-calibration capabilities suitable for single-phase SM applications. Sensor supervision involves assessing the accuracy of energy measurements by supervising both the current and voltage channels. Auto-calibration enables the meter to automatically calibrate the current and voltage channels without the need for additional equipment [140], [142]. This feature is valuable as SMs age over their lifetime, potentially experiencing accuracy drifts.

Figure 3.19 illustrates the connection of the metering AFE to the sensors for measuring and monitoring current and voltage readings [142]. The metering AFE incorporated in the enhanced SM concept and depicted in Figure 3.19 has the following features:

- Phase bypass: When the shunt is short-circuited, it alters the gain. Phase and neutral current monitoring should ideally report similar values thus mismatches indicate a tampering event involving a separate current path at mains frequency.
- CT saturation by and DC magnetic field: The gain changes when the CT is saturated. Traditionally the SMs use hall effect sensor to identify DC magnetic fields tampering attempts.
- Double bypass when both the shunt and CT are short-circuited: The gain of the shunt is altered.
- The sensor monitoring and self-calibration processes are executed without influencing the metrology because the metering AFE overlays a known signal onto the mains, which is then measured.

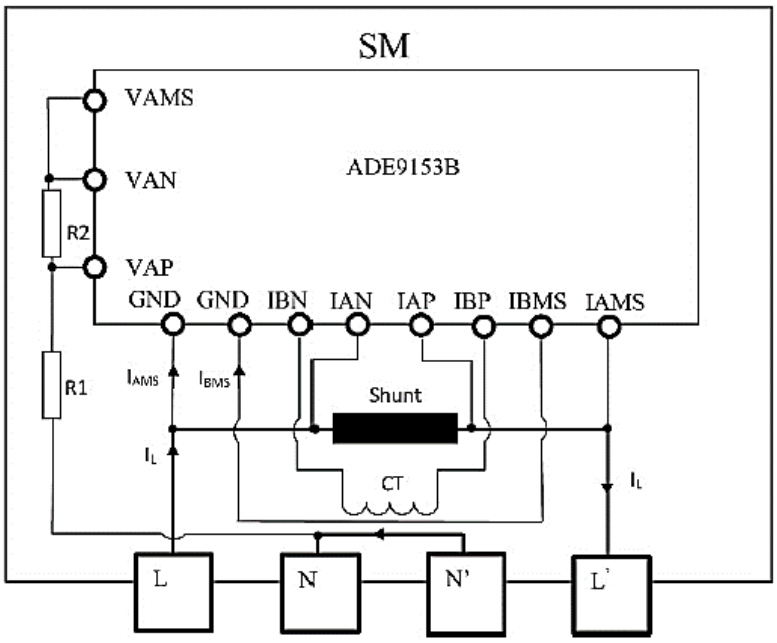

Figure 3.19 Block diagram of the metrology part of the enhanced SM [21]

Metrological values are measured through the conventional signal path using the following AFE analog inputs:

- IAN and IAP differential inputs used to measure over the phase connected shunt.
- IBN and IBP together with a CT monitor the neutral current flow.
- VAP and VAN used for voltage measurement.

Tamper detection and self-calibration are accomplished by injecting and monitoring signals with frequencies higher than the mains frequency through the following AFE pins:

- IAMS applies a control signals through the shunt, requiring four shunt connections for accurate results (two for metrological measurements and two for the control signal).
- IBMS is connected to a wire passing through the CT and going to system GND.
- VAMS is utilized for monitoring the resistive voltage divider integrity.

3.4.4 SM software considerations

The Espressif ESP8266EX is a comprehensive Wi-Fi system-on-chip solution designed for Internet of Things applications [143]. The primary rationale behind selecting this microcontroller is its extensive library support and the user-friendly IDE. The SM uses an ESP12E Wi-Fi module, based on the ESP8266EX chipset, is utilized and connected to a 2.4 GHz PCB Wi-Fi antenna.

The software component was created within the Arduino IDE, building upon the EVAL-ADE9153ASHIELD Arduino libraries that offer fundamental functions for interfacing with the ADE9153A. During SM's development, the libraries from the following sources were employed [148], [149].

Through additional development efforts, the following functionalities within the SM:

- Calibration using a metrological power supply.
- Self-calibration feature for both current and voltage measurement channel.
- Instrumentation value such as current, voltage, frequency, and power factor.
- Detecting tampering events within a 60s timeframe.
- Enabling communication via both Wi-Fi and PLC.
- Displaying all pertinent metrological values on a webpage.

3.4.5 SM functionality testing methods

To assess and validate the capabilities of SM, the demonstrator presented in Figure 3.20 and Figure 3.21 was constructed with the following elements:

- An isolation transformer featuring two coils, one designated for isolated mains supply and the other as phantom loading.
- Shunt wire connected in parallel with the current measuring element.
- Switches and signaling lamps are employed for the voltage and current circuits, along with tamper wire control.
- Phantom loading was achieved by using the low-voltage, high-current coil of the transformer in tandem with a high-power resistor. This configuration effectively separates the voltage and current circuits, simulating a load of 1.4 kW, calculated as P= 230V × 6A, while actually consuming only P= 0.8V x 6A =4.8W for the current circuit.

The states of the enhanced SM demonstrator depicted in Figure 3.21 are elaborated in the Table 3.5, while the actual results from the SM webserver are presented in the next section, 3.4.6.

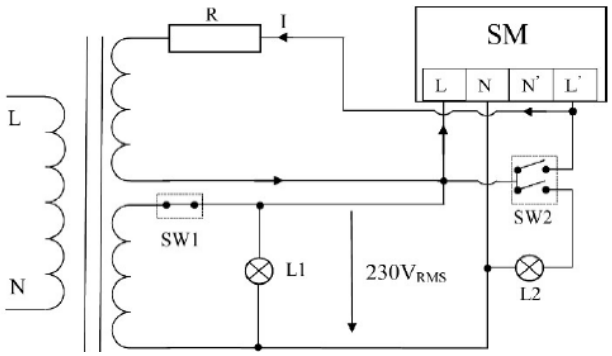

Figure 3.20 Block diagram of the enhanced SM demonstrator [21]

Table 3.5 SM demonstrator states [21]

SW 1 and L1-green	SW 2 and L2-red	Tamper	Description
OFF	OFF	Disconnected	SM unpowered
ON	OFF	Disconnected	SM is operating and I=6A
ON	ON	Connected	SM operating and tamper is active

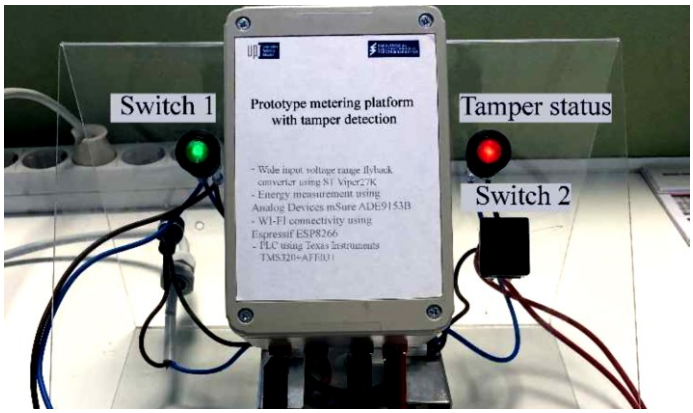

Figure 3.21 Enhanced SM demonstrator [21]

3.4.6 SM functionality testing results

The data of the SM is presented on a webpage through a user-friendly interface enabled by a webserver running on ESP8266EX. The AFE offers various measured and computed values, including instrumentation values, active power, active and reactive power measurements, energy measurements, frequency, PF, as well as estimations derived from sensor monitoring (MS_MON_AICC) and auto-calibration (MS_ACAL_AICC).

Using the test setup presented in section 3.4.5 a tamper was introduced thus, tamper detection is triggered and the SM reports the tamper as shown in Figure 3.22. The tamper detection is triggered by MS_MON_AICC (current reading monitor) difference.

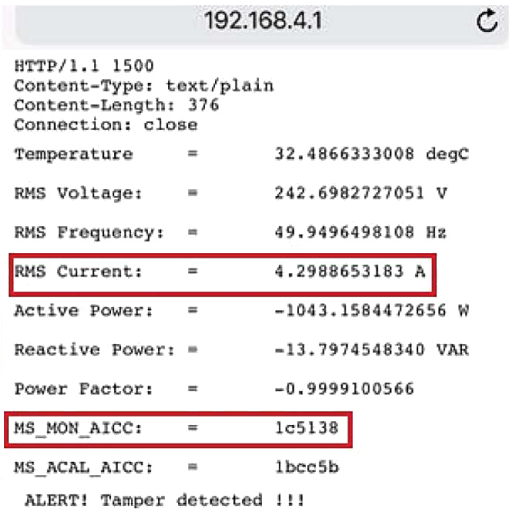

Figure 3.22 Readings and registers indicated by the SM in the webserver interface during tampering [21]

I have conducted practical validation of the PLC functionality in accordance with NB-PLC standards [27], [133]. SM's PLC-G3 modem receiver sensitivity was assessed during an ongoing calibration procedure, utilizing the setup presented in section 3.2.3, no influence was observed in the PLC sensitivity with and without calibration procedure active.

PLC frequency spectrum measurements on low and high simulated power line impedance has been performed without noticing any influence of the calibration signal. Figure 3.23 depicts the frequency spectrum of the PLC-G3 TX broadcast of all 36 carriers over a low simulated power line impedance with calibration procedure active, no perturbation has been measured.

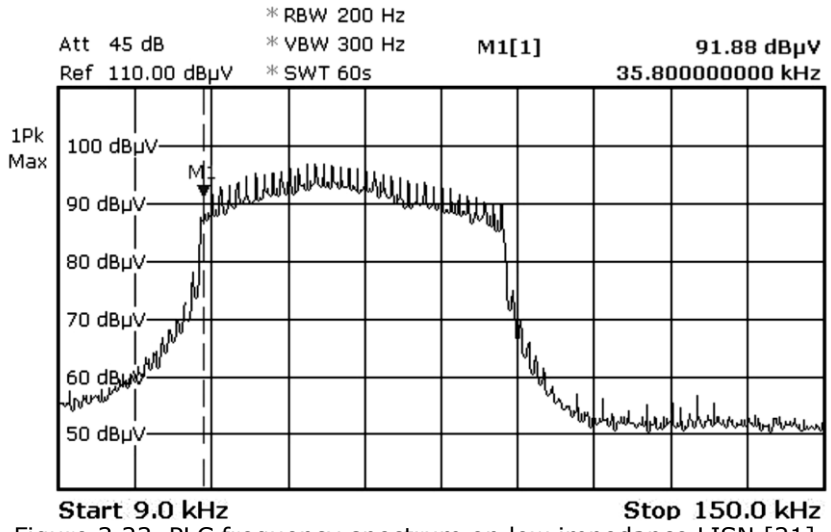

Figure 3.23 PLC frequency spectrum on low impedance LISN [21]

3.5 Chapter summary and future work

In conclusion, this chapter has introduced, presented, and validated a novel approach for identifying CE sources within the PLC frequency band. The method involves correlating load power measurements with quality reports obtained from PLC-G3 modem channels, enabling the detection of interference-causing loads. Practical application includes load detection and interference avoidance through dynamically generated communication schedules when CE-generating loads are inactive.

The significance of this method is underscored by spectrum measurements conducted under both low and high power line impedance conditions, revealing the distinct impact of noise generated by specific loads on the PLC-G3 signal.

Furthermore, an enhanced SM concept has been introduced, incorporating advanced metrology features for precise energy measurements, tamper detection, and self-calibration. This new SM architecture integrates Wi-Fi connectivity alongside PLC, ensuring reliable communication in various scenarios and connectivity with other customer premise devices.

As part of future research endeavors, I plan to advance the conceptual SM outlined in Section 3.4 into a standard one, following the specifications outlined in reference [145]. This enhancement will involve the integration of additional components, including a display, an optical communication port, user interface buttons, relays for load management and consumer disconnection, and the incorporation of a real-time clock. Additionally, there is a compelling need to conduct field experiments to validate the effectiveness of the techniques employed for CE source identification and avoidance.

Results featured in this chapter draw upon my previously published scientific works cited in references [19], [21], [22], [24], [25].

After completing the research activities outlined in this chapter, my contributions include offering research findings as response for one of my initial questions: **What could be non-invasive techniques or solutions available to address the challenges faced by PLC within the SG without the need for grid modifications? If so, what are these techniques, and how can they be effectively implemented?**

A novel method for identifying sources of interference in the PLC frequency band is introduced. This innovative approach leverages the capabilities of SMs to correlate energy measurements from loads with the quality indicators of the PLC-G3 modem channels. This correlation effectively establishes a clear link between energy measurements and the noise generated by specific loads. The practical results further substantiate this correlation, and comprehensive spectrum measurements conducted in laboratory settings offer a robust comparison of noise spectra. This correlation not only validates the method but also enables the development of a transmission schedule based on the activity of noise-producing loads, ultimately enhancing the efficiency of PLC communication.

The **theoretical advancements** stemming from my research endeavors and presented in this chapter are:

- **Introduction of a single phase SM architecture in the context of communication protocols and services present in the power grid.**

A single phase SM architecture with shunt current measurement is introduced within the framework of communication protocols and services found in the electricity network. The architecture aims to incorporate the methods for the identification and avoidance of CE. During its development, off-the-shelf electronic components were

used. Adhesion to international standards was taken into consideration in every step of the SM architecture development. It was progressively developed and is detailed in the subsequent articles [19], [21], [22], [25] and section 3.1 of the doctoral thesis.

- The theoretical contribution involves the development of techniques to identify CE within the NB-PLC frequency band. These techniques harness the inherent components and capabilities of SMs to establish a correlation between power measurements and communication channel quality reports obtained from the PLC-G3 modem.

In Chapter 3 of the thesis, techniques for identifying CE within the frequency band utilized by NB-PLC are formulated. The innovative approach leverages the existing components and functionality of SMs to establish a correlation between power measurements and communication channel quality reports acquired from the PLC-G3 modem. This correlation facilitates the identification of CEs generated by the load and the development of a transmission schedule when the load does not produce CEs (for instance, when it is in a stopped state or operating in a different mode). This novel methodology was published in my article [19].

The **practical advancements** resulting from my research activities and elaborated in this chapter encompass:

- CENELEC A, B, C and D frequency bands CE measurements of common types of loads in NB-PLC frequency using same measurement configuration as per NB-PLC signal spectrum measurements.

I carried out the measurements showcased in Figure 3.7 to underscore and quantify the effect of CE generated by typical loads on the PLC-G3 signal. The results of the measurements have shown that CE identification & avoidance and/ or filtering techniques are a valid research subject. The results have been included in my previous article [19].

- Practical assessments have been carried out in a controlled test environment using channel quality reports from the PLC-G3 modem to evaluate the impact of loads that generate CE on NB-PLC.

Section 3.3 presents the outcomes of the measurements conducted for illustrating the influence of typical loads connected to the low voltage power grid on the PLC-G3 communication protocol. The results outline that the loads connected in its proximity and in the same electrical circuit influence the PLC channel quality reports RSSI and SNR. The results were also published in my previous article [19].

- Practical trials have been conducted to validate the concept of identifying loads generating CE within the frequency band used by NB-PLC using SMs. This validation process involves the correlation of data available within the SM, communication channel quality statistics data from the PLC modem, with power measurements acquired through the metrology ADC, all integrated within the SM. The goal is to pinpoint the loads responsible for generating noise within the power grid and to establish an optimal communication schedule for these specific loads.

Subchapter 3.2 and section 3.3.2 present the validation activities conducted for establishing the feasibility of correlating PLC channel quality information with load power measurements for PLC noisy load detection and its implementation in the SM architecture as a proof of concept. This results of this activity was published in my previous article [19].

- Implementation of an enhanced SM architecture capable of detecting loads generating CE in the PLC frequency band. The enhanced SM has self-metrological check and calibration as well as tamper detection features along with PLC-G3 modem.

In section 3.4 I present an enhanced SM concept that represents an improvement to the one presented in section 3.1. Compared to the architecture presented in section 3.1 it uses the same PLC-G3 modems from Texas Instruments™ but the metrology AFE is capable of self-calibrating together with sensor monitoring and features a power supply design comprising of a non-isolated flyback converter followed by a buck converter. The primary motivation behind the development of the enhanced SM concept was to investigate the potential interference between the mSure™ technology utilized in the metering AFE and PLC. The enhanced SM architecture was presented in my previous article [21] which is an evolution of the architectures presented in my articles [19], [23], [24].

In summary, this section has provided both theoretical and practical novel results such as: techniques for CE detection and avoidance, two SM architectures capable of incorporating these advancements and the adaptation of measurement setups to power line-like impedances. These concepts lay the groundwork for further advancements in SG and PLC.

4 Conducted noise filtering using PLFs

Passive PLFs are employed to address CE in the power grid [150]–[152] or to isolate various PLC network segments [153]. By tackling a few novel problems, I contribute to this field of knowledge. First and foremost, this research serves as a thorough informational resource for developing and evaluating PLFs for NB-PLC filtering applications. It offers an in-depth understanding of the development, integration, and testing aspects related to PLFs for NB-PLC filtering applications by a literature review. The theoretical and practical contributions from this chapter have been expounded upon in the my published work referenced as [20].

The study discussed in this chapter also suggests a novel method for designing and simulating PLFs by using S-parameters. Although S-parameters have been used in design and simulation methodologies before [154], [155], this study is the first to employ this particular strategy to design PLFs for NB-PLC applications.

I have created a 13th order PLF utilizing specially built inductors to show the effectiveness of the suggested design techniques discussed in this section. Below 150 kHz, the intended PLF exhibits substantial insertion loss. With input and output impedances of 3.36, it manages to measure attenuation of more than -130 dB at 50 kHz while still using only 597 mW of power.

This chapter is structured as follows:

- Subchapter 4.1 presents a thorough description of the integration of PLFs into the electrical grid, emphasizing the important grid services and the two primary PLF topology types.
- Subchapter 4.2 acts as a PLF benchmarking guideline outlining the performance tests that must be carried out. There is additional information offered regarding the connection between testing procedures and the actual power grid circumstances.
- Subchapter 4.3, in addition to subchapter 4.2, describes the passive filter standard as well as the safety and immunity tests that need to be performed as part of benchmarking.
- Subchapter 4.4 presents the design, modelling, and assessment of the passive PLF as well as the comparison of the designed PLF with three commercially available PLFs is made. The pragmatic method simplifies the filter design process by using S-parameters.
- In Subchapter 4.5 the PLF whose development is presented in Subchapter 4.4 is subjected to assessment and is juxtaposed with alternative PLFs designed for PLC applications that share comparable traits with the designed PLF. The assessment protocol follows a subset of the previously delineated testing procedures. In order to maintain impartiality, the manufacturers' identities and specific part numbers linked with the PLFs are kept confidential. However, the schematic representations of the reference PLFs, encompassing their constituent values, are unveiled in section 4.5.1.
- Subchapter 4.6 is the concluding section of the research activities presented in chapter 4 in which I propose future research topics in this field of expertise.

4.1 PLF integration, topology and impact in the electricity grid

In this section, I provide an overview of the fundamental types of PLFs, their key characteristics, and explore the interferences that may arise between PLFs and other services within the power grid.

4.1.1 Integration of PLFs in the electricity grid

Typically, PLFs for PLC applications are used in the SG in the following cases:

- Located on the consumer side ideally between the SM and the fuse box to filter the conducted noise produced by the home's equipment [156]. Installing the PLF after the main fuse is not problematic if it does not need a ground connection or if the main fuse is not a RCD. However, if the main fuse is differential or the PLF does need a ground connection, putting the PLF after the main fuse may result in the fuse tripping. In Figure 4.1, this filter use case is designated as PLF Type 1.
- For the purpose of splitting SMs in two PLC areas whilst still connected to the same electrical grid branch. The separation into two sections makes sure that each SM using NB-PLC connects to the appropriate PLC-DC. When many SMs are linked to a branch and an additional DC is installed to increase the throughput, this form of PLF installation is necessary [153]. Figure 4.1 designates this filter use case as PLF Type 2.

The two typical PLF usage scenarios in the low voltage SG are shown in Figure 4.1 [20], [21]. Only single-phase devices are presented for simplicity.

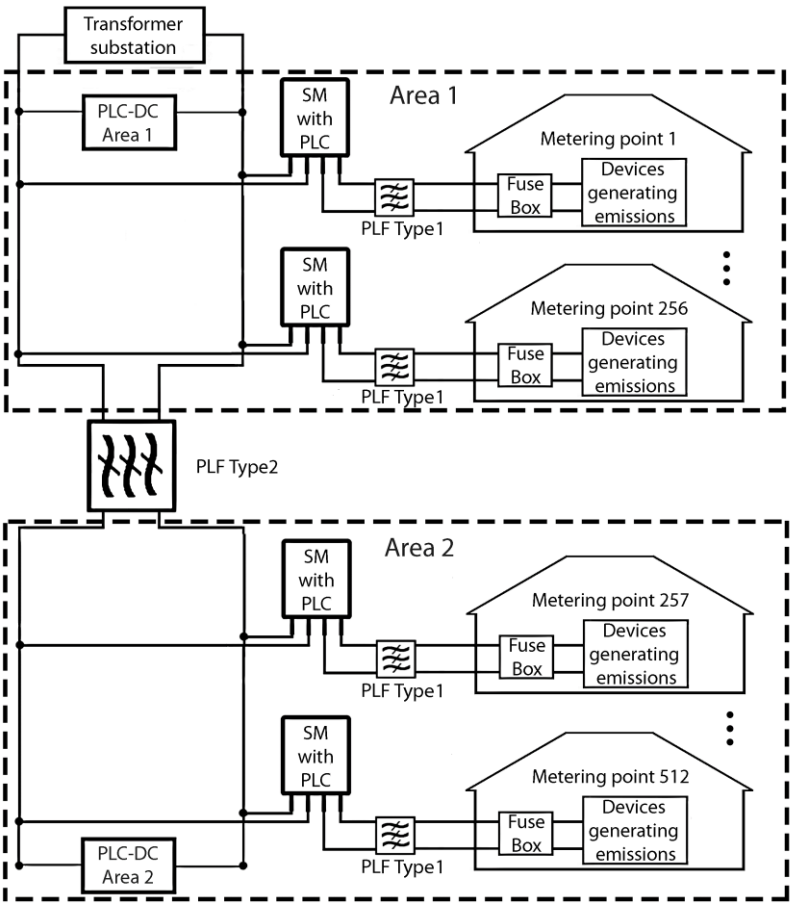

Figure 4.1 PLFs use cases in the SG [20]

4.1.2 PLFs topologies

When it comes to safety ratings, leakage currents, and insertion loss, PLF configurations can be categorized into two main topologies: those with Y capacitors (C_y), which have a central point linked to the protective earth [150], and those without Y capacitors. Figure 4.2 and Figure 4.3 illustrate both types of PLFs, serving as the foundation for various other passive PLF layouts. Additionally, an optional resistor is included to discharge the capacitors and mitigate oscillations at resonance frequencies. Figure 4.2 presents a PLF without a Y capacitor, while Figure 4.3 displays a PLF with a Y capacitor.

The graphic in Figure 4.3 presents the insertion loss, assuming symmetrical loading, of the two PLF configurations depicted in Figure 4.2 and Figure 4.3. These values were obtained through simulation using SPICE. The results indicate that PLFs with Y capacitors, linked to protective earth, tend to provide higher levels of attenuation compared to those without Y capacitors.

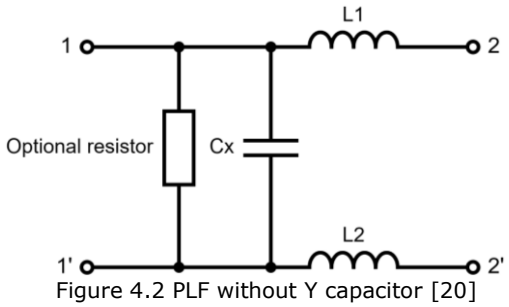

Figure 4.2 PLF without Y capacitor [20]

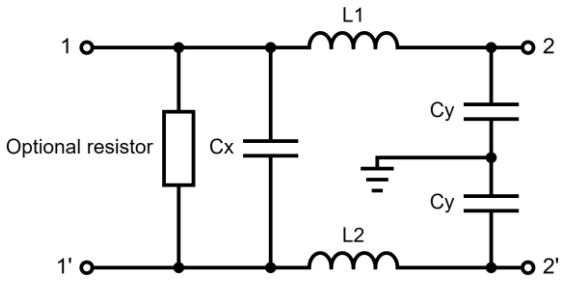

Figure 4.3 PLF with Y capacitor [20]

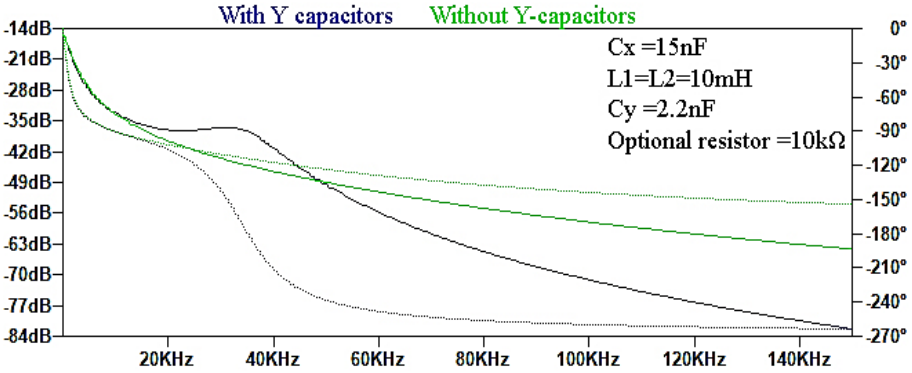

Figure 4.4 PLFs insertion loss using SPICE simulation [20]

4.1.3 Services present in the electrical grid

The grid's features that should not be impacted by the construction of a PLF are highlighted in this section.

4.1.3.1 RCDs

RCDs are employed in the installation as a safeguard against malfunctioning equipment or incorrect user behaviour thus preventing severe electrical injury [157]. Because the most typical tripping current of an RCD is $I_{\Delta n} \leq 30$ mA, installing a PLF with leakage current after the main fuse may present a problem. The tripping current of some RCDs can be changed. It is important to note that Y capacitor leakage might change over time as a result of capacitor aging, which could result in inconsistent RCD tripping.

4.1.3.2 RCS

RCSs are integral components of a remote control system that enables the centralized switching of multiple loads simultaneously. To ensure the proper functioning of this system, it is essential for the signal to reach the receiver sites from the injection point. The frequency band of the ripple control signal ranges from 110 Hz to 3000 Hz [83], making it susceptible to filtration by the PLF.

4.1.3.3 Remote control of the relay disconnect unit

When the power supply is cut off from the SM disconnect unit, some SMs have the capacity to detect the condition of the main fuse. By turning the main fuse on and off, this functionality allows the customer's electricity supply to be restored by remotely closing the SM's disconnect unit [158]–[160]. It is important to note that if a PLF is inserted between the SM and the fuse box, it may affect this feature. Although the precise implementation details are not given, this function often requires signal injection and measurement, which may be impacted by PLF.

4.2 PLF benchmarking

I describe the performance tests that should be performed as part of the benchmarking procedure in this section. The insertion loss, PLC signal filtering capabilities, and impedance are all evaluated throughout these testing.

According to the data from section 3.2.1 compared to standard LISNs, power line impedances encountered in practical settings range from 4 to 15 times lower. The adaptive impedance circuit shown in Figure 3.3 can be used to improve the test setups for insertion loss measurement and PLC signal filtering so that measurements are made on impedances that are more like actual impedances.

4.2.1 Insertion loss

Filters insertion loss can be assessed in laboratory environment by utilizing a VNA [151] or FRA to measure their insertion loss (transfer function). FRAs, in general, are suitable for lower frequency measurements and work well with power line couplers while VNAs are suitable to be used on a broader frequency range but might require careful configuration for low impedance measurements [161]. Figure 4.5 and Figure

4.6 illustrate an offline setup for insertion loss measurement [162], while Figure 4.7 shows an online insertion loss measurement setup employing line couplers [163], an AC power supply, and loads.

Measurement setup from Figure 4.7 can be challenging to implement due to non-standard values of Z_S and Z_L at PLC communication frequencies.

Passive impedance matching circuits can be used to quantify the insertion loss of the filter when the impedance is different from the standard 50Ω. Passive impedance matching circuits can only match impedance at a certain frequency, which is one of its limitations. With impedances other than 50Ω, it may be necessary to employ numerous matching circuits to acquire precise insertion loss measurements. Using baluns [164], [165] which are actually matching transformers, is another method for non-50 measurements. In order to avoid the necessity for an impedance matching circuit and to ensure accurate measurements even when Z_L and Z_S are different to 50Ω, I have found commercially available FRA models that include separate ports for signal measurement and injection to the DUT [166].

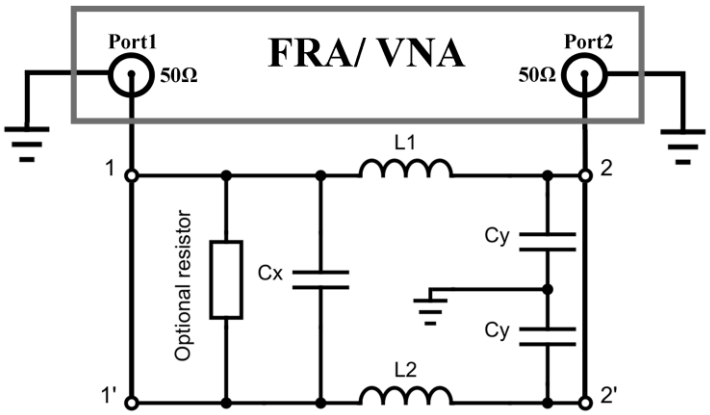

Figure 4.5 PLF offline insertion loss measurement setup, common mode measurement [20]

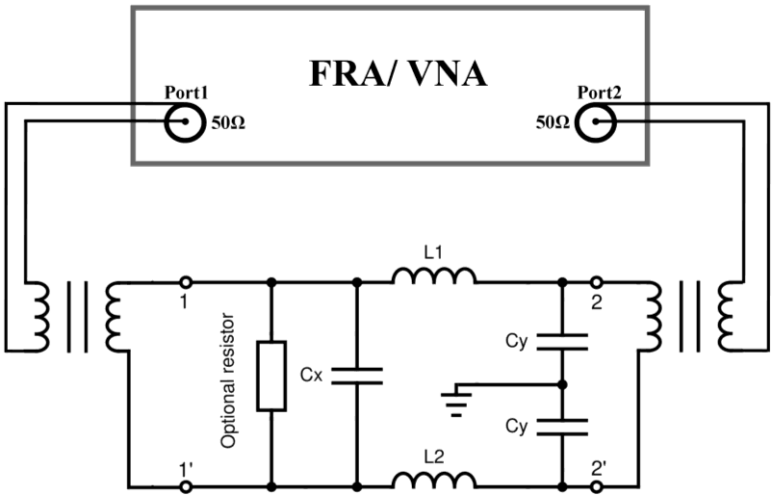

Figure 4.6 PLF offline insertion loss measurement setup, differential mode measurement [20]

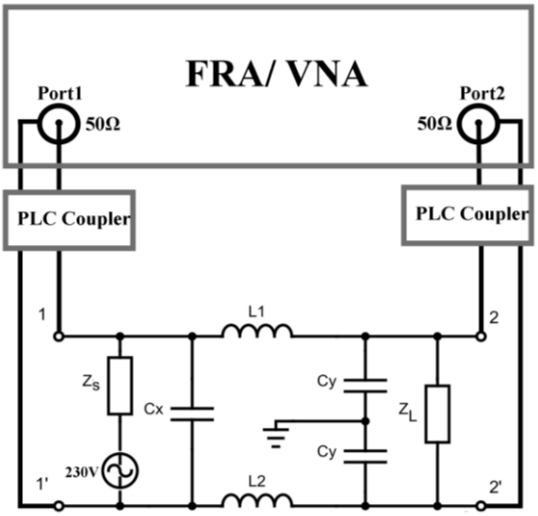

Figure 4.7 PLF online insertion loss measurement setup version 1 [20]

To ensure a controlled input impedance and a noise-free power supply, a LISN along with two PLC couplers were used to create the measurement setup depicted in Figure 4.8. This configuration is derived from PLC and EMC standards [33], [125].

Noteworthy features of the setup include:

- An isolated AC power supply, achieved through the implementation of an isolation transformer.
- A symmetrical V-LISN that enables symmetrical measurements on both the phase and neutral lines. The unused half of the LISN is properly terminated with the standard 50Ω impedance.
- The ability to adjust Z_{in} and Z_L to attain the desired impedance at the filter's port.

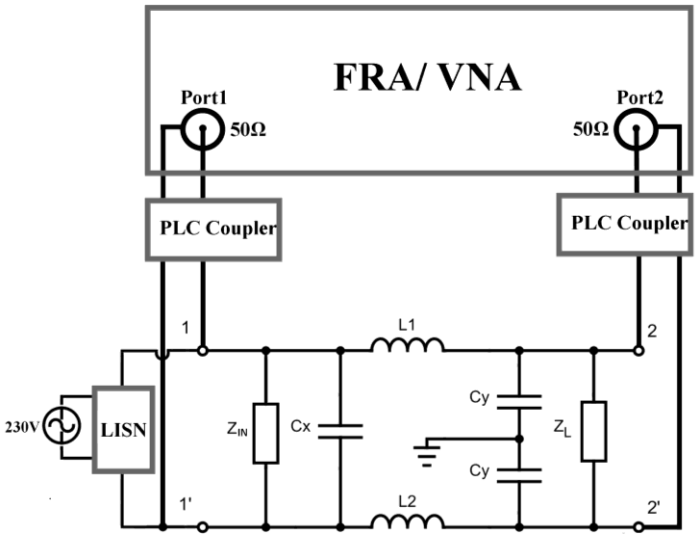

Figure 4.8 PLF online insertion loss measurement setup version 2 [20]

4.2.2 PLC signal filtering

When there is a need to separate PLC devices connected to the same voltage transformer, it becomes necessary to assess the capability of the PLF to block PLC signal. This requirement and its corresponding details are elaborated in section 4.1.

The PLC signal blocking capability of the PLF can be assessed without a FRA or VNA in two pragmatic ways:

- Use PLC modems connected at both ends of the PLF and measure the RSSI and PER, as shown in Figure 4.9.
- Configure a PLC modem in transmit mode and measure the signal level with a spectrum analyser before and after the PLF, as shown in Figure 4.10.

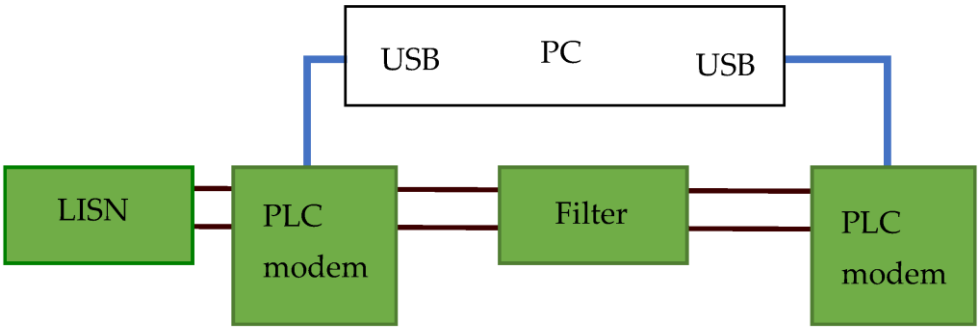

Figure 4.9 PLC signal filtering capability measurement setup version 1 [20]

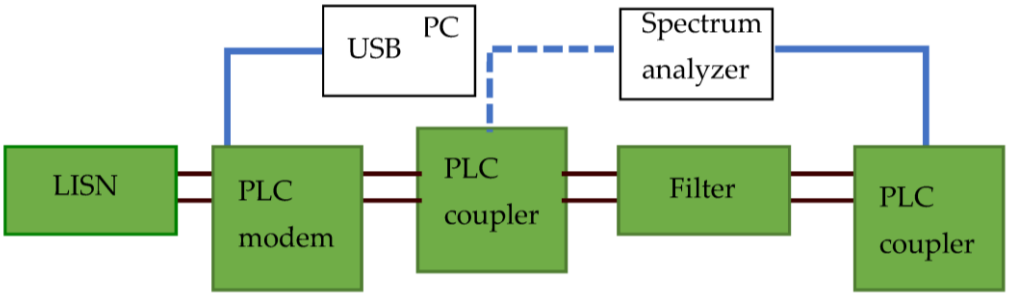

Figure 4.10 PLC signal filtering capability measurement setup version 2 [20]

4.2.3 PLF impedance measurement

The impedance of the PLF should not have a detrimental impact on the performance of the PLC modem. However, in certain situations where the PLF is installed in close proximity to the SM equipped with a PLC modem, it can significantly disrupt the transmitted and received signals. To address this issue, higher filter input & output impedances can be attained by employing multi-stage filters, such as the design I propose in Figure 4.15. This approach allows for improved compatibility between the PLF and the PLC modem, minimizing signal interference.

The methods from Table 4.1 have been identified for measuring the impedance of the PLF at PLC frequencies.

Table 4.1 PLF impedance measurement techniques.

Measurement type	Equipment used	Method description
Offline	RLC meter, impedance analyser, or VNA	Measure directly using specialized impedance measurement equipment as depicted in Figure 4.11
	PLC modem in TX mode, power supply and precision multimeter	Monitoring of the voltage and current consumption of the PLC modem while transmitting carrier frequencies as shown Figure 4.12
Online	Impedance analyser	Measure directly using specialized impedance measurement equipment as shown in Figure 4.13 [133]
	Selective level meter	Using the voltage ratio method as shown in Figure 4.14 [133]

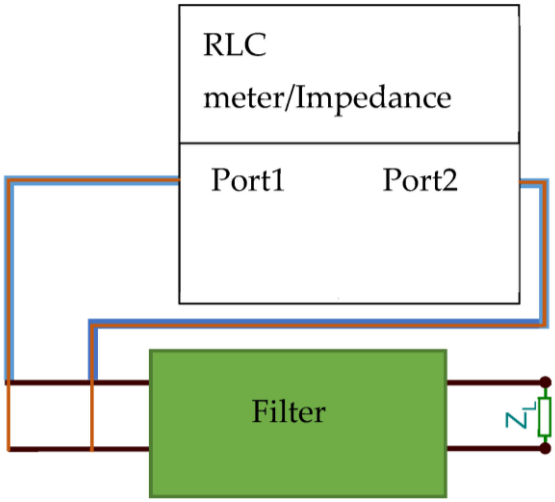

Figure 4.11 Offline impedance measurement setup [20]

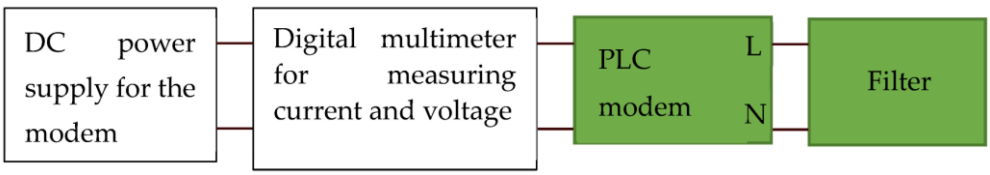

Figure 4.12 Offline impedance measurement setup monitoring the voltage and current consumption of the PLC modem [20]

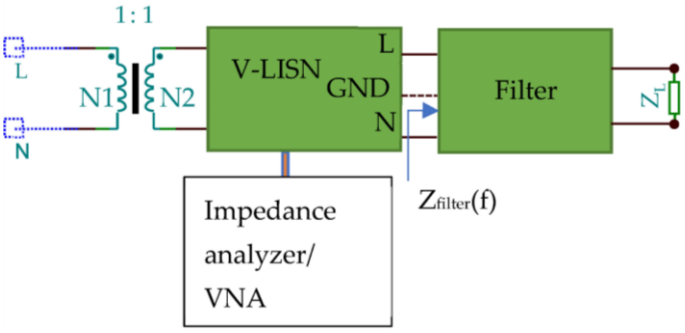

Figure 4.13 Online impedance measurement setup with impedance analyzer [20]

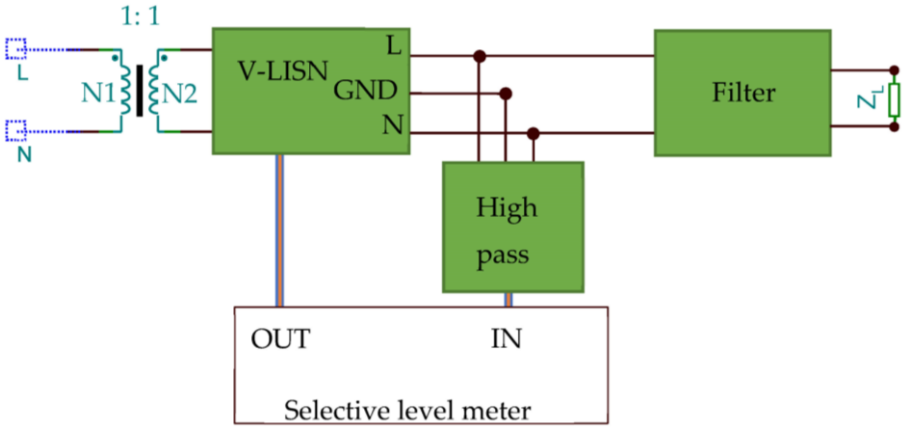

Figure 4.14 Online impedance measurement setup using the voltage ratio method and selective level meter [20]

Single-port measurements S_{11} using a VNA cannot be relied upon for extreme impedance values (i.e., <1Ω) [161]. This limitation arises from the design of VNAs, which primarily focus on measuring the incident wave E^+ entering the DUT and the reflected wave E^- on impedances near 50Ω [161], [167], [168]. The ratio of these two waves is known as the reflection coefficient Γ, utilized to calculate the impedance of the DUT, Z_L. However, the measurement granularity of VNAs is insufficient for single-port measurements at the ends of the measuring range. When Z_{DUT} is exceptionally low, Γ≈ (-1), and when Z_L is extremely high, Γ≈ (+1). Equations (4.1) and (4.2) present the relationship between Γ, E^+, E^- and Z_L.

$$\Gamma = \frac{E^-}{E^+} = \frac{Z_L - 50}{Z_L + 50} \tag{4.1}$$

$$Z_L = 50\frac{(\Gamma + 1)}{(\Gamma - 1)} \tag{4.2}$$

To circumvent the constraints associated with 1-port measurements, the 2-Port VNA measurement technique can be employed which is the equivalent of the 4-wire Kelvin DC method used for resistance measurements. In this approach, one port is utilized to inject signals into the DUT, while the other port measures the voltage

drop across the DUT. By utilizing this 2-Port VNA setup, reliable impedance measurements can be performed [161], [167].

4.3 Supplementary testing methods

In addition to the passive filter standard [169], this section highlights the safety and immunity tests that should be conducted as part of the testing process. These tests encompass heating, surge, overcurrent, and short circuit assessments.

Considering that the PLF will be installed under similar conditions as the SM, it is important to conduct appropriate testing to ensure its proper and safe functionality [145].

4.3.1 Heating

During the PLF's operation at maximum rated conditions, the enclosure shall not reach temperatures that pose a fire hazard or affect the performance of the PLF or nearby devices. To assess this, a thermal view camera [152] can be used to inspect the PLF while subjecting it to the maximum current. The testing guidelines are derived from the general electricity-metering standard [53]:

- The PLF should withstand the maximum rated current and voltage for a duration of 2 hours.
- With a surrounding temperature of 40°C, the temperature increase on the exterior surface should not be more than 65°C.

4.3.2 Surge

The test should be conducted in accordance with the applicable surge testing standard [170], adhering to the conditions from Table 4.2:

Table 4.2 PLF surge testing.

Test setup and DUT settings	PLF should be powered up with nominal voltage +5% but without any loads attached.
	One meter of cable connecting the surge generator and PLF.
	Tested in differential mode (line to line) and optionally in common mode (line/neutral and ground), if the PLF uses a ground connection
Generator settings	Pulses should be applied at Π/3 and 4Π/3 with respect to the mains zero crossing.
	Generator impedance: 2 Ω
	Number of pulses: five positive and five negative
	Repetition rate of maximum 1 pulse/ minute
	Surge pulse voltage of 4 kV

4.3.3 Overcurrent

If there is no fuse installed prior to the PLF, which is often the case when the PLF is used to separate two sections of the PLC grid (as depicted in Figure 4.1), it is advisable to perform this test. The PLF should demonstrate the capability to withstand a short-duration overcurrent of 30 times the maximum rated current for a single mains half-cycle [144]. Additionally, no characteristics of the PLF should altered following this test.

4.3.4 Short circuit

Short circuit condition is achieved when; the output of the PLF is short-circuited, while the input is supplied with double the maximum rated current until it reaches an open circuit state. It is essential to ensure that the PLF remains in a safe condition throughout the testing process until it reaches an open circuit state.

4.3.5 Overvoltage

The overvoltage scenarios simulated in this test include those that can occur in the grid because of failures like earth faults, phase reversals, and voltage unbalances. All these circumstances result in an increase in the line or phase voltage. The calculation for the worst-case scenario that could happen in a system with a phase voltage V_{L-N}=230 V is provided below [144], [171]:

$$V_{(L-N)max} = 1.1 \times 230\,V = 253\,V \quad (4.3)$$

$$V_{(L-L)max} = \sqrt{3} \times V_{(L-N)max} \cong 440\,V \quad (4.4)$$

4.4 PLF design, simulation and benchmarking

In this section, the design, simulation, and evaluation of the passive PLF for NB-PLC applications is presented.

4.4.1 PLF design

The design of the PLF was guided by the following requirements:

- Achieve a minimum attenuation of -120 dB at 50 kHz to effectively block the PLC signal, considering the maximum PLC signal level of 120 dBµV [27].
- Optimize mains quiescent power consumption.
- Ensure a rated current of at least 30 A to enable installation as type 2 PLF between the SM and the building's electrical system (e.g., main fuse).
- To prevent interfering with communication, keep the input/output impedance high in the NB-PLC frequency band. The impedance should be more than 2 Ω as a minimum requirement because PLC modems are built and verified to transmit on low impedance [27].
- Designing the PLF and choosing its components should be done in a way that makes it easy to comply with the tests listed in Section 4.3 and any other testing specifications.

To meet these requirements, I have designed a 13th order PLF as depicted in Figure 4.15, adhering to the specifications mentioned earlier. In this specific instance, the 13th-order filter is the highest filter order required to achieve the maximum necessary attenuation for filtering CE that affects PLC. This accounts for scenarios where there is no inherent attenuation between the noise source and the PLC modem, meaning there's no attenuation introduced by the power line connecting to the filter. In field conditions, considering the diversity of electrical installations, it may be feasible to lower the filter order based on the attenuation introduced by the power line segment connecting the filter to the installation. The necessary filter insertion loss and order can be determined through attenuation measurements on the power line segment connecting the filter. Compliance and performance evaluation of the PLF are discussed in section 4.2 and results presented in section 4.5.

The selection of electronic components plays an important role in the successful implementation of the PLF. Table 4.3 contains a detailed bill of materials explaining

the component selection of the designed PLF and the reference to the plot representing individual impedance measurement.

Table 4.3 PLF components

Reference designator	Component Descriptions and Use Case Explanation
TMOV	The designed PLF integrates a TMOV from LittleFuse™, specifically the TMOV20RP460E [172]. Unlike traditional MOVs, the TMOV offers surge protection while guaranteeing non-conduction at mains voltage preventing overheating and potential fire hazards [173]. The chosen TMOV starts to conduct at 460 V, ensuring the PLF's safe operation during overvoltage conditions where $V_{(L\text{-}L)max}$≈440 V. By analyzing the single-port impedance measurement of the TMOV, as depicted in polar form in Figure 4.16, it becomes visible that at NB-PLC frequencies, the TMOV behaves as a relatively high impedance in comparison to the power line impedance.
R1, R2 and R3	Three resistors connected in series are used in this PLF to passively dampen potential oscillations in the grid [174]. To address surge safety requirements, the Surge Safety Resistors SSR300J10K0TKZTB500 from Firstohm™ [175] were selected. The choice of a series connection is preferred to prevent arcing caused by insufficient clearance and creepage distances [176]. The single port impedance measurement of R1, R2 and R3 shown in polar form in Figure 4.17 reveal that it does not impact the PLC signal because it has a very high impedance even at NB-PLC frequencies ~10kΩ.
C1 and C5	Polyester film capacitors able to withstand $V_{(L\text{-}L)max}$=440 V were utilized in the designed PLF. Specifically, I used the JGGC series capacitors from JB® [102]. The single port impedance measurement of C1 and C5 shown in polar form in Figure 4.18 indicate that the impedance modulus of these two capacitors at NB-PLC frequencies is |Z|< 1.3Ω.
L1 to L8	Toroidal cores made of Sendust MS-184075-2 manufactured by Micrometals™ were used in the design and construction of the inductors [177]. Sendust material is well-suited for applications demanding high permeability, low coercivity, high resistivity, and strong magnetization, making it ideal for inductors employed in filtering applications [178]. To achieve an inductance value L=100 μH and a current rating stranded enameled conductor. The single port impedance measurement of L1 to L8 is shown in polar form in Figure 4.19 and reveal that each inductor has an impedance |Z|> 5Ω which makes them suitable as part of the L-C LPF.
C2, C3, C4	Polyester film capacitors able to withstand $V_{(L\text{-}L)max}$=438 V were used in the design. Specifically, I used the JGGC series capacitors from JB® [102]. The capacitance value was chosen to balance between power consumption in mains conditions, attenuation, and input/output impedance thus having a value of 2.2 μF. The single port impedance measurement of C2, C3 and C4 shown in polar form in Figure 4.20 indicates that the impedance |Z|< 2Ω at NB-PLC frequencies which makes them suitable as part of the L-C LPF.

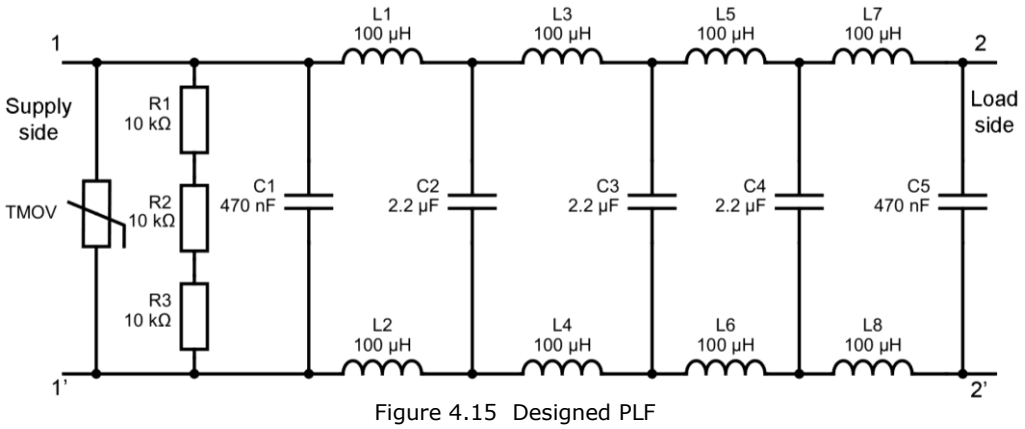

Figure 4.15 Designed PLF

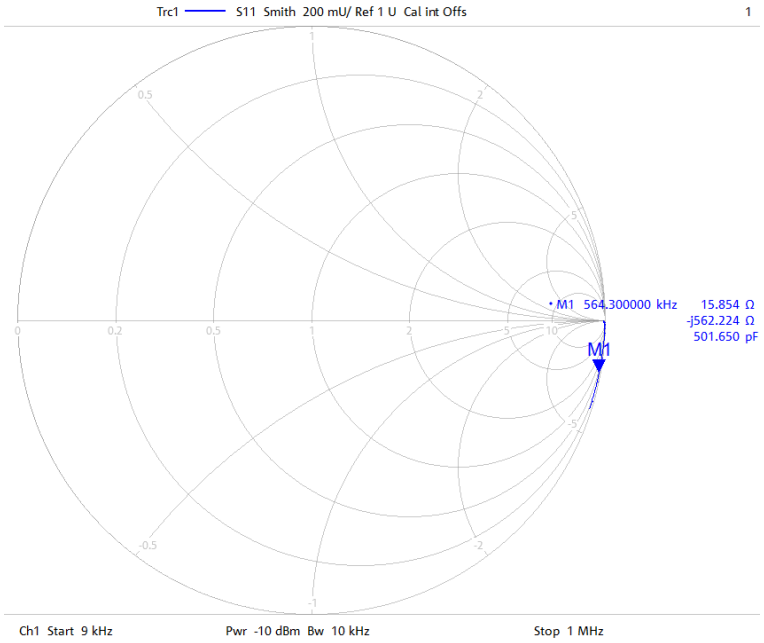

Figure 4.16 S_{11} measurement of TMOV

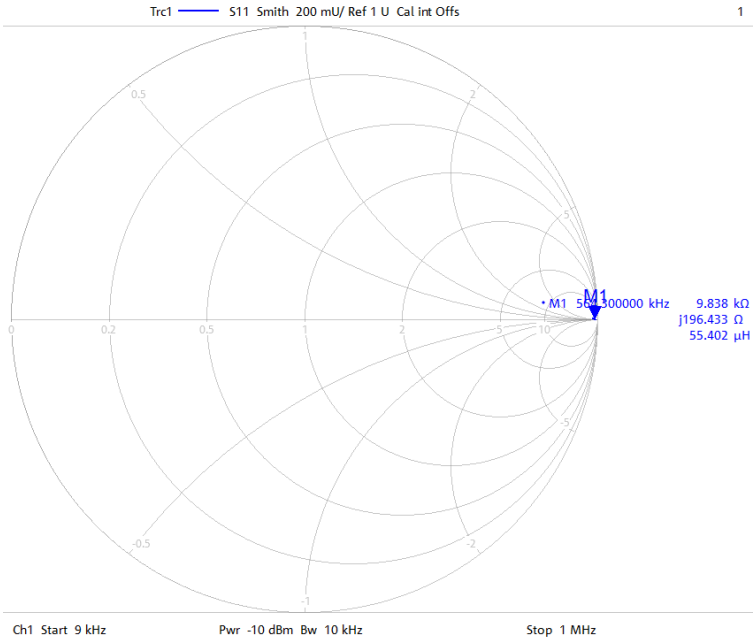

Figure 4.17 S_{11} measurement of R1, R2 and R3

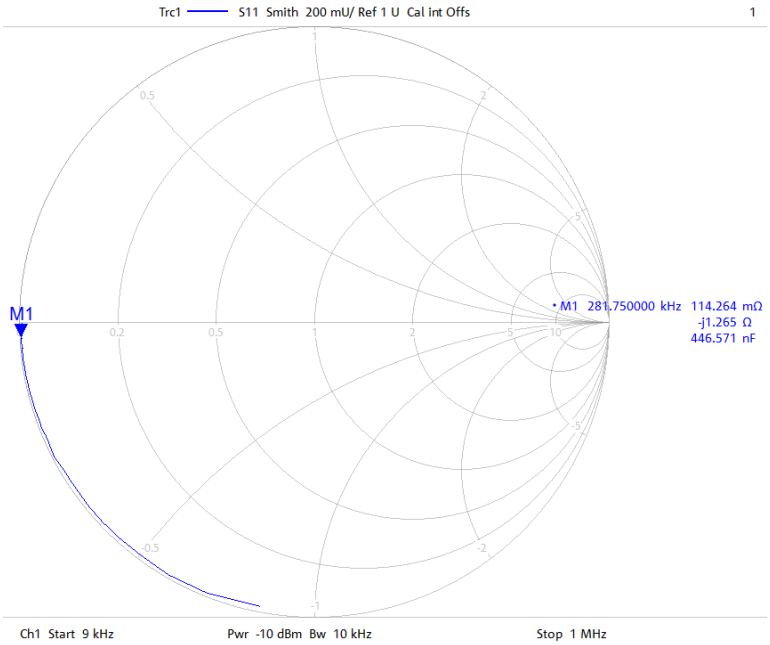

Figure 4.18 S_{11} measurement of C1 and C5

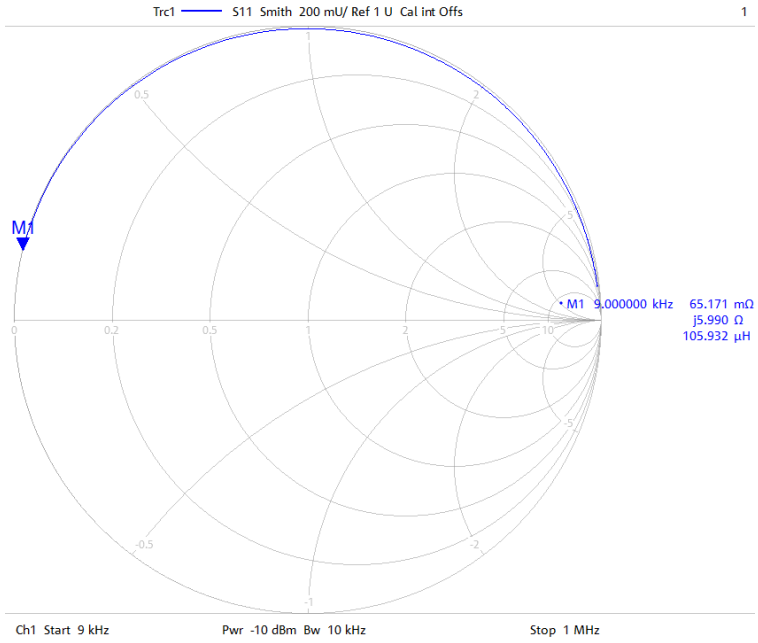

Figure 4.19 S_{11} measurement of L1 to L8

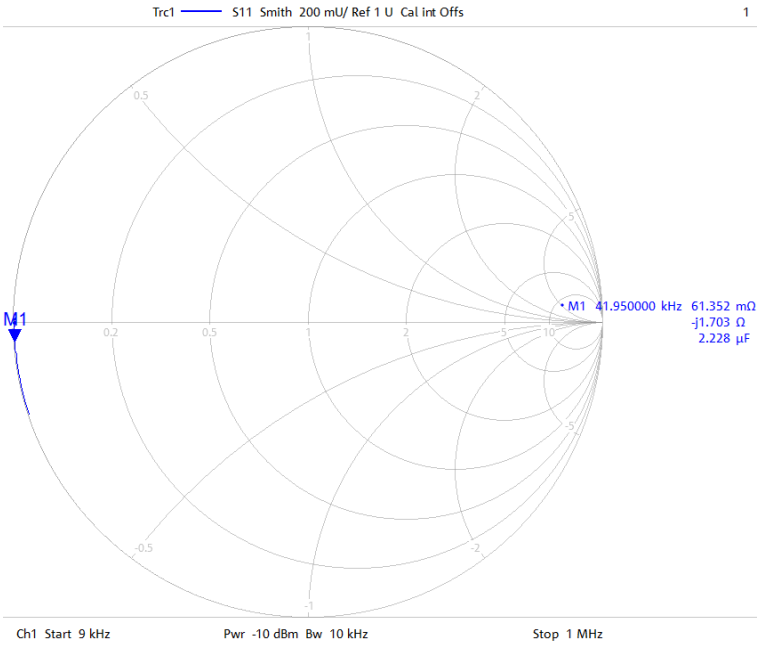

Figure 4.20 S_{11} measurement of C2, C3 and C4

4.4.2 PLF simulation using S-parameters simulator

Using a VNA, the S11 parameters of each component were measured. The resulting Touchstone files [65] were then employed to simulate the PLF using the RFSim99 S-Parameters simulator. RFSim99 is a circuit simulator that operates on linear S-parameters that solves matrix equations for two-port devices.

Figure 4.21 is the graphical representation of a two-port network [179], [180] in which the incident waves for Port1 and Port2 are a_1 and a_2 analogously the reflected waves of these two ports are b_1 and b_2. The ratio of the waves gives the forward transmission coefficients from port 1 to port 2 called S_{21} and port 2 to port $1 S_{12}$. Incident and reflect waves ratio provides the reflection coefficients S_{11} is the input reflection coefficient while S_{22} is the output reflection coefficient

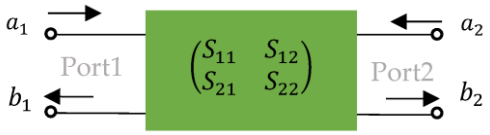

Figure 4.21 Generalized two-port network [20]

Below is the matrix algebraic representation of two port S-parameters [179], [180] which is also used by RFSim99 simulator [20]:

$$S_{11} = \frac{b_1}{a_1} \tag{4.5}$$

$$S_{12} = \frac{b_1}{a_2} \tag{4.6}$$

$$S_{21} = \frac{b_2}{a_1} \tag{4.7}$$

$$S_{22} = \frac{b_2}{a_2} \tag{4.8}$$

$$\begin{pmatrix} b_1 \\ b_2 \end{pmatrix} = \begin{pmatrix} S_{11} & S_{12} \\ S_{21} & S_{22} \end{pmatrix} \times \begin{pmatrix} a_1 \\ a_2 \end{pmatrix} \tag{4.9}$$

For the measurements, PLF online insertion loss test from Figure 4.8 was implemented with the following equipment being used ZNC3 VNA, HM6050-2 LISN both from R&S™ and PLT-22 PLC coupler from Echelon™. The image of the implemented measurement setup is shown in Figure 4.22 while Figure 4.23 presents the designed PLF schematic as it was simulated in RFSim99. The simulation takes into consideration all the components from the actual measurement setup.

The following parameters and conventions were used to perform measurements and create the graph from Figure 4.24:

- Reference impedance for measurement apparatus: $Z_0 = 50\,\Omega$.
- The recorded S21 [dB] parameter is thought to represent the PLF's insertion loss [181].
- Because of the VNA's dynamic range and noise floor, measurements can start low, at -130 dB [182]. Although the simulated S21 magnitude values are as low as −300 dB, all magnitude values ≤−140 dB were scaled to −140 dB in order to facilitate graphical representation.

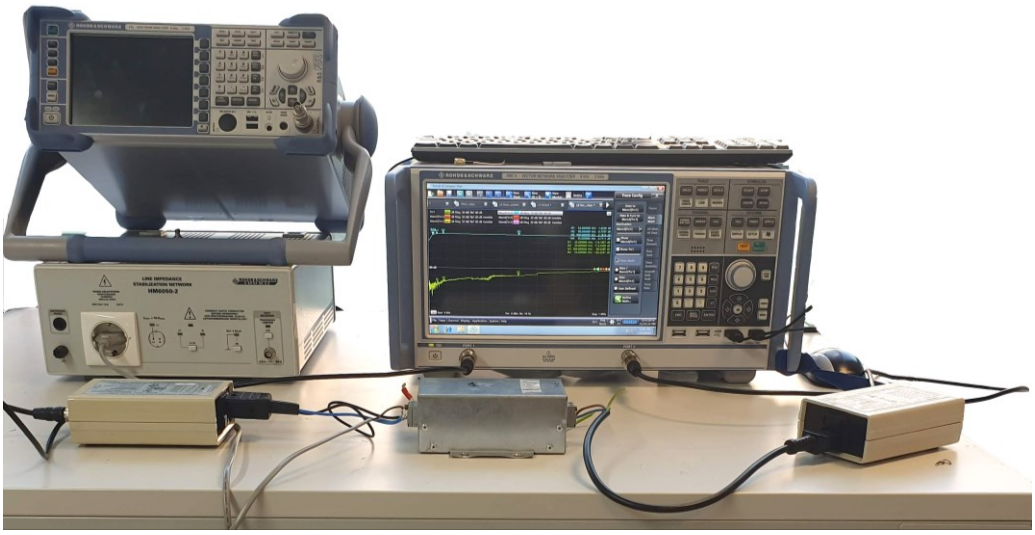

Figure 4.22 PLFs online insertion loss measurement setup version 2 [20]

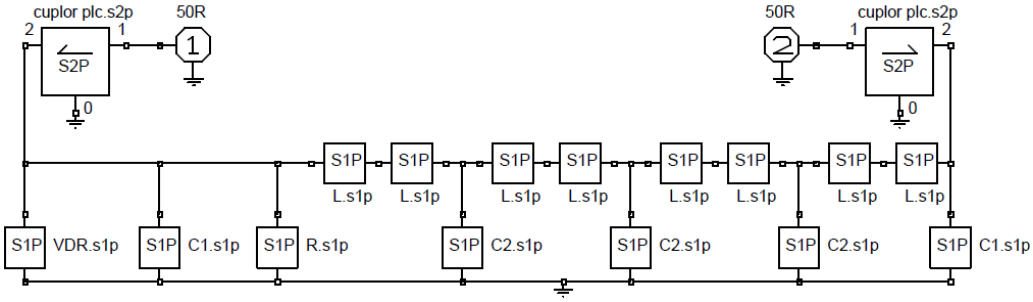

Figure 4.23 Designed PLF simulation in RFSim99

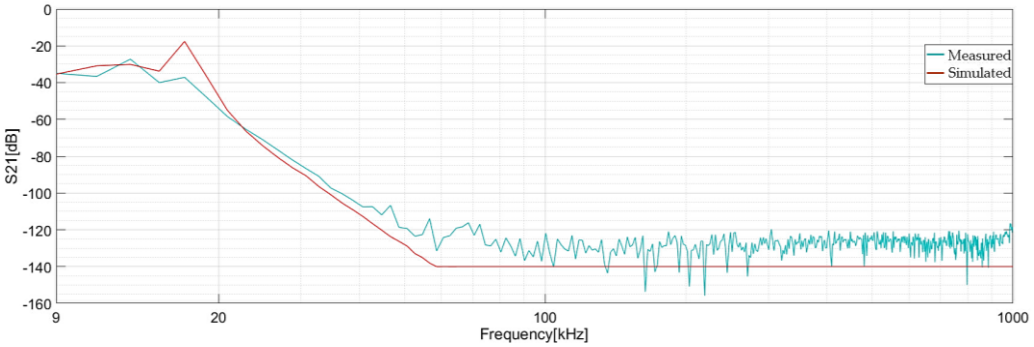

Figure 4.24 Comparison between measured and simulated insertion loss [20]

4.5 Designed PLF Evaluation and Comparison to Commercially Available PLFs

The PLF depicted in Figure 4.15 undergoes evaluation and is compared to three PLFs marketed for PLC applications, reporting similar datasheet properties with the designed PLF. The evaluation process follows a subset of the test methods outlined earlier. To ensure neutrality, the identities of manufacturers and part numbers associated with the PLFs are concealed. Nevertheless, the schematic diagrams of the benchmarked PLFs, including their component values, are disclosed in Section 4.5.1.

4.5.1 PLF insertion loss and power consumption measurements

The following conditions were used for the insertion loss measurement of the PLFs:

- PLF online insertion loss measurement setup 2 from Figure 4.8 was used.
- The initial step involved validating the measurement setup by directly connecting the PLC couplers to each other. This validation check is referred to as "PLC Couplers" in the subsequent figures.
- Subsequently, measurements were conducted with the PLF installed in three ways: "Unenergised" (no mains voltage), "Energised" (mains voltage applied), and "Energised with 2000 W load" (2 kW load with mains voltage applied). The figures displaying the results of insertion loss measurements maintain a consistent naming convention.

Figure 4.25 specifically depicts the insertion loss results for the designed PLF.

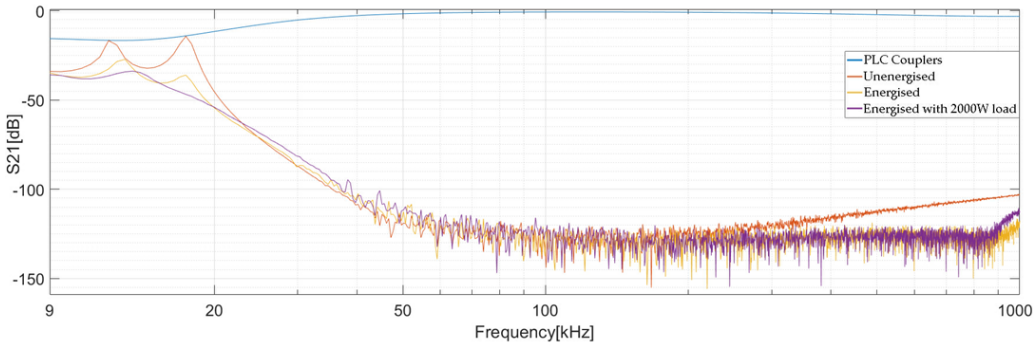

Figure 4.25 Designed PLF insertion loss measurement [20]

The datasheet schematic of PLF 1 is depicted in Figure 4.26. During measurements, the ground connection of the Y-capacitors positioned between C2 and C3 was intentionally left unconnected. As a result, the PLF was connected in a similar manner to an eighth-order passive PLF or a two-stage PLF shown in Figure 4.3. The insertion loss of PLF 1 is presented in Figure 4.27.

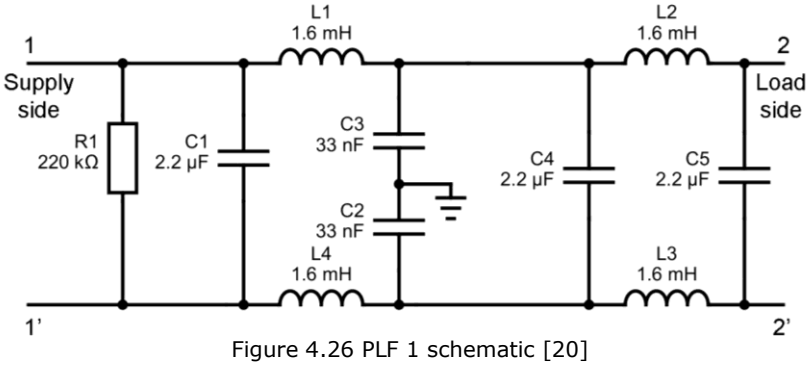

Figure 4.26 PLF 1 schematic [20]

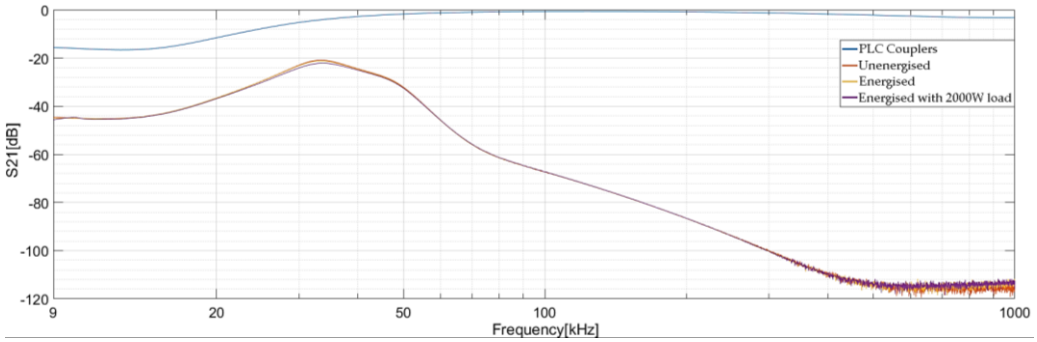

Figure 4.27 PLF 1 insertion loss measurement [20]

Figure 4.28 showcases the reverse-engineered schematic of PLF 2, as the original schematic was not available in the datasheet. This PLF belongs to the resonant type, with a resonance frequency ranging between 20 kHz and 30 kHz, which can be seen in Figure 4.29 where the S21 [dB] attenuation exhibits its minimum value. It is worth noting that these types of PLFs possess the drawback of having attenuation highly dependent on the input and output impedance. This fact is substantiated by the substantial difference in attenuation (10 dB to 40 dB) displayed in Figure 4.29, comparing the attenuation when the PLF is energized versus the scenario when the PLF is subjected to a 2 kW load.

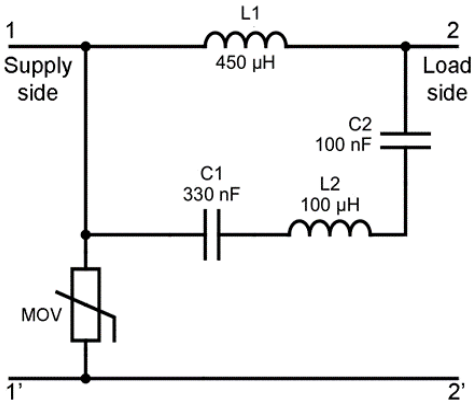

Figure 4.28 PLF 2 schematic [20]

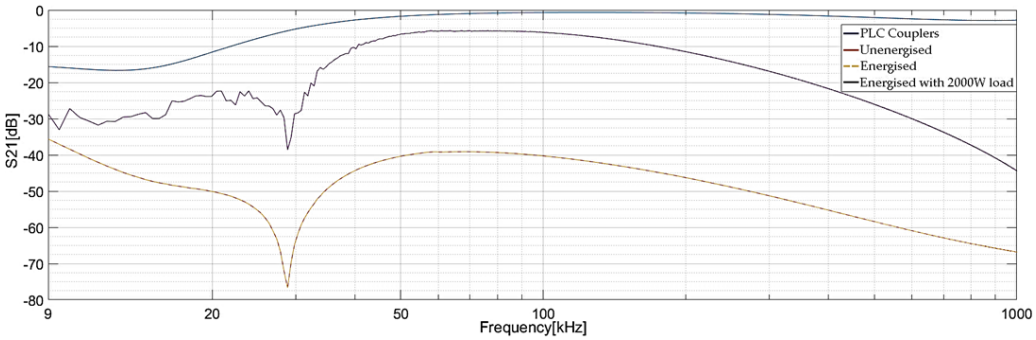

Figure 4.29 PLF 2 insertion loss measurement [20]

Figure 4.30 shows the schematic sourced from the datasheet of PLF 3 which is a 6th order passive PLF, similar topology as the proposed filter. Figure 4.31 presents the insertion loss of PLF 3.

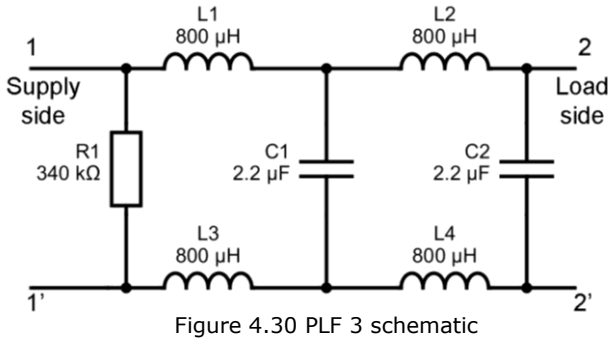

Figure 4.30 PLF 3 schematic

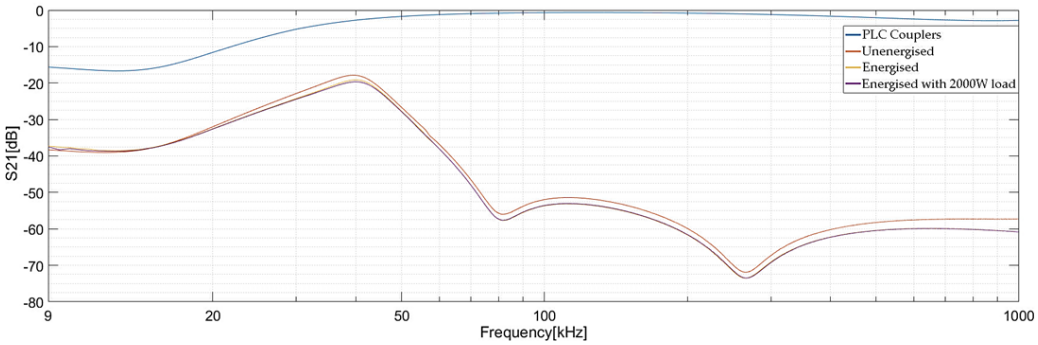

Figure 4.31 PLF 3 insertion loss measurement [20]

Table 4.4 lists the results of the measurements of insertion loss and power consumption, along with comparisons to datasheet values. The table contains the maximum rated current value as a benchmark for the PLFs' comparability.

The data in Table 4.4 is obtained using the following techniques and resources:

- Measurements of PLF power consumption were conducted at 230 V 50 Hz with no load connected.
- Insertion loss from the datasheet and practical measurements.
- Measurement of the insertion loss gap as a difference between the PLF attenuation and the attenuation at which communication ceases is seen by these data. The measurement setup used is represented in Figure 4.9.

Table 4.4 PLFs overview-using values from the datasheets and practical measurements.

PLF Number	Rated Current [A]	Power Consumption [mW]	Insertion loss datasheet value [dB]	Measured insertion loss with PLF Energized and 2 kW Load [dB]	PLF Insertion Loss delta until PLC ceases [dB]
Designed PLF	30 *	597	−130 *	−120	0
PLF 1	25	524	−40	−32	53
PLF 2	45	33	−40	−7	59
PLF 3	25	215	−20	−28	55

* Designed and simulated value.

The PLF developed in this study demonstrates superior characteristics. It achieves the best insertion loss across a wide frequency range, exhibiting a significant three-fold better attenuation at 50 kHz (more than -130 dB) compared to the best commercially available PLF (-40 dB).

4.5.2 Impedance estimation of the PLFs

In this section I introduce a method for estimating the impedance of the PLFs. It involves measuring the current consumption of the PLC-G3 modem in TX mode while broadcasting all 36 beacons within the frequency range of 36 kHz to 90.6 kHz. This current consumption data is used to calculate the impedance of the PLFs relative to a Z= 1 Ω. The measurements are taken at both the input and output connections of the PLFs.

The measurement results are presented in Table 4.5, which provides information about the modem's current consumption in TX mode and the calculated impedance within the PLC-G3 frequency range. The table also identifies the measurement location of each PLF, whether it is placed at the input or output of the system.

Table 4.5 Modem current consumption in TX mode and calculated impedance in the frequency range 36–90.6 kHz.

PLF identification	PLF location	RMS current consumption [mA]	Calculated |Z| [Ω]
Designed	output	125	3.36
PLF	input	125	3.36
PLF 1	output	275	1.53
	input	275	1.53
PLF 2	output	25	16.8
	input	75	5.6
PLF 3	output	225	1.87
	input	205	2.05

During the measurement, the modem's power consumption in TX mode was found to be 420 mA when transmitting signals on resistive shunt of Z= 1 Ω.

Figure 4.12 illustrates the measurement technique used to determine the current consumption of the PLFs, and Figure 4.32 shows the setup employed for these current consumption measurements.

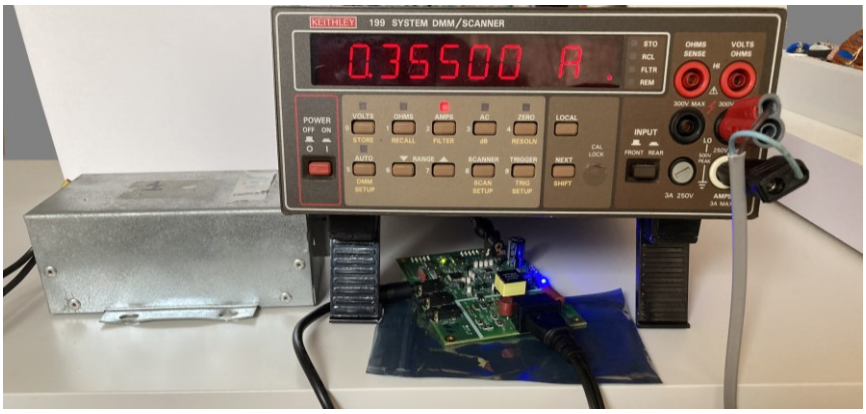

Figure 4.32 Current consumption measurement setup

Overall, the purpose of this section is to assess the impedance characteristics of the PLFs and understand how they affect the performance of the PLC-G3 modem, particularly in TX mode. The input/ output impedance values are important for evaluating and optimizing the PLFs in the PLC system.

4.5.3 Benchmarking the PLFs using PLC-G3 frequency spectrum measurements

In this section PLC-G3 frequency spectrum measurements of three commercially available PLFs as well as the proposed PLF are presented and discussed. I have used PLC signal filtering capability measurement setup version 2 presented in Figure 4.10 with Agilent™ N9010A spectrum analyser, R&S™ HM6050-2 LISN and the PLC evaluation kit MAX79356 from Maxim Integrated™ [110]. From a technical perspective, these measurements conducted in laboratory environment are particularly stringent. This is primarily due to the fact that the PLC-G3 modem is transmitting directly in close proximity to the filter, resulting in minimal additional attenuation caused by power line segments. In this controlled environment, the evaluation accurately reflects the performance of the filters, as they are subjected to the most challenging conditions, ensuring that their attenuation capabilities can be thoroughly assessed.

The following test steps were performed as part of this benchmarking:

1st Step: Noise floor measurements with the setup energised at 230V 50Hz. Figure 4.34 presents the noise floor measurement result performed before measuring each PLF, the results were close to the noise floor of the spectrum analyser in all the cases which shows that the measurement setup is noiseless and stable.

2nd Step: Configure the PLC modem before the PLF in TX mode and the PLC modem after the PLF in RX mode. Figure 4.33 presents how the PLC-G3

modems were configured using Zeno Simple Connect interface running on a PC, which is connected to the modems via a USB to UART converter.
3rd Step: Measure the PLC frequency spectrum before and after the PLF.

The PLC-G3 frequency spectrum results for the proposed PLF, PLF 1, PLF 2 and PLF 3 are shown in figures as follows:

- Figure 4.35 is the TX PLC-G3 frequency spectrum measurement of the proposed PLF while Figure 4.36 is the frequency spectrum of the RX PLC-G3 signal before the proposed PLF.
- Figure 4.37 is the TX PLC-G3 frequency spectrum measurement of PLF 1 while Figure 4.38 is the frequency spectrum of the RX PLC-G3 signal before PLF 1.
- Figure 4.39 is the TX PLC-G3 frequency spectrum measurement PLF 2 while Figure 4.40 is the frequency spectrum of the RX PLC-G3 signal before PLF 2.
- Figure 4.41 is the TX PLC-G3 frequency spectrum measurement of PLF 3 while Figure 4.42 is the frequency spectrum of the RX PLC-G3 signal before PLF 3.

Table 4.6 summarizes the evaluation of PLFs based on their frequency spectrum measurements from Figure 4.35 to Figure 4.42, attenuation ranking, and their impact on communication performance, showing how different PLFs affect the reception of frames in a PLC system.

Table 4.6 Summary of the PLFs PLC-G3 frequency spectrum measurements.

PLF	Frequency spectrum measurement	Attenuation ranking and explanation	Communication
Designed PLF	Figure 4.35 Figure 4.36	1st position because it has same frequency spectrum as the noise floor	No frames are received
PLF 1	Figure 4.37 Figure 4.38	4th position because at least one of the PLC-G3 sub bands is not attenuated at all	All frames are received
PLF 2	Figure 4.39 Figure 4.40	2nd position because the spectrum is still detectable, the attenuation is flat which allows to estimate 60 dB of attenuation	All frames are received
PLF 3	Figure 4.41 Figure 4.42	3rd position because one of the PLC-G3 sub bands is only slightly attenuated	All frames are received

After a thorough analysis of the measurement results, it becomes clear why communication remains feasible with commercially available filters. Among the six PLC-G3 sub-bands, at least one sub-band experiences minimal attenuation or distortion thus making communication possible. However, it is necessary to note that the low attenuation observed in the commercially evaluated PLF may not necessarily translate to reduced performance in real-world field conditions. There might be the case that there is a distance of power line between the source of CE or the PLC modem and the filter, which further contribute to the overall attenuation. Because of the diversity in electricity installations and the time-varying nature of power lines, the contribution of power line attenuation is unpredictable and unreliable.

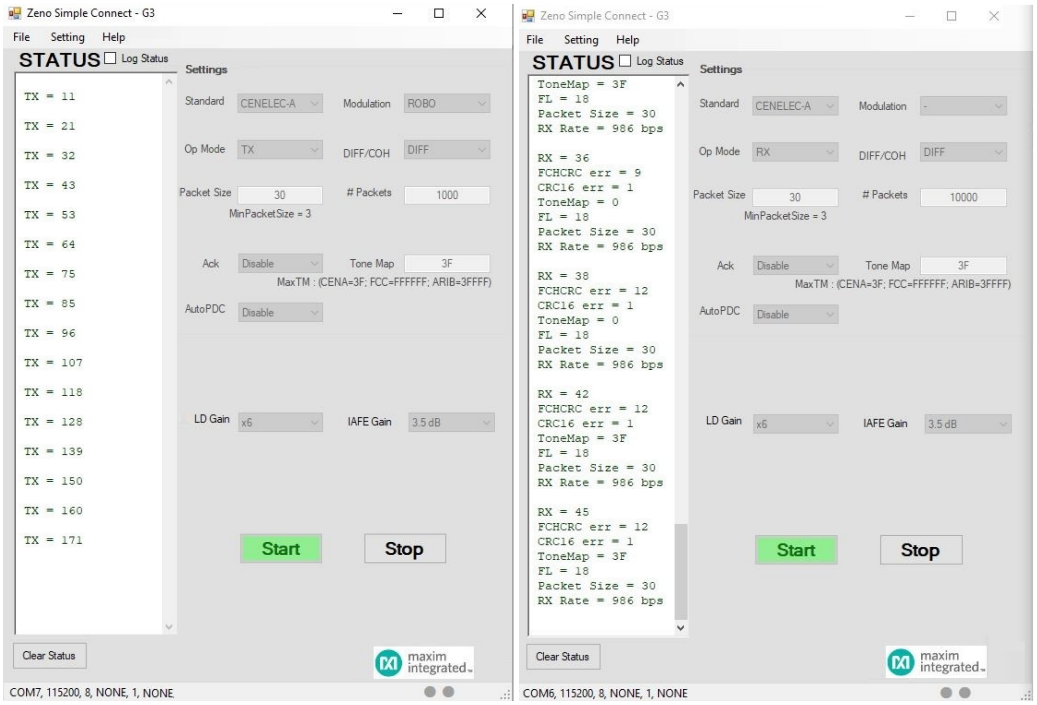

Figure 4.33 Modems configuration

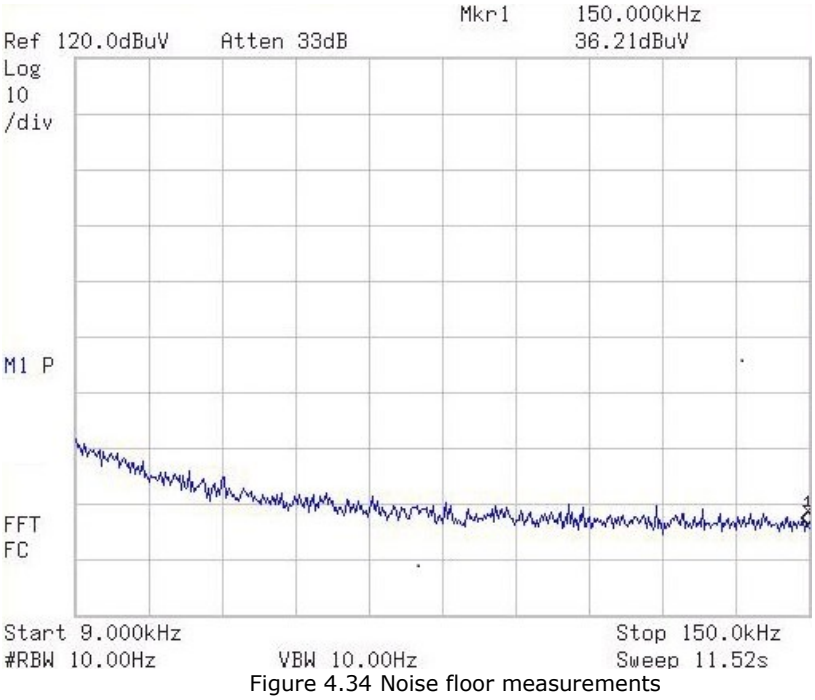

Figure 4.34 Noise floor measurements

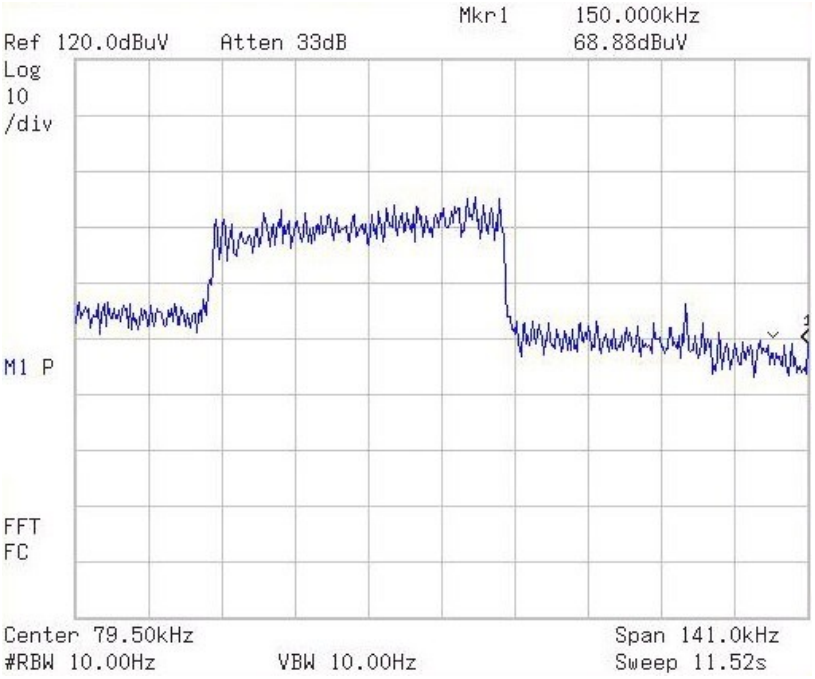

Figure 4.35 Proposed PLF TX signal- before the PLF

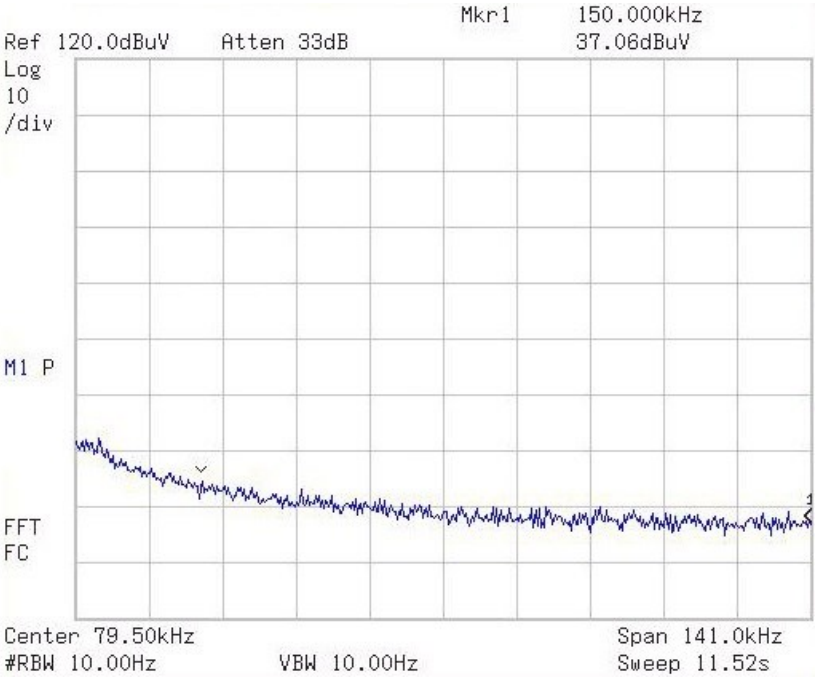

Figure 4.36 Proposed PLF RX signal- after the PLF

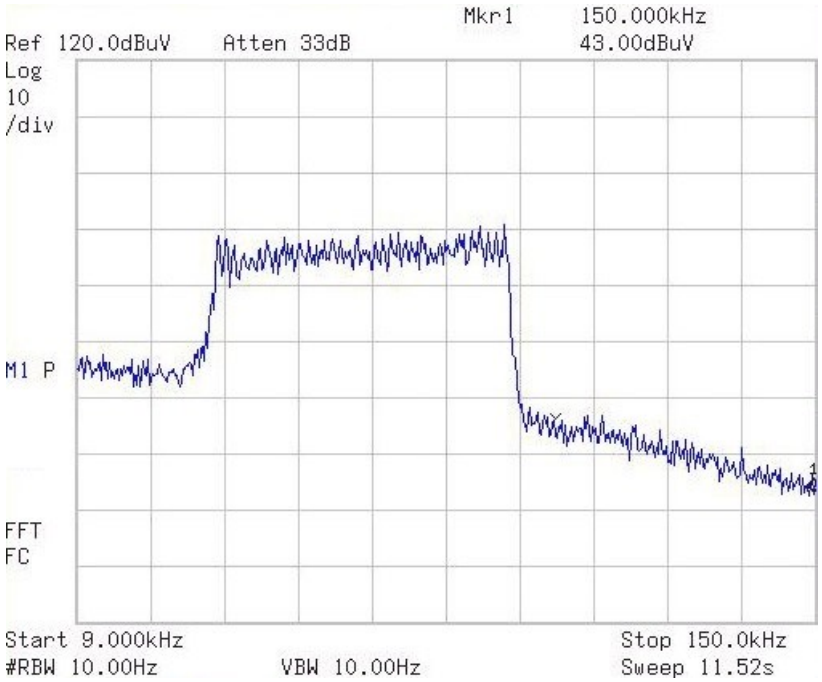

Figure 4.37 PLF 1 TX signal- before the PLF

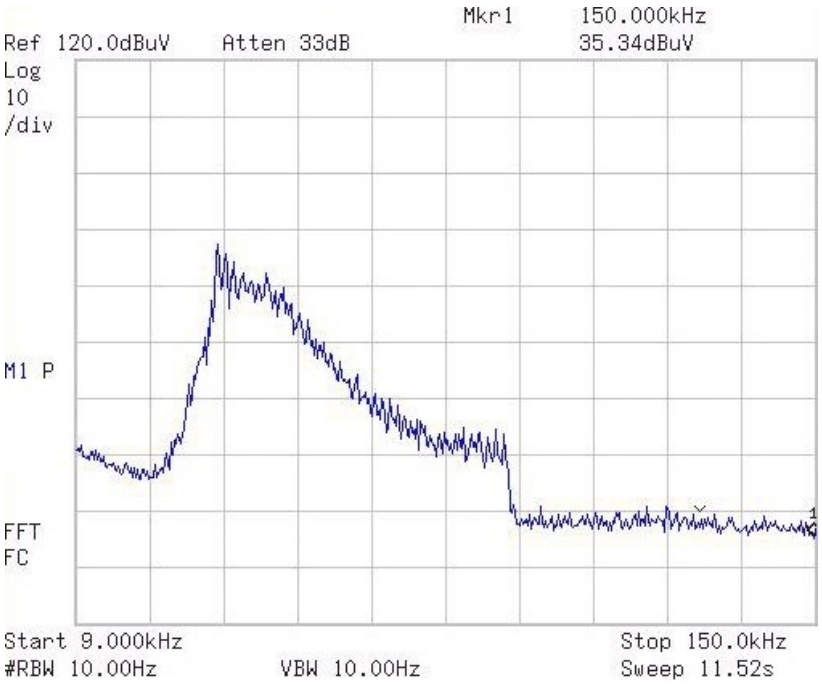

Figure 4.38 PLF 1 RX signal- after the PLF

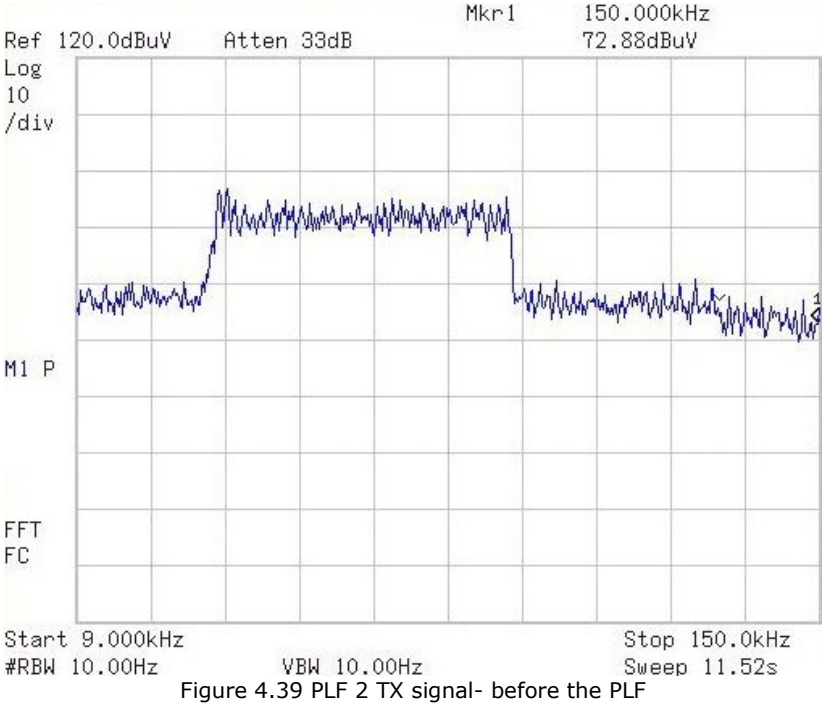

Figure 4.39 PLF 2 TX signal- before the PLF

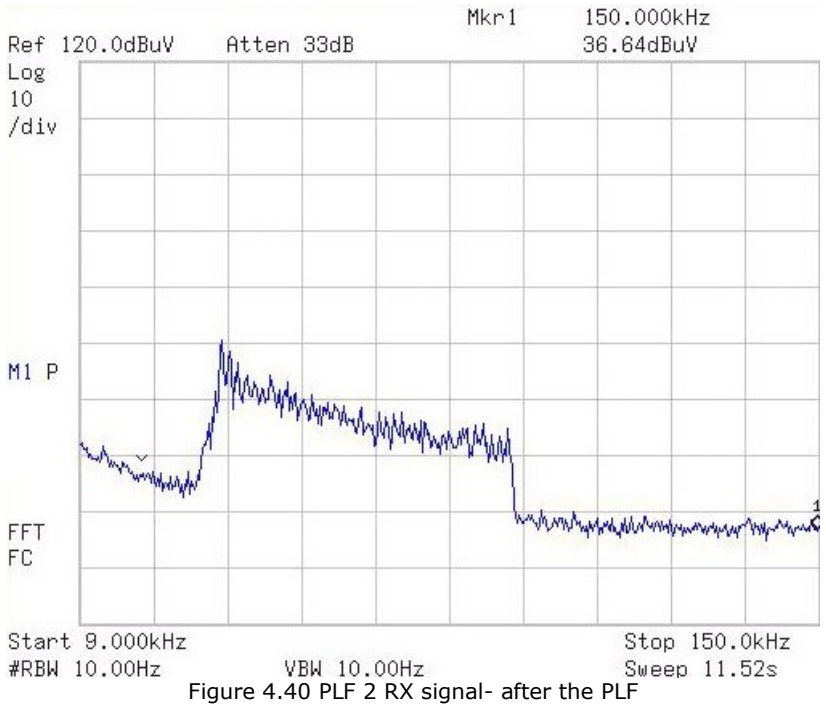

Figure 4.40 PLF 2 RX signal- after the PLF

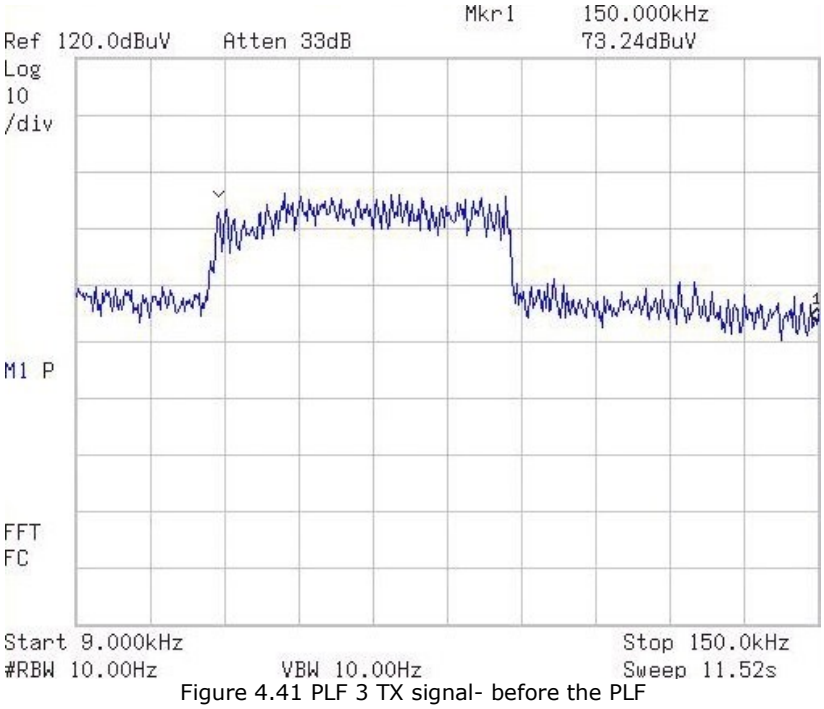

Figure 4.41 PLF 3 TX signal- before the PLF

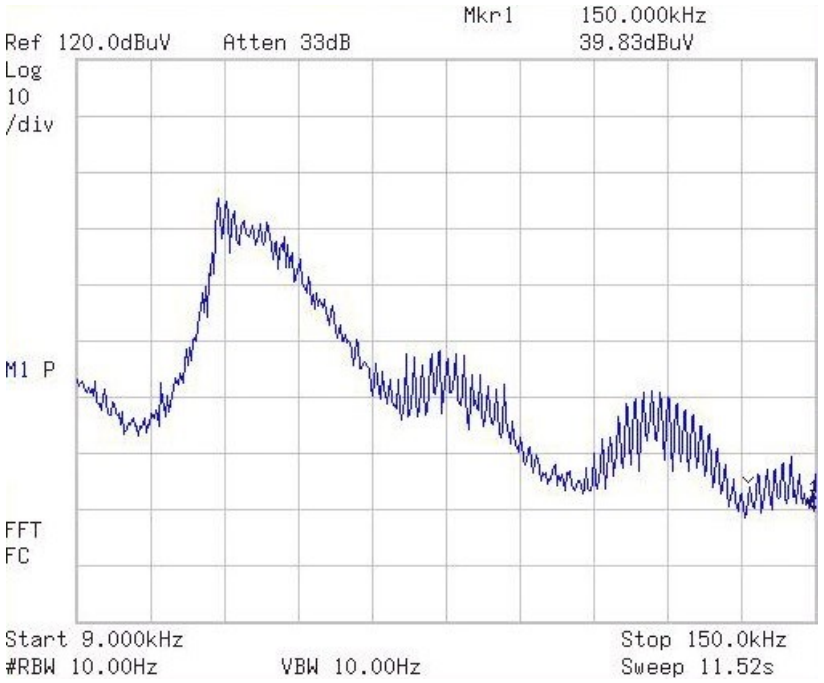

Figure 4.42 PLF 3 RX signal- after the PLF

4.6 Chapter summary and future work

In this chapter, I provided a comprehensive analysis of evaluation and design methodologies, which allowed me to propose a novel framework for PLFs development and performance assessment. The design and evaluation framework for PLFs, was designed for frequencies below 150 kHz but it can be easily extended.

Using the proposed design methods I have successfully built a PLF using passive components and an S-parameters simulator. A thorough explanation of component selection and PLF construction has been provided, and actual measurements have been used to confirm the correctness of the simulated results. Benchmarking against three PLFs that are readily accessible commercially reveals that the developed PLF is the best option for efficient filtering below 150 kHz.

With the best insertion loss across the NB-PLC frequency range, a threefold increase in attenuation at 50 kHz (more than -130 dB) compared to the best commercially available PLF (-40 dB), and a power consumption of 597 mW, which is comparable to the other commercial PLFs, the designed PLF exhibits exceptional qualities. Additionally, in the frequency range between 36 kHz and 90.6 kHz, the proposed PLF achieves the second-best input and output impedance of 3.36 Ω.

The designed PLF, as stated in Section 4.1.1, is appropriate as a type 1 PLF but unsuitable as a type 2 PLF for separating two portions of the electrical grid because of its maximum rated current of 30 A. As follow-up research, I want to investigate how to design a type 2 PLF using the techniques covered in this chapter.

I propose future benchmarking of additional PLFs using the test benchmarking methods outlined in 4.2 and 4.3. Additionally, designing and testing a hybrid PLF that blends resonant and conventional PLF types with the goal of lowering the filter's order while retaining sufficient attenuation below 150 kHz is interesting.

As a result of my research activities presented in this chapter I was able to answer the following initial question: **In order to enhance PLC performance, what potential modifications or improvements might be required in the power grid infrastructure, and what strategies can be employed to successfully implement these modifications?**

Filtering out CE in a PLC system is commonly approached through the use of a LPF. However, this straightforward method presents challenges due to the relatively low frequencies (below 150 kHz) utilized for NB-PLC communication. Additionally, the power grid contains various services, and its impedance differs significantly from commercially available PLF designs. Section 4.1 of this work delves into the integration of PLFs in the electricity grid, exploring the PLF topology and its impact on grid operations. Addressing these complexities, a novel methodology for designing PLFs specifically for NB-PLC using S-parameters is proposed in section 4.4. This innovative approach aims to tackle the unique requirements posed by the power grid's characteristics and the specific frequency range used for NB-PLC communication.

In this chapter, I offered a comprehensive contribution to the field of NB-PLC improvement techniques. This major theoretical advance encompasses:

- **CE filtering techniques and overview of the integration of PLFs into the electricity grid, highlighting the services and features present in the grid as well as main types of PLFs.** After conducting an extensive review of the literature, I identified filtering techniques for CE and the integration of PLFs into the electrical network. This documentation revealed two methods for connecting passive filters within the low-voltage electricity supply network: one between the SM and the main fuse, and the other between two segments of the supply network. These findings were presented

in section 4.1 of the doctoral thesis and elaborated upon in articles [20] and [21].

As an experimental contribution to the field of passive filtering in NB-PLC, as presented in this chapter, I have conducted the following:

- **Implementation and evaluation of a passive PLF for NB-PLC frequency band.** I have designed and implemented a 13th order passive PLF which uses carefully selected components so that it offers enough attenuation in order to block CE and PLC signal while it presents a sufficiently high impedance at both ends thus not disturbing the intended PLC communication. The design steps of the PLF are extensively presented in sections 4.4.1 and 4.4.2 as well as in my previous article [20].
- **Comparing the designed PLF to the ones that are currently on the market.** The designed PLF exhibits exceptional qualities, including the lowest insertion loss across the NB-PLC frequency range, a threefold increase in attenuation at 50 kHz (more than -130 dB) compared to the best commercially available PLF (-40 dB). Additionally it has a power consumption of only 597 mW, which is comparable to the other commercial PLFs. Additionally; the suggested PLF achieves the second-best input and output impedance of 3.36 Ω in the frequency range between 36 kHz and 90.6 kHz. The benchmarking process and results are shown in chapter 4.2 and validated by my previous article [20].

A path for future research and development activities could involve a modular design with considerations for attenuation and current rating. Given the various types of electrical installations, it may be feasible to reduce the filter order depending on the amount of attenuation introduced by the power line segment. To determine the appropriate filter order, one could conduct attenuation measurements on the power line segment.

Both the theoretical principles and experimental outcome presented in this chapter originate from my prior scientific publications as referenced in [20], [21].

5 Conclusions, contributions and future work

In this concluding chapter, I bring together the various aspects of my research journey, presenting a comprehensive synthesis of the methods for enhancing PLC over Low Voltage Networks. I will begin by addressing the initial questions, which guided my activity, providing concise and answers that shed light on the core objectives of my study. Subsequently, I will delve into the theoretical and practical contributions generated by this research, highlighting the novel perspectives and valuable knowledge I have contributed to the academic and practical realms. Furthermore, I will outline potential paths for future work and research, paving the way for continued exploration and advancement in the field. This chapter serves as the culmination of my research endeavors, offering a comprehensive understanding of the significance of my study and its impact on both theory and practice.

Overall, my research activity during the PhD studies significantly contributes to the advancement of PLC technologies, offering valuable methods for noise identification, avoidance and suppression as well as the design and evaluation of PLFs. The outcomes of this thesis can potentially enhance the reliability and efficiency of PLC systems, paving the way for broader applications in various industrial and residential settings.

5.1 Conclusions

In conclusion, the significance and widespread adoption of NB-PLC in SG applications have been demonstrated. However, it is clear that there are existing gaps in standardization and the coexistence of grid-connected devices operating at frequencies below 150 kHz as well as insufficient practical ways to address NB-PLC communication issues arising from the fact that the power distribution network was not intended for communication. These factors underscore the importance of addressing these issues to ensure uninterrupted communication among SG devices. As the demand for SG technologies continues to grow, it becomes necessary to bridge these gaps and enhance the reliability and efficiency of NB-PLC in SG applications. By doing so, the full potential of SGs can be unlocked, enabling them to meet the ever-increasing demands of modern power distribution and management.

The first approach introduced a method for identifying noise-generating loads within the PLC frequency band. By correlating SM power measurements of the load with channel quality reports obtained from the PLC-G3 modem, a clear connection between power measurements and noise originating from specific loads was established. This connection enabled the creation of a PLC transmission schedule based on the operation of noise-generating loads. The practical results showcased the efficacy of this method, emphasizing its potential for real-world implementation and enhancing PLC system performance.

The second approach focused on the development and evaluation of PLFs, particularly targeting the CENELEC A, B, C, and D communication bands. The design of a PLF was achieved using simulation methods and passive components. Detailed information on component selection and PLF design was presented. The simulated values were validated through practical measurements, confirming the accuracy of the designed PLF. Comparative benchmarking against commercial PLFs revealed that the designed PLF outperformed other PLFs, exhibiting exceptional characteristics, including superior insertion loss, significant attenuation at 50 kHz, and low power

consumption. The proposed PLF, though suitable as a type 1 PLF, serves as a basis for future work exploring the design of a type 2 PLF using the methodologies presented in this thesis.

At the end of my research activities, I was able to answer the questions that I raised at the beginning in section 1.4:

1. **How and why is PLC integrated into the electricity grid, and what are its primary objectives and benefits?**

I have shown in sections 2.4, 2.5 and 2.6 how and why is PLC used as communication protocol in the power line. The electricity grid already has an extensive network of power lines which allow integrating PLC into the grid by utilizing this existing infrastructure for communication purposes without the need to lay additional dedicated communication cables or deploy costly wireless systems. PLC is mostly used in the electricity grid as last mile communication protocol between SM and DC.

2. **What specific challenges does NB-PLC encounter within the power distribution grid, and how do these challenges impact its performance and reliability?**

There are many challenges that PLC must overcome in order to ensure proper communication: conducted noise (caused by standardization gaps), signal attenuation and low power line impedance.

The power grid is a noisy environment, and PLC is affected by various sources of CE from other electrical devices, radio frequency interference from radio broadcasts and impulse noise from power equipment. This CE impact the PLC signal quality and affects communication reliability. The types of noise present in the electricity distribution grid are presented in section 2.2.1 and section 2.2.2

Signal Attenuation: As PLC signals travel through power lines, they experience attenuation due to line losses and impedance mismatches. This limits the range and coverage of PLC communication, especially over long distances or in areas with poor power line conditions. This is presented in section 2.2.3.

Power line impedance is much lower compared to what standard equipment used in the design process can achieve. A survey of these extremely low values as well as adaptations of the design methods are presented in sections 2.2.4 and 3.2.1.

3. **What could be non-invasive techniques or solutions available to address the challenges faced by PLC within the SG without the need for grid modifications? If so, what are these techniques, and how can they be effectively implemented?**

A novel approach for identifying noise-generating loads within the PLC frequency band is presented in chapter 3. By leveraging SMs to correlate energy measurements of the load with PLC-G3 modem channel quality indicators, a clear connection between energy measurements and noise originating from specific loads has been established. The practical results further validate this correlation, and spectrum measurements conducted on power lines with both low and high impedance provide a comprehensive comparison with the noise spectrum. This correlation enables the creation of a transmission schedule based on the operation of loads generating noise, enhancing the efficiency of PLC communication.

4. **In order to enhance PLC performance, what potential modifications or improvements might be required in the power grid infrastructure,**

and what strategies can be employed to successfully implement these modifications?

Filtering out CE affecting a PLC system is commonly approached through the use of a LPF. However, this straightforward method presents challenges due to the relatively low frequencies (below 150 kHz) utilized for NB-PLC communication. Additionally, the power grid contains various services, and its impedance differs significantly from commercially available PLF designs. Section 4.1 of this work delves into the integration of PLFs in the electricity grid, exploring the PLF topology and its impact on grid operations. Addressing these complexities, a novel methodology for designing PLFs specifically for NB-PLC using S-parameters is proposed in section 4.4. This innovative approach aims to tackle the unique requirements posed by the power grid's characteristics and the specific frequency range used for NB-PLC communication.

5.2 Theoretical contributions

This section outlines the theoretical contributions I have introduced to this specialized field of study throughout the research activities of my doctoral program:

1. **Challenges of NB-PLC communication in the context of SGs.**

I have researched and documented the interference caused by CE in the power supply network on NB-PLC. These emissions are categorized, their sources identified, and their impact emphasized. The need to enhance NB-PLC by detecting, avoiding, and filtering out CE within the NB-PLC communication frequency band is underscored. Furthermore, the gaps in standardization related to CE affecting NB-PLC are identified and addressed. This in-depth analysis is extensively covered in section 2.2 of my thesis and is also discussed in the articles [19], [20].

2. **Identification of SM architecture in the context of communication protocols and services present in the power grid.**

A SM architecture is introduced within the framework of communication protocols and services found in the electricity network. The architecture aims to incorporate the methods for the identification and avoidance of CE. During its development, off-the-shelf electronic components were used. Adhesion to international standards was taken into consideration in every step of the SM architecture development. It was progressively developed and is detailed in the subsequent articles [19], [21], [22], [25] and section 3.1 of the doctoral thesis.

3. **Proposal of a technique for identifying CE in the NB-PLC Frequency Band.**

In Chapter 3 of the thesis, technique for identifying CE within the frequency band utilized by NB-PLC are formulated. The innovative approach leverages the existing components and functionality of SMs to establish a correlation between power measurements and communication channel quality reports acquired from the PLC-G3 modem. This correlation facilitates the identification of CEs generated by the load and the development of a transmission schedule when the load does not produce CEs (for instance, when it is in a stopped state or operating in a different mode). This novel methodology was published in my article [19].

4. **CE filtering techniques and overview of the integration of PLFs into the electricity grid, highlighting the services and features present in the grid as well as main types of PLFs.**

After conducting an extensive review of the literature, I identified filtering techniques for CE and the integration of PLFs into the electrical network. This documentation revealed two methods for connecting passive filters within the low-voltage electricity supply network: one between the meter and the main fuse, and the other between two segments of the supply network. These findings were presented in section 4.1 of the doctoral thesis and elaborated upon in articles [20] and [21].

5. **Performance, safety and immunity tests that ought to be conducted as part of PLF benchmarking.**

In sections 4.2 and 4.3 I propose filter benchmarking methods and insertion loss measurement techniques, PLC signal attenuation and PLF impedance measurements which have been optimized in order to obtain results as close as possible to the real power line. The main improvement that I brought to the setup was the implementation of 2Ω LISN impedance, which is a good practical approximation of the real power line impedance. The proposed benchmarking methods are present in my previous article [20].

6. **Design and simulation methods for PLFs.**

In sections 4.4.1 and 4.4.2 I propose the design of PLFs using S-parameters and RFSim99. While the design methods themselves are not novel, they have not been previously applied to low-frequency applications like PLF design for PLC. This became feasible due to the advancement of measuring equipment capable of providing S-parameters measurements in the kHz range. The proposed benchmarking methods are presented in my previous article [20].

5.3 Practical contributions

For validating the theoretical contributions brought to this field of research, I conducted a series of experiments in a laboratory setting that closely replicated real-world conditions. This section enumerates the practical advancements achieved in this specialized field through the research undertaken during the doctoral studies:

1. **CENELEC A, B, C and D frequency bands CE measurements in NB-PLC frequency bandwidth of common types of loads.**

I carried out the measurements showcased in Figure 3.7 to underscore and quantify the effect of CE generated by typical loads on the PLC signal. The results of the CE frequency measurements have shown that CE identification & avoidance and/ or filtering techniques are a valid research subject. The results have been included in my previous article [19].

2. **Study of the impact of loads generating CE on NB-PLC communication.**

Section 3.3 presents the outcomes of the measurements conducted for illustrating the influence of typical loads connected to the low voltage power grid on the PLC signal. The results reveal that the loads connected in its proximity and in the same electrical circuit influence the PLC channel quality, this assessment is done through PLC-G3 modem channel reports RSSI and SNR as well as frequency spectrum

measurements using a spectrum analyzer. The results were also published in my previous article [19].

3. **Practical trials for validating the concept of identifying loads generating CE in the frequency band used by PLC by correlating PLC channel quality data and power measurements for the identification of loads generating noise and determination of optimum time schedule for communication.**

Sections 3.2 and 3.3.2 present the validation activities conducted for establishing the feasibility of correlating PLC channel quality information with load power measurements for PLC noisy load detection and its implementation in the SM architecture as a proof of concept. This results of this activity was published in my previous article [19].

4. **Implementation of an enhanced SM architecture with self-calibration and tampering features capable of detecting loads generating CE in the PLC frequency band.**

In section 3.4, I present an enhanced SM concept that represents an improvement to the one presented in section 3.1. Compared to the architecture presented in section 3.1 it uses the same PLC-G3 modems from Texas Instruments™ but the metrology AFE is capable of self-calibrating together with sensor monitoring and features a power supply design comprising of a non-isolated flyback converter followed by a buck converter. The primary motivation behind the development of the enhanced SM concept was to investigate the potential interference between the mSure™ technology utilized in the metering AFE and PLC. The enhanced SM architecture was presented in my previous article [21] which is an evolution of the architectures presented in my articles [19], [23], [24].

5. **Implementation and evaluation of a passive PLF for NB-PLC frequency band.**

I have designed and implemented a 13^{th} order passive PLF which uses carefully selected components so that it offers enough attenuation in order to block CE and PLC signal while it presents a sufficiently high impedance at both ends thus not disturbing the intended PLC communication. The 13^{th} order filter was selected in order provide sufficient attenuation so that it delivers noise-floor like output in NB-PLC frequency band considering that, there is no attenuation between the power line and the filter. The design steps of the PLF are extensively presented in sections 4.4.1 and 4.4.2 as well as in my previous article [20].

6. **Benchmarking the designed PLF against ones that are currently on the market.**

The designed PLF exhibits exceptional qualities, including the lowest insertion loss across the NB-PLC frequency range, a threefold increase in attenuation at 50 kHz (more than -130 dB) compared to the best commercially available PLF (-40 dB). Additionally it has a power consumption of only 597 mW, which is comparable to the other commercial PLFs. Additionally; the suggested PLF achieves the second-best input and output impedance of 3.36 Ω in the frequency range between 36 kHz and 90.6 kHz. The benchmarking process and results are shown in chapter 4.2 and validated by my previous article [20].

5.4 Future work

In the context of continuing the research activities, I intend to build upon the activities laid out in this thesis and published articles by pursuing the following objectives:

- Develop the enhanced SM concept presented in section 3.4 into a standard SM [145] by adding the following peripherals: display, optical communication port, buttons, relays for load management and consumer disconnection, and a real-time clock.
- The designed PLF is appropriate for use as a type 1 PLF but inadequate for serving as a type 2 PLF (for isolating two sections of the power grid) because it has maximum rated current of 30 A as shown in Section 4.1.1. I want to implement a type 2 PLF using the techniques covered in section 4.4.
- Assess more PLFs using the testing procedures detailed in section 4.2. Furthermore, it is of interest to explore the design and evaluation of a hybrid PLF that combines resonant and n^{th} order types of PLFs, aiming to decrease the filter order while still ensuring attenuation and impedance suitable for type 1 and type 2 PLF.
- Determine whether it is possible to reduce the order of the PLF to less than 13, as in real-world scenarios, the CE affecting the PLC is typically not in close proximity to the filter, and therefore has already been attenuated by the power line. Reducing the filter order has the benefit of lowering the number of components, resulting in decreased size and cost, while retaining the practical benefits of utilizing a PLF for CE within the NB-PLC frequency band.
- Conduct field trials to validate the methodologies for improving PLC over low voltage networks should be performed as the ultimate validation step for the solutions investigated during my doctoral research.

6 References

[1] S. Vitiello, N. Andreadou, M. Ardelean, and G. Fulli, "Smart Metering Roll-Out in Europe: Where Do We Stand? Cost Benefit Analyses in the Clean Energy Package and Research Trends in the Green Deal," *Energies*, vol. 15, no. 7, Art. no. 7, Jan. 2022, doi: 10.3390/en15072340.

[2] Directorate-General for Energy (European Commission), Tractebel Impact, C. Alaton, and F. Tounquet, *Benchmarking smart metering deployment in the EU-28: final report*. LU: Publications Office of the European Union, 2020. Accessed: Jan. 28, 2023. [Online]. Available: https://data.europa.eu/doi/10.2833/492070

[3] "AMI and Power Line Communications." Accessed: Jan. 29, 2023. [Online]. Available: https://www.networkedenergy.com/en/news-events/ami-and-power-line-communications

[4] "CEN-CENELEC-ETSI Smart Grid Coordination Group Smart Grid Reference Architecture." CEN-CENELEC-ETSI Smart Grid Coordination Group, Nov. 08, 2012. Accessed: Jan. 07, 2023. [Online]. Available: https://www.cencenelec.eu/media/CEN-CENELEC/AreasOfWork/CEN-CENELEC_Topics/Smart%20Grids%20and%20Meters/Smart%20Grids/reference_architecture_smartgrids.pdf

[5] G. F. Bartak and A. Abart, "EMI in the frequency range 2-150 kHz," in *Proc. Int Symp on Electromagnetic Compatibility, Tokyo, Japan*, 2014, pp. 577–580.

[6] L. C. Long, W. E. Sayed, V. Munesswaran, N. Moonen, R. Smolenski, and P. Lezynski, "Assessment of Conducted Emission for Multiple Compact Fluorescent Lamps in Various Grid Topology," *Electronics*, vol. 10, no. 18, Art. no. 18, Jan. 2021, doi: 10.3390/electronics10182258.

[7] A. Gallarreta *et al.*, "A Light Measurement Method for 9–150 kHz Disturbances in Power Grids Comparable to CISPR Quasi-Peak," *IEEE Trans. Instrum. Meas.*, vol. 71, pp. 1–10, 2022, doi: 10.1109/TIM.2022.3195255.

[8] M. Girotto and A. M. Tonello, "EMC Regulations and Spectral Constraints for Multicarrier Modulation in PLC," *IEEE Access*, vol. 5, pp. 4954–4966, 2017, doi: 10.1109/ACCESS.2017.2676352.

[9] J. Garrido, A. Moreno-Munoz, A. Gil-de-Castro, V. Pallares-Lopez, and T. Morales-Leal, "Supraharmonics emission from LED lamps: A reduction proposal based on random pulse-width modulation," *Electr. Power Syst. Res.*, vol. 164, pp. 11–19, Nov. 2018, doi: 10.1016/j.epsr.2018.07.032.

[10] S. Lodetti *et al.*, "On the suitability of the CISPR 16 method for measuring conducted emissions in the 2–150kHz range in low voltage grids," *Electr. Power Syst. Res.*, vol. 216, p. 109011, Mar. 2023, doi: 10.1016/j.epsr.2022.109011.

[11] Dept. of Communications Engineering, University of the Basque Country. (UPV/EHU), Escuela de Ingeniería de Bilbao. Spain *et al.*, "Characterization of Non Intentional Conducted Emissions Up to 500 kHz in Urban Environment," *Renew. Energy Power Qual. J.*, vol. 1, pp. 663–668, Apr. 2018, doi: 10.24084/repqj16.425.

[12] W. E. Sayed, P. Lezynski, R. Smolenski, N. Moonen, P. Crovetti, and D. W. P. Thomas, "The Effect of EMI Generated from Spread-Spectrum-Modulated SiC-Based Buck Converter on the G3-PLC Channel," *Electronics*, vol. 10, no. 12, Art. no. 12, Jan. 2021, doi: 10.3390/electronics10121416.

[13] I. Fernandez *et al.*, "Characterization of non-intentional emissions from distributed energy resources up to 500 kHz: A case study in Spain," *Int. J.*

Electr. Power Energy Syst., vol. 105, pp. 549–563, Feb. 2019, doi: 10.1016/j.ijepes.2018.08.048.

[14] I. Fernández, D. de la Vega, A. Arrinda, I. Angulo, N. Uribe-Pérez, and A. Llano, "Field Trials for the Characterization of Non-Intentional Emissions at Low-Voltage Grid in the Frequency Range Assigned to NB-PLC Technologies," *Electronics*, vol. 8, no. 9, Art. no. 9, Sep. 2019, doi: 10.3390/electronics8091044.

[15] C. Szymczyk, C. Nieß, and G. Bumiller, "An On-Line Measurement Approach for EMI Filter Characterization," in *2021 IEEE International Symposium on Power Line Communications and its Applications (ISPLC)*, Oct. 2021, pp. 90–95. doi: 10.1109/ISPLC52837.2021.9628534.

[16] N. Uribe-Pérez, I. Angulo, L. Hernández-Callejo, T. Arzuaga, D. De la Vega, and A. Arrinda, "Study of Unwanted Emissions in the CENELEC-A Band Generated by Distributed Energy Resources and Their Influence over Narrow Band Power Line Communications," *Energies*, vol. 9, no. 12, Art. no. 12, Dec. 2016, doi: 10.3390/en9121007.

[17] "FCC ONLINE TABLE OF FREQUENCY ALLOCATIONS." FEDERAL COMMUNICATIONS COMMISSION OFFICE OF ENGINEERING AND TECHNOLOGY POLICY AND RULES DIVISION, Aug. 23, 2022. Accessed: Jul. 01, 2023. [Online]. Available: https://www.fcc.gov/file/21474/download

[18] "Power Line Communication Equipment (10kHz-450kHz)." Nov. 27, 2002. Accessed: Jul. 01, 2023. [Online]. Available: https://www.arib.or.jp/english/std_tr/telecommunications/desc/std-t84.html

[19] S. Avram, "Power line communication channel noise source detection using smart meters," in *2016 12th IEEE International Symposium on Electronics and Telecommunications (ISETC)*, Oct. 2016, p. 106. doi: 10.1109/ISETC.2016.7781067.

[20] S. Avram and R. Vasiu, "Passive Power Line Communication Filter Design and Benchmarking Using Scattering Parameters," *Appl. Sci. 2023*, vol. 13, no. 11, doi: https://doi.org/10.3390/app13116821.

[21] S. Avram, R. Vasiu, D. Chiciudean, L.-N. Paven, and M. L. Crauciuc, "Hardware and Software Implementation of a Self-Calibrating Smart Meter with Tamper Detection," in *2021 10th International Conference on ENERGY and ENVIRONMENT (CIEM)*, Oct. 2021, pp. 1–5. doi: 10.1109/CIEM52821.2021.9614900.

[22] S. Avram, V. Plotenco, and L.-N. Paven, "Design and development of an electricity Meter Test Equipment," in *2017 International Conference on Optimization of Electrical and Electronic Equipment (OPTIM) & 2017 Intl Aegean Conference on Electrical Machines and Power Electronics (ACEMP)*, May 2017, pp. 96–101. doi: 10.1109/OPTIM.2017.7974954.

[23] S. Avram, A.-M. Safta, C. Căleanu, and R. Vasiu, "Hardware and software implementation of an embedded metering webserver," Jul. 2017, p. 46. doi: 10.1109/TSP.2017.8075933.

[24] S. Avram, C. D. Căleanu, R. Vasiu, A.-M. Safta, and H. G. Belei, "Hardware and Software Integration of an Electrophoretic display on a smart meter," *ITM Web Conf.*, vol. 29, p. 03003, 2019, doi: 10.1051/itmconf/20192903003.

[25] S. Avram, A.-M. Safta, C. Daniel Căleanu, and R. Vasiu, "Hardware and software implementation of an embedded metering webserver," in *2017 40th International Conference on Telecommunications and Signal Processing (TSP)*, Jul. 2017, pp. 43–46. doi: 10.1109/TSP.2017.8075933.

[26] A. Majumder and J. Caffery, "Power line communication: An overview," *Potentials IEEE*, vol. 23, pp. 4–8, Nov. 2004, doi: 10.1109/MP.2004.1343222.
[27] "EN 50065-1:2011 - Signalling on low-voltage electrical installations in the frequency range 3 kHz to 148,5 kHz. General requirements, frequency bands and electromagnetic disturbances." Accessed: May 07, 2019. [Online]. Available: https://shop.bsigroup.com/ProductDetail/?pid=000000000030235497
[28] M. A. Ogunlade, S. L. Gbadamosi, I. E. Owolabi, and N. I. Nwulu, "Noise Measurement, Characterization, and Modeling for Broadband Indoor Power Communication System: A Comprehensive Survey," *Energies*, vol. 16, no. 3, Art. no. 3, Jan. 2023, doi: 10.3390/en16031535.
[29] R. Vines, H. Trissell, L. Gale, and J. O'neal, "Noise on Residential Power Distribution Circuits," *IEEE Trans. Electromagn. Compat.*, vol. EMC-26, no. 4, pp. 161–168, Nov. 1984, doi: 10.1109/TEMC.1984.304217.
[30] G. López, J. Moreno, E. Sanchez, C. Martínez, and F. Martín, "Noise Sources, Effects and Countermeasures in Narrowband Power-Line Communications Networks: A Practical Approach," *Energies*, vol. 10, Aug. 2017, doi: 10.3390/en10081238.
[31] M. Zimmermann and K. Dostert, "Analysis and modeling of impulsive noise in broad-band powerline communications," *IEEE Trans. Electromagn. Compat.*, vol. 44, no. 1, pp. 249–258, Feb. 2002, doi: 10.1109/15.990732.
[32] W. E. Sayed, P. Lezynski, R. Smolenski, N. Moonen, P. Crovetti, and D. W. P. Thomas, "The Effect of EMI Generated from Spread-Spectrum-Modulated SiC-Based Buck Converter on the G3-PLC Channel," *Electronics*, vol. 10, no. 12, Art. no. 12, Jan. 2021, doi: 10.3390/electronics10121416.
[33] "EN 55015:2013+A1:2015 - Limits and methods of measurement of radio disturbance characteristics of electrical lighting and similar equipment." Accessed: May 07, 2019. [Online]. Available: https://shop.bsigroup.com/ProductDetail?pid=000000000030333650
[34] "EN 55014-1:2017 Electromagnetic compatibility. Requirements for household appliances, electric tools and similar apparatus. Emission." Accessed: May 07, 2019. [Online]. Available: https://shop.bsigroup.com/ProductDetail?pid=000000000030284477
[35] J. Lin, F. Magnago, and J. M. Alemany, "Chapter 1 - Optimization Methods Applied to Power Systems: Current Practices and Challenges," in *Classical and Recent Aspects of Power System Optimization*, A. F. Zobaa, S. H. E. Abdel Aleem, and A. Y. Abdelaziz, Eds., Academic Press, 2018, pp. 1–18. doi: 10.1016/B978-0-12-812441-3.00001-X.
[36] "Power Electronics: Circuits, Devices & Applications." Accessed: May 24, 2023. [Online]. Available: https://www.pearson.com/en-us/subject-catalog/p/power-electronics-circuits-devices--applications/P200000003551/9780137982097
[37] T. Sangsuwan, S. Thepphaeng, and C. Pirak, "Experimental performance analysis of powerline communication technologies in AMI systems," in *The 20th Asia-Pacific Conference on Communication (APCC2014)*, Oct. 2014, pp. 382–386. doi: 10.1109/APCC.2014.7092841.
[38] S. Souissi, O. B. Rhouma, and C. Rebai, "Design of coupling interface for narrowband Power Line Communication channel characterization".
[39] C. J. Kikkert and G. Reid, "Radiation and attenuation of communication signals on power lines," in *2009 7th International Conference on Information,*

Communications and Signal Processing (ICICS), Macau, China: IEEE, Dec. 2009, pp. 1–5. doi: 10.1109/ICICS.2009.5397568.
[40] M. H. L. Chan and R. W. Donaldson, "Attenuation of Communication Signals on Residential and Commercial Intrabuilding Power-Distribution Circuits," *IEEE Trans. Electromagn. Compat.*, vol. 28, no. 4, pp. 220–230, 1986, doi: 10.1109/TEMC.1986.4307293.
[41] G. S. Lima and A. De Conti, "Narrowband PLC Channel Attenuation Due to a Multi-Grounded Neutral," *IEEE Trans. Power Deliv.*, vol. 36, no. 2, pp. 639–650, Apr. 2021, doi: 10.1109/TPWRD.2020.2987755.
[42] A. M. Pasdar, I. H. Cavdar, and Y. Sozer, "Power-Line Impedance Estimation at FCC Band Based on Intelligent Home Appliances Status Detection Algorithm Through Their Individual Energy and Impedance Signatures," *IEEE Trans. Power Deliv.*, vol. 29, no. 3, pp. 1407–1416, Jun. 2014, doi: 10.1109/TPWRD.2013.2286154.
[43] Ł. Chruszczyk, "Low-voltage grid impedance measurements in 10 kHz – 1 MHz frequency range," in *2015 IEEE 3rd Workshop on Advances in Information, Electronic and Electrical Engineering (AIEEE)*, Nov. 2015, pp. 1–6. doi: 10.1109/AIEEE.2015.7367291.
[44] I. Fernández *et al.*, "Comparison of Measurement Methods of LV Grid Access Impedance in the Frequency Range Assigned to Nb-Plc Technologies," *Electronics*, vol. 8, no. 10, Art. no. 10, Oct. 2019, doi: 10.3390/electronics8101155.
[45] M. Schwartz, "Carrier-wave telephony over power lines: Early history [History of Communications]," *IEEE Commun. Mag.*, vol. 47, no. 1, pp. 14–18, Jan. 2009, doi: 10.1109/MCOM.2009.4752669.
[46] M. Schwartz, "The origins of carrier multiplexing: Major George Owen Squier and AT&T," *Commun. Mag. IEEE*, vol. 46, pp. 20–24, Jun. 2008, doi: 10.1109/MCOM.2008.4511639.
[47] N. Marumi, "Simultaneous Transmission and Reception in Radio Telephony," in *IRE*, Jun. 1920, pp. 199–219.
[48] G. Dreßler, *Hochfrequenz-Nachrichtentechnik für Elektrizitätswerke*. Springer-Verlag, 1941.
[49] P. A. Brown, "Power Line Communications - Past Present and Future," in *International Symposium on Power Line Communications and Its Applications (ISPLC)*, Lancaster UK, Sep. 1999, pp. 1–8. [Online]. Available: https://hal.science/hal-01066411/document
[50] S. Ramseier and H. Spiess, "Making the power lines sing." Accessed: Jul. 28, 2023. [Online]. Available: https://library.e.abb.com/public/15c5b679bb9f0b93c12572640048e8ab/review_e.indd_1.pdf
[51] D. Dzung, I. Berganza, and A. Sendin, "Evolution of powerline communications for smart distribution: From ripple control to OFDM," in *2011 IEEE International Symposium on Power Line Communications and Its Applications*, Udine, Italy: IEEE, Apr. 2011, pp. 474–478. doi: 10.1109/ISPLC.2011.5764444.
[52] D. Dzung, T. V. Hoff, and J. Stoupis, "The nervous system of the smart grid." Accessed: Jul. 28, 2023. [Online]. Available: https://library.e.abb.com/public/c124268b04b4fbc1c125770c00357f08/33-37%201M011_ENG_72dpi.pdf

[53] A. Neuberg, "Ripple control in the Czech Republic and Demand Side Management," in *CIRED 2009 - 20th International Conference and Exhibition on Electricity Distribution - Part 1*, Jun. 2009, pp. 1–5. doi: 10.1049/cp.2009.0806.
[54] A. Unhauzer, "THE FUTURE OF CENTRALIZED RIPPLE CONTROL SYSTEM IN HUNGARY – STATE-OF-THE-ART TRENDS".
[55] O. Selinger-Lutz, I. Katz, R. Hollinger, and C. Wittwer, "Lessons Learned From Field Test Data of a Robust Smart Grid Concept," in *2018 IEEE PES Innovative Smart Grid Technologies Conference Europe (ISGT-Europe)*, Sarajevo, Bosnia and Herzegovina: IEEE, Oct. 2018, pp. 1–6. doi: 10.1109/ISGTEurope.2018.8571565.
[56] "IEC 62054-11:2004+AMD1:2016, Electricity metering (a.c.) - Tariff and load control - Part 11:Particular requirements for electronic ripple control receivers." Accessed: Jul. 28, 2023. [Online]. Available: https://webstore.iec.ch/publication/26234
[57] D. Westermann and A. John, "Demand Matching Wind Power Generation With Wide-Area Measurement and Demand-Side Management," *Energy Convers. IEEE Trans. On*, vol. 22, pp. 145–149, Apr. 2007, doi: 10.1109/TEC.2006.889551.
[58] W. Hagmann, "A spread spectrum communication system for load management and distribution automation," *IEEE Trans. Power Deliv.*, vol. 4, no. 1, pp. 75–81, Jan. 1989, doi: 10.1109/61.19190.
[59] A. Sendin *et al.*, "Adaptation of Powerline Communications-Based Smart Metering Deployments to the Requirements of Smart Grids," *Energies*, vol. 8, no. 12, Art. no. 12, Dec. 2015, doi: 10.3390/en81212372.
[60] "Introduction to the LonWorks® Platform Revision 2." Accessed: Jul. 24, 2023. [Online]. Available: https://www.echelon.com/assets/blt893a8b319e8ec8c7/078-0183-01B_Intro_to_LonWorks_Rev_2.pdf
[61] S. T. Mak and T. G. Moore, "TWACS™, A New Viable Two-Way Automatic Communication System for Distribution Networks. Part II: Inbound Communication," *IEEE Trans. Power Appar. Syst.*, vol. PAS-103, no. 8, pp. 2141–2147, Aug. 1984, doi: 10.1109/TPAS.1984.318524.
[62] "IEC 61334-5-1:2001 - Distribution automation using distribution line carrier systems - Part 5-1: Lower layer profiles; The spread frequency shift keying (S-FSK) profile | Joinup." Accessed: Jul. 29, 2023. [Online]. Available: https://joinup.ec.europa.eu/collection/ict-standards-procurement/solution/iec-61334-5-12001-distribution-automation-using-distribution-line-carrier-systems-part-5-1-lower
[63] "IEC TS 61334-5-2:1998, Distribution automation using distribution line carrier systems - Part 5-2: Lower layer profiles - Frequency shift keying (FSK) profile." Accessed: Jul. 29, 2023. [Online]. Available: https://webstore.iec.ch/publication/5309
[64] "Smart Houses Interacting with Smart Grids to achieve next-generation energy efficiency and sustainability," European Commision, Oct. 2010. Accessed: Jul. 29, 2023. [Online]. Available: https://www.smartgrid.gov/files/documents/SmartHouse_SmartGrid_D12_Technology_Trends_for_SmartHouse_Sm_201007.pdf
[65] C. Lavenu, C. Chauvenet, P. Treffiletti, M. Varesio, and K. Hueske, "Standardization Challenges, Opportunities and Recent Evolutions for the G3-PLC Technology," *Energies*, vol. 14, no. 7, Art. no. 7, Jan. 2021, doi: 10.3390/en14071937.

[66] "IEC TS 61334-5-5:2001, Distribution automation using distribution line carrier systems - Part 5-5: Lower layer profiles - Spread spectrum - fast frequency hopping (SS-FFH) profile." [Online]. Available: https://webstore.iec.ch/publication/5312

[67] E. Comellini, R. Gargiuli, G. Gelli, R. Tonon, and P. Mirandola, "An Enhanced Distribution Automation System Based On New Communication Technology At ENEL," ETDE-IT092-29, 1991. Accessed: Jul. 29, 2023. [Online]. Available: https://inis.iaea.org/collection/NCLCollectionStore/_Public/24/007/24007954.pdf

[68] M. Cotti and R. Millan, "CERVANTES PROJECT AND 'METERS AND MORE': THE STATE OF THE ART OF SMART METERING IMPLEMENTATION IN EUROPE," no. 0829, 2011.

[69] K. D. Craemer and G. Deconinck, "Analysis of State-of-the-art Smart Metering Communication Standards".

[70] S. Ramseler, M. Arzberger, and A. Hauser, "MV and LV powerline communications: new proposed IEC standards," in *1999 IEEE Transmission and Distribution Conference (Cat. No. 99CH36333)*, New Orleans, LA, USA: IEEE, 1999, pp. 235–239 vol.1. doi: 10.1109/TDC.1999.755350.

[71] "IEC TS 61334-5-4:2001, Distribution automation using distribution line carrier systems - Part 5-4: Lower layer profiles - Multi-carrier modulation (MCM) profile." Accessed: Jul. 29, 2023. [Online]. Available: https://webstore.iec.ch/publication/5311

[72] C. A. Wülfing, F. G. Reck, F. G. Carloto, C. H. Barriquello, P. R. Marin, and E. Nascimento, "Evaluation of DLMS/COSEM Data Processing Setups Applied to Smart Metering," in *2022 14th Seminar on Power Electronics and Control (SEPOC)*, Nov. 2022, pp. 1–6. doi: 10.1109/SEPOC54972.2022.9976442.

[73] M. Knezic, Z. Ivanovic, and B. Dokic, *GPRS-Based Electrical Energy Monitoring System*. 2012.

[74] G. Artale *et al.*, "A PLC based monitoring and remote control architecture for Distributed Generation and Storage systems in LV smart grids," in *2021 IEEE 6th International Forum on Research and Technology for Society and Industry (RTSI)*, Sep. 2021, pp. 255–260. doi: 10.1109/RTSI50628.2021.9597316.

[75] A. Sendin, J. Simon, I. Urrutia, and I. Berganza, *PLC deployment and architecture for Smart Grid applications in Iberdrola*. 2014, p. 178. doi: 10.1109/ISPLC.2014.6812374.

[76] K. Namrata, A. Dayal, A. Ranjan, K. Arun, D. Tolia, and A. Samadhiya, "IOT Enabled Smart Grid Coordinated Control Using Hierarchical PLC Architecture," in *Smart Energy and Advancement in Power Technologies*, K. Namrata, N. Priyadarshi, R. C. Bansal, and J. Kumar, Eds., in Lecture Notes in Electrical Engineering. Singapore: Springer Nature, 2023, pp. 89–105. doi: 10.1007/978-981-19-4971-5_7.

[77] L. Lu, R. Brito, and Y. Song, "QoS and performance of REMPLI PLC network," Oct. 2005, [Online]. Available: https://inria.hal.science/inria-00000758/preview/QoS_and_performance_of_REMPLI_PLC_network.pdf

[78] S. Liu, F. Yang, D. Li, R. Yao, and J. Song, "Power Line Communication with Robust Timing and Carrier Recovery against Narrowband Interference for Smart Grid," *Sensors*, vol. 22, no. 11, Art. no. 11, Jan. 2022, doi: 10.3390/s22114013.

[79] W. Kabir, "Orthogonal Frequency Division Multiplexing (OFDM)," in *2008 China-Japan Joint Microwave Conference*, Shanghai, China: IEEE, Sep. 2008, pp. 178–184. doi: 10.1109/CJMW.2008.4772401.

[80] P. Patil, M. R. Patil, S. Itraj, and U. L. Bomble, "A Review on MIMO OFDM Technology Basics and More," in *2017 International Conference on Current Trends in Computer, Electrical, Electronics and Communication (CTCEEC)*, Mysore, India: IEEE, Sep. 2017, pp. 119–124. doi: 10.1109/CTCEEC.2017.8455114.
[81] "Alliance | PRIME Alliance." Accessed: Jul. 30, 2023. [Online]. Available: https://www.prime-alliance.org/alliance/
[82] Md. Rahman, C. Hong, S. Lee, J. Lee, Md. Razzaque, and J. Kim, "Medium access control for power line communications: an overview of the IEEE 1901 and ITU-T G.hn standards," *IEEE Commun. Mag.*, vol. 49, no. 6, pp. 183–191, Jun. 2011, doi: 10.1109/MCOM.2011.5784004.
[83] J. Toonen, S. Bhattacharyya, and S. Cobben, "Impacts of ripple control signals at low voltage customer's installations," in *22nd International Conference and Exhibition on Electricity Distribution (CIRED 2013)*, Stockholm, Sweden: Institution of Engineering and Technology, 2013, pp. 0256–0256. doi: 10.1049/cp.2013.0636.
[84] D. E. Nordell, "Communication systems for Distribution Automation," in *2008 IEEE/PES Transmission and Distribution Conference and Exposition*, Chicago, IL, USA: IEEE, Apr. 2008, pp. 1–14. doi: 10.1109/TDC.2008.4517284.
[85] D. Luo, D. Xiao, X. Zhang, X. Zhang, X. Tang, and L. Zheng, "Design and implementation of HPLC Communication module in Smart Grid," *J. Phys. Conf. Ser.*, vol. 1738, p. 012012, Jan. 2021, doi: 10.1088/1742-6596/1738/1/012012.
[86] E. Kabalci and Y. Kabalci, "Chapter 4 - Power line communication technologies in smart grids," in *From Smart Grid to Internet of Energy*, E. Kabalci and Y. Kabalci, Eds., Academic Press, 2019, pp. 119–171. doi: 10.1016/B978-0-12-819710-3.00004-1.
[87] A. Ikpehai, B. Adebisi, and K. M. Rabie, "Broadband PLC for Clustered Advanced Metering Infrastructure (AMI) Architecture," *Energies*, vol. 9, no. 7, Art. no. 7, Jul. 2016, doi: 10.3390/en9070569.
[88] Mlynek, J. Misurec, P. Silhavy, R. Fujdiak, J. Sláčik, and Z. Hasirci Tuğcu, "Simulation of Achievable Data Rates of Broadband Power Line Communication for Smart Metering," *Appl. Sci.*, vol. 9, p. 1527, Apr. 2019, doi: 10.3390/app9081527.
[89] P. Mlýnek, M. Rusz, L. Benešl, J. Slácik, and P. Musil, "Possibilities of Broadband Power Line Communications for Smart Home and Smart Building Applications," *Sensors*, vol. 21, Jan. 2021, doi: https://doi.org/10.3390/s21010240.
[90] M. Giraneza and K. Abo-Al-Ez, "Power line communication: A review on couplers and channel characterization," *AIMS Electron. Electr. Eng.*, vol. 6, no. 3, Aug. 2022, doi: 10.3934/electreng.2022016.
[91] L. G. D. S. Costa, A. C. M. De Queiroz, B. Adebisi, V. L. R. Da Costa, and M. V. Ribeiro, "Coupling for Power Line Communications: A Survey," *J. Commun. Inf. Syst.*, vol. 32, no. 1, pp. 8–22, 2017, doi: 10.14209/jcis.2017.2.
[92] P. Mulroy and I. Gilbert, "COMPARISON OF COUPLING METHODS IN MV EQUIPMENT FOR POWERLINE COMMUNICATIONS," no. 0870, 2011.
[93] J. Yoo, S. Choe, and N. Pine, "SISO/MIMO-OFDM Based Power Line Communication Using MRC," in *Electrical Engineering and Control*, M. Zhu, Ed., in Lecture Notes in Electrical Engineering. Berlin, Heidelberg: Springer, 2011, pp. 853–860. doi: 10.1007/978-3-642-21765-4_106.

[94] R. Han and D. J. Rogers, "Zero-Additional-Hardware Power Line Communication for DC–DC Converters," *IEEE Trans. Power Electron.*, vol. 37, no. 11, pp. 13107–13118, Nov. 2022, doi: 10.1109/TPEL.2022.3178020.
[95] G. Artale *et al.*, "A New Coupling Solution for G3-PLC Employment in MV Smart Grids," *Energies*, vol. 12, no. 13, 2019, doi: https://doi.org/10.3390/en12132474.
[96] T. F. A. Nogueira *et al.*, "Inductive coupling-based narrowband PLC systems for overhead MV power distribution networks: New insights," *Int. J. Electr. Power Energy Syst.*, vol. 147, p. 108715, May 2023, doi: 10.1016/j.ijepes.2022.108715.
[97] C. A. Boddie, "Telephone Communication over Power Lines by High Frequency Currents," *Proc. IRE*, vol. 15, no. 7, pp. 559–640, Jul. 1927, doi: 10.1109/JRPROC.1927.221237.
[98] J. I. Morales-Aragonés *et al.*, "A Resonant Ring Topology Approach to Power Line Communication Systems within Photovoltaic Plants," *Appl. Sci.*, vol. 12, no. 16, p. 7973, Aug. 2022, doi: 10.3390/app12167973.
[99] A. Beer, A. Sheri, J. Vinck, I. Frank Nonso, and H. Ferreira, *Contactless Power Line Communications at 2.45GHz*. 2017.
[100] F. N. Igboamalu, A. R. Ndjiongue, and H. C. Ferreira, "PLC-RF diversity: channel outage analysis," *Telecommun. Syst.*, vol. 73, no. 4, pp. 521–530, Apr. 2020, doi: 10.1007/s11235-019-00624-1.
[101] D. Poljak, V. Doric, and S. Sesnic, "Coupling from HF Transmitter to Power Line Communications System using Antenna Theory - Analytical versus Numerical Approach," in *VXV International Symposium on Theoretical Engineering*, Jun. 2009, pp. 1–3.
[102] "JFG - Axial Metallized Polyester & Polypropylene Film Capacitor - jb." Accessed: Apr. 30, 2023. [Online]. Available: https://www.jbcapacitors.com/pdf/JFG-Axial-Metallized-Polyester-Polypropylene-Film-Capacitor.pdf
[103] "AFE031 Powerline Communications Analog Front-End." Jun. 2019. Accessed: Jul. 30, 2023. [Online]. Available: https://www.ti.com/lit/gpn/afe031
[104] X. Wang and X. Gao, "The typical designs of PLC network in MV distribution network," in *2012 IEEE International Symposium on Power Line Communications and Its Applications*, Beijing, China: IEEE, Mar. 2012, pp. 19–23. doi: 10.1109/ISPLC.2012.6201332.
[105] "Inductive Couplers for Signal Transmission - Grupo Premo." Accessed: Aug. 05, 2023. [Online]. Available: https://www.grupopremo.com/en/596-inductive-couplers
[106] D.-S. In, S. Shon, and J.-J. Lee, "A study on the implementation of inductive coupler with rogowski coil for BPLC," in *2008 International Conference on Advanced Technologies for Communications*, Oct. 2008, pp. 327–330. doi: 10.1109/ATC.2008.4760588.
[107] J.-J. Lee, D.-S. In, H.-M. Oh, S. Shon, and D.-H. Nam, "Neutral inductive coupling for improved underground medium voltage BPLC," in *ISPLC2010*, Mar. 2010, pp. 67–71. doi: 10.1109/ISPLC.2010.5479947.
[108] Z. W. Swana, P. A. Janse van Rensburg, and H. C. Ferreira, "Is resistive coupling feasible for the reception of power-line communications data?," in *2015 IEEE International Symposium on Power Line Communications and Its Applications (ISPLC)*, Mar. 2015, pp. 47–52. doi: 10.1109/ISPLC.2015.7147588.

[109] Z. Sadowski, "Comparison of PLC-PRIME and PLC-G3 protocols," in *2015 International School on Nonsinusoidal Currents and Compensation (ISNCC)*, Lagow, Poland: IEEE, Jun. 2015, pp. 1–6. doi: 10.1109/ISNCC.2015.7174704.
[110] "MAX79356 Evaluation Kit." Maxim Integrated, 2016. Accessed: Aug. 05, 2023. [Online]. Available: https://www.analog.com/media/en/technical-documentation/data-sheets/MAX79356CAEVK1.pdf
[111] "ST8500 power line communication system-on-chip G3-PLC characterization." Jan. 2021. Accessed: Aug. 01, 2023. [Online]. Available: https://www.st.com/resource/en/application_note/an5525-st8500-poer-line-communication-systemonchip--g3plc-charachterization-stmicroelectronics.pdf
[112] "Specification for PoweRline Intelligent Metering Evolution." Sep. 14, 2021. [Online]. Available: https://www.prime-alliance.org/media/2021/12/PRIME-Spec_v1.420210914.pdf
[113] "Narrowband OFDM PLC specifications for G3-PLC networks." Jun. 2021. Accessed: Aug. 15, 2023. [Online]. Available: https://g3-plc.com/download/90/specifications/2578/g3-plc_alliance_-_g3-plc_specifications_-_cenelec_-_arib_-_fcc__-_revision__2021__clean.pdf
[114] "SOMPLC-F28PLC83 System on Module for Power Line Communication, User's Guide." Jun. 2015. Accessed: Jul. 09, 2023. [Online]. Available: https://www.ti.com/lit/pdf/spruhr4
[115] A. E. Dulay, R. I. R. Astillero, P. G. P. La Rosa, R. J. L. L. Tan, A. D. Tapang, and A. Santos, "Performance evaluation of G3 narrowband PLC standard for transmission through single and paired transformer," in *2016 3rd MEC International Conference on Big Data and Smart City (ICBDSC)*, Mar. 2016, pp. 1–6. doi: 10.1109/ICBDSC.2016.7460333.
[116] M. Hoch, "Comparison of PLC G3 and PRIME," in *2011 IEEE International Symposium on Power Line Communications and Its Applications*, Apr. 2011, pp. 165–169. doi: 10.1109/ISPLC.2011.5764384.
[117] A. Fernandez Olivera, A. Sendin, I. Urrutia Galdos, J. Mateo Arenas, P. Angueira, and J. J. Ferro Vázquez, "Analysis of PRIME PLC Smart Metering Networks Performance," *Renew. Energy Power Qual. J.*, pp. 613–618, Mar. 2013, doi: 10.24084/repqj11.387.
[118] J. C.-I. Chuang, "Comparison of coherent and differential detection of BPSK and QPSK in a quasi-static fading channel," in *IEEE International Conference on Communications, - Spanning the Universe.*, Jun. 1988, pp. 749–755 vol.2. doi: 10.1109/ICC.1988.13661.
[119] Keysight, "Digital Modulation in Communications Systems | Keysight." Accessed: Oct. 20, 2023. [Online]. Available: https://www.keysight.com/us/en/assets/7018-09093/application-notes/5965-7160.pdf
[120] "Power Line Modem with E-meter Platform White Paper." Texas Intruments, Feb. 04, 2004. Accessed: Apr. 08, 2023. [Online]. Available: https://www.ti.com/lit/an/slla164/slla164.pdf
[121] "ITU-T G.9903 Narrowband orthogonal frequency division multiplexing power line communication transceivers for G3-PLC networks." TELECOMMUNICATION STANDARDIZATION SECTOR OF ITU, Aug. 2017. [Online]. Available: https://www.itu.int/rec/dologin_pub.asp?lang=e&id=T-REC-G.9903-201708-I!!PDF-E&type=items
[122] P. Guyard, R. Fiorelli, and J. Houee, "STCOMET smart meter and power line communication system-on-chip development kit." 2017. Accessed: Aug. 01, 2023. [Online]. Available:

https://www.st.com/resource/en/application_note/an4732-stcomet-smart-meter-and-power-line-communication-systemonchip-development-kit-stmicroelectronics.pdf
[123] P. Sausen, A. Sausen, M. Campos, L. F. Sauthier, A. Oliveira, and R. Emmel, "Power Line Communication Applied in a Typical Brazilian Urban Power Network," *IEEE Access*, vol. PP, pp. 1–1, May 2021, doi: 10.1109/ACCESS.2021.3078697.
[124] M. Nassar, J. Lin, Y. Mortazavi, A. Dabak, I. Kim, and B. Evans, "Local Utility Power Line Communications in the 3–500 kHz Band: Channel Impairments, Noise, and Standards," *IEEE Signal Process. Mag.*, vol. 29, no. 5, pp. 116–127, Sep. 2012, doi: 10.1109/MSP.2012.2187038.
[125] "EN 55016-1-2:2014+A1:2018 - Specification for radio disturbance and immunity measuring apparatus and methods. Radio disturbance and immunity measuring apparatus. Coupling devices for conducted disturbance measurements." Accessed: May 14, 2019. [Online]. Available: https://shop.bsigroup.com/ProductDetail/?pid=000000000030330243
[126] J. A. Malack and J. R. Engstrom, "RF Impedance of United States and European Power Lines," *IEEE Trans. Electromagn. Compat.*, vol. EMC-18, no. 1, pp. 36–38, Feb. 1976, doi: 10.1109/TEMC.1976.303453.
[127] G. Chu, J. Li, and W. Liu, "Narrow band power line channel characteristics for low voltage access network in China," in *2013 IEEE 17th International Symposium on Power Line Communications and Its Applications*, Mar. 2013, pp. 297–302. doi: 10.1109/ISPLC.2013.6525867.
[128] C. J. Kikkert and S. Zhu, "Resistive Shunt On-line Impedance Analyzer," in *2016 International Symposium on Power Line Communications and its Applications (ISPLC)*, Mar. 2016, pp. 150–155. doi: 10.1109/ISPLC.2016.7476269.
[129] I. Cavdar and K. Engin, "Measurements of Impedance and Attenuation at CENELEC Bands for Power Line Communications Systems," *Sensors*, vol. 8, Dec. 2008, doi: 10.3390/s8128027.
[130] "LISN / AMN." Accessed: Oct. 15, 2023. [Online]. Available: https://www.schwarzbeck.de/en/lisn-line-impedance-stabilisation-networks.html
[131] "CISPR 16-1-2:2014+AMD1:2017 CSV | IEC Webstore | electromagnetic compatibility, EMC, smart city." Accessed: Jul. 09, 2023. [Online]. Available: https://webstore.iec.ch/publication/61924
[132] "Operating Manual Spectrum Analyzer R&S FSL." Accessed: Aug. 01, 2023. [Online]. Available: https://www.rohde-schwarz.com/it/file/FSL_OperatingManual_en_12.pdf
[133] "EN 50065-7 - Signalling on Low-Voltage Electrical Installations in the Frequency Range 3 kHz to 148,5 kHz - Part 7: Equipment Impedance." Accessed: May 23, 2019. [Online]. Available: https://standards.globalspec.com/std/134252/EN%2050065-7
[134] K. B. Clark, "Isolation and Regulation Transformer Operating Principles and Transients Response." Dec. 14, 2004. [Online]. Available: https://www.surgesuppresion.com/images/DotNetSite/TechPhttps://www.surgesuppression.com/images/DotNetSite/TechPapers/IsolationTransformersPassTransientsRev07.pdf
[135] "LISN Line Impedance Stabilisation Networks / AMN Artificial Mains Network." Accessed: Jul. 09, 2023. [Online]. Available:

https://www.schwarzbeck.de/en/lisn-line-impedance-stabilisation-networks.html
[136] R. & S. G. & C. KG, "R&S®HM6050-2 Line Impedance Stabilization Network User Manual." Accessed: Jul. 09, 2023. [Online]. Available: https://www.rohde-schwarz.com/hk/manual/r-s-hm6050-2-line-impedance-stabilization-network-user-manual-manuals_78701-156546.html
[137] "STPM32 - ASSP for metering applications with up to four independent 24-bit 2nd order sigma-delta ADCs, 4 MHz OSF and 2 embedded PGLNA - STMicroelectronics." Accessed: Jul. 09, 2023. [Online]. Available: https://www.st.com/resource/en/datasheet/stpm32.pdf
[138] Trialog, "Technical overview of G3-PLC," Trialog. Accessed: Oct. 21, 2023. [Online]. Available: https://www.trialog.com/en/technical-overview-of-g3-plc/
[139] "Calmet TE30 Datasheet." Jul. 2022. Accessed: Aug. 01, 2023. [Online]. Available: https://www.calmet.com.pl/images/pdf/TE30-Three-Phase-Working-Standard-Data-Sheet-EN.pdf
[140] "Energy Metering IC with Sensor Monitoring and Self-Calibration." Analog Devices. Accessed: Apr. 08, 2023. [Online]. Available: https://www.analog.com/media/en/technical-documentation/data-sheets/ADE9153B.pdf
[141] "EV-ADE9153ASHIELDZ User Guide UG-1253." Analog Devices. Accessed: Apr. 08, 2023. [Online]. Available: https://www.analog.com/media/en/technical-documentation/userguides/ ev-ade9153ashieldz-ug-1253.pdf
[142] M. Nousiainen, J. Lohvansuu, and D. Lath, "Electricity Meter Accuracy Monitoring Enabled by ADI's mSure Technology."
[143] "ESP8266EX Datasheet." Jun. 2023. [Online]. Available: https://www.espressif.com/sites/default/files/documentation/0a-esp8266ex_datasheet_en.pdf
[144] "EN 50470-3:2006+A1:2018 Electricity metering equipment (a.c.). Particular requirements. Static meters for active energy (class indexes A, B and C)." Accessed: May 28, 2021. [Online]. Available: https://shop.bsigroup.com/ProductDetail?pid=000000000030361405
[145] "EN 50470-1:2006+A1:2018 Electricity metering equipment (a.c.). General requirements, tests and test conditions. Metering equipment (class indexes A, B and C)." Accessed: May 28, 2019. [Online]. Available: https://shop.bsigroup.com/ProductDetail?pid=000000000030361398
[146] ST MicroElectronics, "Viper26K Datasheet, DS12978 Rev 1." Accessed: Jan. 25, 2021. [Online]. Available: https://www.st.com/resource/en/datasheet/viper26k.pdf
[147] Texas Instruments, "TPS62177DQCR datasheet." Accessed: Jan. 25, 2021. [Online]. Available: https://www.ti.com/lit/ds/slvsb35c/slvsb35c.pdf
[148] "Arduino/libraries/ESP8266WiFi/src/ESP8266WiFi.h at master · esp8266/Arduino," GitHub. Accessed: Aug. 15, 2023. [Online]. Available: https://github.com/esp8266/Arduino/blob/master/libraries/ESP8266WiFi/src/ESP8266WiFi.h
[149] "ADE9153A arduino library," GitHub. Accessed: Aug. 15, 2023. [Online]. Available: https://github.com/analogdevicesinc/arduino/blob/master/Arduino%20Uno%20R3/libraries/ADE9153A/ADE9153A.h

[150] V. Tarateeraseth, "EMI filter design: Part III: Selection of filter topology for optimal performance," *IEEE Electromagn. Compat. Mag.*, vol. 1, no. 2, pp. 60–73, Second 2012, doi: 10.1109/MEMC.2012.6244975.
[151] D. Varajão, R. Esteves Araújo, L. M. Miranda, and J. A. Peças Lopes, "EMI Filter Design for a Single-stage Bidirectional and Isolated AC–DC Matrix Converter," *Electronics*, vol. 7, no. 11, p. 318, Nov. 2018, doi: 10.3390/electronics7110318.
[152] K. Bernacki, D. Wybrańczyk, M. Zygmanowski, A. Latko, J. Michalak, and Z. Rymarski, "Disturbance and Signal Filter for Power Line Communication," *Electronics*, vol. 8, no. 4, p. 378, Apr. 2019, doi: 10.3390/electronics8040378.
[153] A. Vukicevic, M. Bittner, A. Rubinstein, M. Rubinstein, and F. Rachidi, "A concept to enhance system data rate for PLC access networks," in *2008 IEEE International Symposium on Power Line Communications and Its Applications*, Jeju City, Jeju Island, South Korea: IEEE, Apr. 2008, pp. 105–110. doi: 10.1109/ISPLC.2008.4510407.
[154] S. Liu, Y. Zhang, and D. Yu, "Research and design of EMI digital filters using scattering parameters," in *2009 International Conference on Wireless Communications Signal Processing*, Nov. 2009, pp. 1–5. doi: 10.1109/WCSP.2009.5371392.
[155] P. C. Sekhar, Y. Gopal, and T. rao, "DESIGN OF S PARAMETERS FOR VARIOUS FILTERS," 2013. Accessed: Aug. 09, 2023. [Online]. Available: http://www.tjprc.org/publishpapers/--1366185303-11.-Design%20of%20s%20parameters.full.pdf
[156] "Blocking Filter - Grupo Premo." Accessed: Aug. 01, 2023. [Online]. Available: https://www.grupopremo.com/content/102-blocking-filter
[157] "EN 61140:2016 - Protection against electric shock. Common aspects for installation and equipment." Accessed: May 07, 2019. [Online]. Available: https://shop.bsigroup.com/ProductDetail/?pid=000000000030275023
[158] "Instruction leaflet for the linky smart meter." Accessed: Aug. 08, 2023. [Online]. Available: https://www.enedis.fr/media/2208/download
[159] "What should you do when the electricity goes off?," Endesa. Accessed: Aug. 09, 2023. [Online]. Available: https://www.endesa.com/en/blogs/endesa-s-blog/light/what-to-do-fuse-box-trips
[160] "Qué es el ICP y para qué sirve | i-DE - Grupo Iberdrola." Accessed: Aug. 09, 2023. [Online]. Available: https://www.i-de.es/averias-cortes-luz/que-es-el-icp-para-que-sirve
[161] "Keysight Technologies Ultra-Low Impedance Measurements Using 2-Port Measurements Online:literature.cdn.keysight.com/litweb/pdf/5989-5935EN.pdf (Accessed on 14 April 2023)." Accessed: May 25, 2019. [Online]. Available: http://literature.cdn.keysight.com/litweb/pdf/5989-5935EN.pdf
[162] TDK, "General technical information, Available online:https://www.tdk-electronics.tdk.com/en/155646/tech-library (accessed on 15 March 2023)."
[163] "STEVAL-XPLM01CPL - Power line communication AC coupling circuit - STMicroelectronics." Accessed: Apr. 14, 2023. [Online]. Available: https://www.st.com/en/evaluation-tools/steval-xplm01cpl.html
[164] J. D. W. Onoufrios Theofylaktos, *Calibration Procedure for Measuring S-Parameters in Balun Applications on 150-Ω High-Speed Cables*. National Aeronautics and Space Administration, 2023. [Online]. Available: https://ntrs.nasa.gov/api/citations/20120008524/downloads/20120008524.pdf

[165] "Using Baluns and RF Components for Impedance Matching." Jan. 26, 2021. Accessed: Apr. 22, 2023. [Online]. Available: https://www.coilcraft.com/pdfs/Doc1077_Baluns_and_Impedance_Matching.pdf
[166] "SLM3505 User Manual." Accessed: Aug. 08, 2023. [Online]. Available: https://www.newtons4th.com/media/docs/D000200-SLM3505-User-Manual.pdf
[167] M. Randus and K. Hoffmann, "A simple method for extreme impedances measurement - experimental testing," in *2008 72nd ARFTG Microwave Measurement Symposium*, Dec. 2008, pp. 40–44. doi: 10.1109/ARFTG.2008.4804276.
[168] I. Novak, "Why S11 VNA Measurements Don't Work for PDN Measurements." Accessed: Apr. 04, 2023. [Online]. Available: http://www.electrical-integrity.com/Quietpower_files/QuietPower-4.pdf
[169] "IEC 60939-3:2015 Passive filter units for electromagnetic interference suppression – Part 3: Passive filter units for which safety tests are appropriate." Accessed: May 30, 2023. [Online]. Available: https://webstore.iec.ch/publication/23091
[170] "EN 61000-4-5:2014+A1:2017 Electromagnetic compatibility (EMC) – Part 4-5: Testing and measurement techniques. Surge immunity test." Accessed: May 28, 2019. [Online]. Available: https://shop.bsigroup.com/ProductDetail/?pid=000000000030348871
[171] "EN 50160:2010+A1:2015 Voltage characteristics of electricity supplied by public electricity networks." Accessed: Jun. 04, 2019. [Online]. Available: https://shop.bsigroup.com/ProductDetail/?pid=000000000030320121
[172] "TMOV - Littelfuse." Accessed: Apr. 30, 2023. [Online]. Available: https://www.littelfuse.com/products/varistors/thermally-protected/tmov.aspx
[173] "Varistors - an overview Available online: https://www.sciencedirect.com/topics/earth-and-planetary-sciences/varistors (accessed on 30 April 2023)," Accessed: Apr. 30, 2023. [Online]. Available: https://www.sciencedirect.com/topics/earth-and-planetary-sciences/varistors
[174] W. Wu *et al.*, "Analysis and suppression of high-frequency oscillation between converter-based source and loads in an island power system," *Int. J. Electr. Power Energy Syst.*, vol. 117, p. 105616, May 2020, doi: 10.1016/j.ijepes.2019.105616.
[175] R.-M. O. Corporation, "Surge Safety Resistor - SSR | Made in Taiwan MELF Resistors Manufacturer - FIRSTOHM," First resistor & condenser Co. Ltd. Accessed: Apr. 30, 2023. [Online]. Available: https://www.firstohm.com.tw/en/category/CATE-surge_safety_resistor-SSR.html?page=13
[176] "Creepage Distance - an overview | ScienceDirect Topics." Accessed: Apr. 30, 2023. [Online]. Available: https://www.sciencedirect.com/topics/engineering/creepage-distance
[177] "MS-184075-2-DataSheet.pdf, Available Online:https://datasheets.micrometals.com/MS-184075-2-DataSheet.pdf (Accessed on 12 April 2023)." Accessed: Apr. 30, 2023. [Online]. Available: https://datasheets.micrometals.com/MS-184075-2-DataSheet.pdf
[178] A. Inoue and F. Kong, "Soft Magnetic Materials," in *Encyclopedia of Smart Materials*, A.-G. Olabi, Ed., Oxford: Elsevier, 2022, pp. 10–23. doi: 10.1016/B978-0-12-803581-8.11725-4.
[179] F. Caspers, "RF engineering basic concepts: S-parameters." CERN. Accessed: Aug. 08, 2023. [Online]. Available: https://cds.cern.ch/record/1415639/files/p67.pdf

[180] S. Liu, Y. Zhang, and D. Yu, "Research and design of EMI digital filters using scattering parameters," in *2009 International Conference on Wireless Communications Signal Processing*, Nov. 2009, pp. 1–5. doi: 10.1109/WCSP.2009.5371392.
[181] "Taking Advantage of S-Parameter." Accessed: Aug. 08, 2023. [Online]. Available: https://product.tdk.com/en/products/emc/guidebook/eemc_basic_03.pdf
[182] "R&S®ZNB Vector Network Analyzer Specifications." Accessed: Aug. 08, 2023. [Online]. Available: https://scdn.rohde-schwarz.com/ur/pws/dl_downloads/dl_common_library/dl_brochures_and_datasheets/pdf_1/service_support_30/ZNB_dat-sw_en_5214-5384-22_v0900_96dp.pd